ISSN: 2227-6912
E-ISSN: 2790-0479

Azerbaijan Technical University

MACHINE SCIENCE

2
2024

International scientific-technical journal

MACHINE SCIENCE

MAŞINŞÜNASLIQ МАШИНОВЕДЕНИЕ

International scientific-technical journal
Beynəlxalq elmi-texniki jurnal
Международный научно-технический журнал

Number 2
2024
10.61413/KPJE9807

Founder: The Ministry of Education of Azerbaijan Republic
Təsisçi: *Azərbaycan Respublikası Təhsil Nazirliyi*
Учредитель: *Министерство образования Азербайджанской Республики*

The journal is included into the list confirmed by Higher Attestation Commission of the Azerbaijan Republic of editions for the publication of works of competitors for scientific degrees

Jurnal Azərbaycan Respublikası Ali Atestasiya Komissiyasının təsdiq etdiyi elmi dərəcə iddiaçılarının əsərlərinin çap edildiyi dövri elmi nəşrlərin siyahısına daxil edilmişdir.

Журнал входит в перечень, утвержденных ВАК Азербайджанской Республики, изданий для публикации трудов соискателей ученых степеней

Journal was founded according the order No1861 Ministry of Education of Azerbaijan Republic on the date 25.11.2011. Registration No 3521. Journal is published at least twice a year.

Jurnal Azərbaycan Respublikası Təhsil Nazirliyinin 25.11.2011-ci il tarixli 1861 saylı əmri əsasında təsis edilmişdir. Qeydiyyat No 3521. İldə ən azı iki nömrə nəşr edilir.

Учреждено приказом за №1861 от 25.11.2011 года Министерства образования Азербайджанской Республики. Регистрация № 3521. Ежегодно публикуется два номера.

It has been published since 2001. Published in 2001 - 2011 with a name "*Mechanics-machine building*"
2001-ci ildən nəşr edilir. 2001 – 2011-ci illərdə "Mexanika-maşınqayırma" adı ilə çap edilmişdir.
Издается с 2001 года. В 2001 – 2011 годах издано под названием "Механика-машиностроение"

The "MACHINE SCIENCE" journal is supported by Azerbaijan Technical University, which means there are no publication fees for authors.
"MAŞINŞÜNASLIQ" jurnalı Azərbaycan Texniki universiteti tərəfindən dəstəklənir və məqalələrin nəşri üçün müəlliflərdən hər hansı ödəniş tələb olunmur.
Журнал «МАШИНОВЕДЕНИЕ» поддерживается Азербайджанским Техническим Университетом, что означает, что с авторов не взимается плата за публикацию статей.

Editorial address*:** ***Redaksiyanın ünvanı: ***Адрес редакции:***	Baku, AZ1073, H.Javid ave., 25. AzTU Tel: (+994 12) 539 12 25 E-mail: msj@aztu.edu.az	© Machine Science, 2024 **ISSN:** 2227-6912 **E-ISSN:** 2790-0479

EDITORIAL COMMITTEE

MACHINE SCIENCE

ISSN: 2227-6912
E-ISSN: 2790-0479

2024, № 2. Pages 4 – 12

OPTIMIZATION OF THE NUMBER OF MACHINING STAGES WORKPIECES FOR MECHANICAL ENGINEERING PARTS

Viktor GUZEEV[1a], Nizami YUSUBOV[2b], Heyran ABBASOVA[2c*], Ramil DADASHOV[2d]

[1]*South Ural State University, Chelyabinsk, Russia*
[2]*Department of Machine Building Technology, Azerbaijan Technical University, Baku, Azerbaijan*

E-mail: [a]guzeevvi@susu.ru, [b]nizami.yusubov@aztu.edu.az, [c*]abbasova.heyran@aztu.edu.az, [d]dadashov@aztu.edu.az

https://doi.org/10.61413/VZRV4922

Abstract: The productivity of machining in the production of machine parts is determined by the time spent on shaping surfaces according to the drawing and the number of machining stages required to achieve the specified accuracy of the part from workpieces of varying accuracy. Due to the well-known property of the technological system related to the technological inheritance of errors from the workpiece to the part, the refinement of the workpiece dimensions is carried out in several stages. The required number of machining (refining) stages for the workpiece depends both on the characteristics of the technological system itself and on the degree of variation in the workpiece's input parameters and its machining conditions. In addition, since the process of reducing the workpiece error depends on the dispersion of its dimensions, the required number of machining stages to achieve the specified accuracy is primarily determined by the change in the dimension of the dynamic setup at each stage. At the same time, the dimension itself is typically adjusted by changing the static setup. The dimension of the dynamic setup arises due to the elastic displacements of the elements of the technological system under the influence of cutting forces. The greater the difference between the dynamic setup dimension and the setup dimension (static setup dimension), the larger the error in the resulting dimension. Errors caused by fluctuations in the dynamic setup dimensions are difficult to compensate for, as they depend on many parameters: the strength properties of the material being machined, cutting conditions, cutting tool parameters and its wear, the rigidity of the technological system, and others. The article presents an approach to finding combinations of technological process parameters that ensure the shortest production time for parts and the specified accuracy. For parametric optimization, the identified patterns of the influence of the main technological process parameters on the refinement coefficient of the workpiece dimensions at each machining stage are discussed.

Keywords: *machining stages, cutting conditions, turning, properties of the material being machined*

Introduction.

Considering the technological inheritance of workpiece errors, it is customary to process the workpiece in several stages (phases) [1]. At each stage, the dimension of the workpiece is refined by a certain amount – the refinement coefficient. For example, in turning operations, four stages are typically used: roughing, semi-finishing, finishing, and polishing [2]. The required number of machining stages depends on the dimensional accuracy of the workpiece and part, the rigidity of the technological system, the cutting conditions, and other factors. Each machining stage may be performed in one or several passes. The number of machining stages collectively determines the total time for completing the technological transition and the technological operation as a whole. This requires finding the optimal number of machining stages when designing the technological process [3–14].

To solve this problem, it is necessary to analyze the influence of individual technological process parameters on the refinement coefficient of the workpiece at each stage.

The refinement coefficient of the workpiece at each machining stage largely depends on the load-bearing capacity of the technological system. It determines the magnitude of the error in the dynamic setup dimension. The greater the cutting force and the lower the rigidity of the technological system, the smaller the refinement coefficient of the dimensions at that machining stage. In turn, the components of the cutting force are largely determined by the cutting conditions, and many researchers suggest finding the optimal values for feed rate and cutting speed [15–17, 18, 19–26]. At the same time, decisions regarding the number of stages and the refinement coefficient of dimensions at each stage are made by the machining engineer, guided by their experience.

The task of determining the optimal values of the refinement coefficients at each machining stage is reduced to finding the conditions that ensure the shortest total machining time while achieving the specified dimensional accuracy. To optimize the magnitude of the refinement coefficient and determine the required number of machining stages, it is necessary to identify the degree of influence of the main parameters of the technological system on them.

The influence of the feed rate on the refinement coefficient in turning operations. Technological limitations that must be considered during turning operations include restrictions on the power of the machine's main drive, the strength of the feed drive mechanism, the maximum torque, and the strength of the tool holder and cutting insert. Technological limitations also include restrictions on the required accuracy and surface roughness of the machined surface. Additionally, there are limitations related to the design features of the machines, such as the ranges of feed values and spindle speed.

The search for the optimal option can be illustrated by an example of machining a cylindrical surface with a diameter of Ø60h10, length L = 40 mm, and a required surface roughness of Ra = 2.5 μm for a "Bushing" part made of steel 45 (σ_i = 1380 MPa) on a 16K20T1 machine using a cutting tool with a T15K6 insert, 2101-0637, according to GOST 18883-73.

The required 10th grade from a 16th grade workpiece with a surface diameter of 60 mm can be achieved in 4 machining stages, with a refinement coefficient of 1 grade at each stage. The refinement route for this case can be represented as a sequence of grades: 16 → 14 → 13 → 12 → 10. The task of selecting the optimal number of machining stages and corresponding cutting conditions is reduced to a discrete problem of determining the shortest time path for refinement between the specified accuracy of the part and the workpiece.

The time required for each machining stage depends on the feed rate and the length of the working stroke. For feed rate values chosen in consideration of all restrictions, the main time for the corresponding stages is provided in Table 1.

Table 1. Main time spent on machining stages

No	Machining stages, grade	Main time, min
1	16→14	0,073
2	16→ 13	0,2
3	16→ 12	0,44
4	16→ 10	1,3
5	14 →13	0,093
6	14 →12	0,11
7	14 →10	0,8
8	13 →12	0,105
9	13 →10	0,5
10	12 →10	0,27

From Table 2, it can be seen that it is not always advantageous to work with the maximum permissible feed rate, as in this case, the accuracy requirements for the workpiece at each machining stage increase, leading to a higher number of stages. For example, if all machining stages are performed with the maximum feed rate allowed by the limitations, four machining stages will be required (refinement route 16→14→13→12→10), and the cycle time for automatic operation (Tca) increases to 0.708 minutes (see Table 2). However, choosing the minimum possible feed rate values, although it reduces the number of refinement stages, increases the time of each technological transition. For example, the refinement sequence 16→14→10 results in a cycle time (T_{ca}) of 0.953 minutes, although the number of stages is only two. In this example, the shortest cycle time (T_{ca} = 0.573 minutes) is achieved with the refinement option over three stages – 16→14→12→10.

Table 2. Options for forming machining stages

No	Refinement route, grade	Cycle time, min
1	16→ 14→ 13→ 12→10	0,708
2	16 →13 →12 →10	0,695
3	16 →14 →12 →10	0,573
4	16 →12 →10	0,79
5	16 →14 →13 →10	0,786
6	16 →13 →10	0,78
7	16 →14 →10	0,953
8	16→ 10	1,3

Options with the intermediate 11th grade precision were excluded because the stage 11→10 requires a feed rate of 0.19 mm/rev, which exceeds the permissible limit for surface roughness.

Thus, determining the optimal number of machining stages should be accompanied by the optimization of cutting conditions (feed rate and cutting speed).

The influence of tool wear on the refinement coefficient of the workpiece. Tool wear leads to an increase in cutting force, which in turn changes (increases) the dynamic setup dimension of the specified part dimension. This change in the dynamic setup dimension causes an additional dispersion field of the performed dimension and deteriorates the machining accuracy.

To determine the extent of the influence of tool wear on the flank surface on the number of required machining stages, let us refer to the previous example of machining the part "Bushing," which has a surface Ø60h10. We will calculate the automatic machine cycle time according to the program (T_{ca}) for different refinement sequence options, assuming a wear value ($l_з$) of 0.8 mm, which is the criterion for the standard tool life.

The schemes of machining options with the indication of the time required for each stage are provided in Tables 1 and 2. Calculations using the direct enumeration method show that, in this case, the optimal option is machining in four refinement stages (refinement route: 16→14→13→12→10). This option results in a cycle time of **T_{ca} = 0.708 minutes**.

If the calculations assume a minimum wear value of 0.05 mm, the time will increase by **24%**.

The influence of the principal cutting edge angle on the optimal number of machining stages. The cutting (cutting edge) angles determine the directions of the components of the cutting force. Consequently, changes in these angles alter the load on the feed drive mechanism and the carriage-part assembly. This can lead to additional elastic deformations in the machine elements and influence the refinement coefficient of the workpiece at different machining stages.

Figure 1 shows graphs of the changes in main time required to perform a single machining stage of a hypothetical surface, depending on the angle φ. The graphs indicate that changing the cutting angle from 30° to 90° increases the main time by a factor of 1.3 to 1.6. This confirms the practical recommendations of using tools with small principal cutting edge angles for rough machining. Figure 2 illustrates the dependence of the required number of machining stages on changes in the cutting angle. The graph confirms the appropriateness of using tools with cutting angles of 30°–45° for rough stages and angles close to 90° for finishing stages.

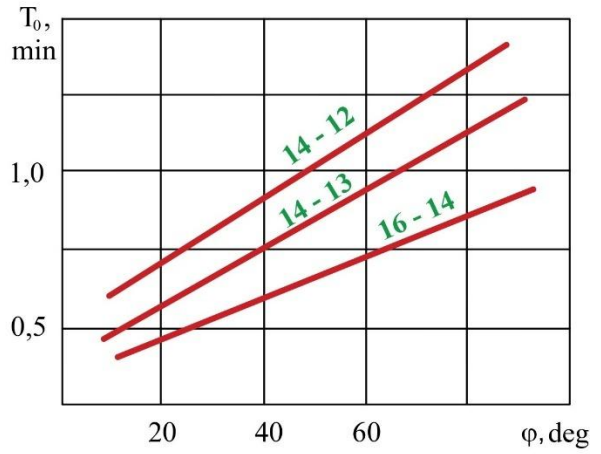

Fig. 1. Dependence of the main time of execution of the rough stage of machining on the cutting angle of the tool

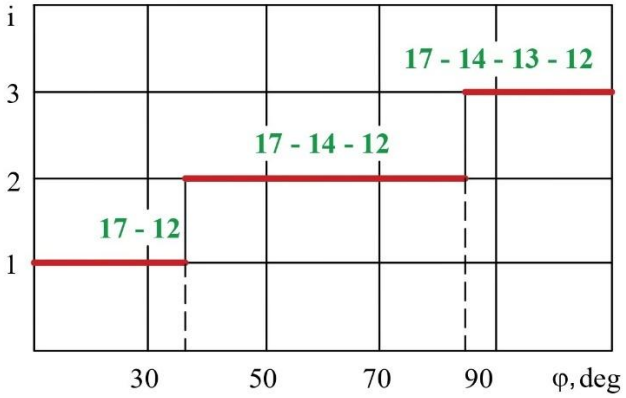

Fig. 2. Influence of the principal cutting angle on the refinement route of the workpiece under the condition L/D ≤ 1

As the rigidity of the technological system decreases, the nature of the influence of the cutting angle on the target function changes. This is because, with low rigidity of the technological system, the active limitation on the feed rate is determined by the accuracy of the dynamic setup dimensions. Figure 3 shows the dependence of the main time on the cutting angle during the machining of a part with an **L/D ratio of 10**, while Figure 4 presents the corresponding dependence of the number of machining stages on this angle. From these graphs, it can be observed that in the case of a low-rigidity technological system, using a tool with a cutting angle close to 90° results in shorter machining times, and the required accuracy is achieved in fewer refinement stages. These findings confirm the existing experience in machining parts, providing indirect validation of the proposed method for determining the necessary number of machining stages.

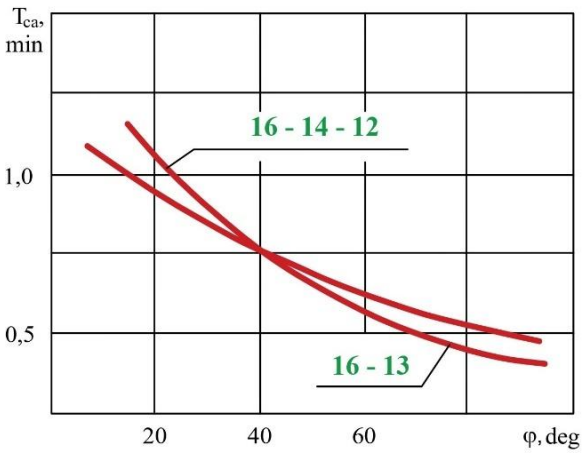

Fig. 3. Effect of cutting edge angle on machining cycle time at L/D = 10

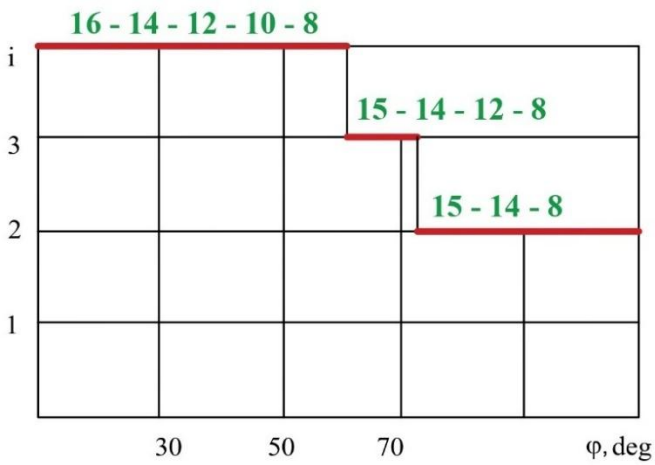

Fig. 4. Influence of the cutting edge angle on the refinement route of the workpiece under the condition L/D = 10

The influence of the strength properties of the workpiece material on the refinement coefficient at all machining stages. The intensity of stresses in the cutting zone, σ_i, most accurately characterizes the material's ability to resist the cutting process. This value is part of the formula for determining the cutting force and, consequently, directly influences the dimensional accuracy errors of the dynamic setup.

Figure 5 presents graphs showing the dependence of the main time required to complete a single machining stage on the stress intensity in the cutting zone (σ_i), obtained through calculations. The

graphs indicate that the influence of σ_i on machining efficiency varies across different refinement stages.

This is due to the fact that when determining the feed rate at different stages, different constraints may be active. For instance, at the finishing stages, the feed rate is limited by surface roughness requirements. In such cases, higher values of σi allow for the selection of larger feed rates, which consequently reduces the main transition time. This occurs because, at higher σi values, surface roughness decreases (at cutting speeds exceeding 100 m/min).

Figure 6 illustrates the influence of stress intensity on the refinement route of the workpiece.

Calculations show that as the rigidity of the technological system (j) increases, the refinement coefficient for all machining stages rises, while the number of stages decreases.

Since the values of σ_i and the rigidity of the technological system are most often uncontrollable parameters, these dependencies can be used to determine the boundary values of σi and j for specific conditions.

Industrial Verification of the Methodology for Determining the Optimal Number of Machining Stages. The methodology was tested at sixteen enterprises. The verification involved assigning the calculated number of machining stages and their corresponding cutting conditions in the control program, followed by machining a batch of parts with these parameters according to the program. After each machining stage, the resulting dimension was measured. Based on the measurement results, distribution curves of the dimensions were constructed, and conclusions were drawn about the accuracy of the machining stage performed. The randomness of the sample parts was verified using the Pearson criterion.

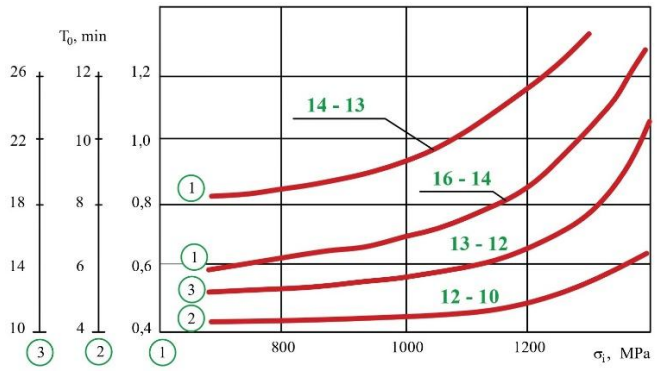

Figure 5. Influence of the properties of the machined material on the main time

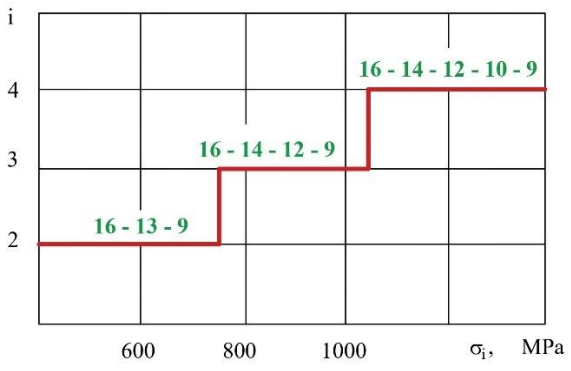

Figure 6. The refinement route of the workpiece depending on the properties of the machined material

Let us examine the data from the methodology testing on specific parts. Table 3 provides the machining parameters for the part "Bushing". Workpiece material: Steel 20. Machine tool: ATPr-2M12SN (АТПр-2М12СН). Cutting tool: T15K6 2102-0307 in accordance with GOST 6743-61 (Т15К6 2102-0307 ГОСТ 6743-61).

From Table 3, it is evident that the machining option with the optimal refinement route for the workpiece reduces the labor intensity of the technological transition by 24%.

To verify compliance with the specified grade at each intermediate machining stage, statistical control of the intermediate dimensions $Ø55_{-0,74}$ and $Ø52,4_{-0,3}$ was performed.

Figures 7 and 8 show the graphs of the empirical and theoretical distribution curves of the part dimensions after the roughing and semi-finishing stages, respectively.

Table 3. Machining parameters of the "Bushing" part

Parameters	Refinement route, grades	Feed rate, mm/rev	Main time, minutes	Time for the complex, min.
Old parameters of machining	16 ↓ 13 ↓ 11 ↓ 8	0,246 0,18 0,143	0,24 0,33 0,21	0,78
New parameters of machining	16 ↓ 14 ↓ 12 ↓ 8	0,45 0,34 0,10	0,13 0,174 0,29	0,59
Labor intensity of the new option as a percentage of the current option.	76,3%			

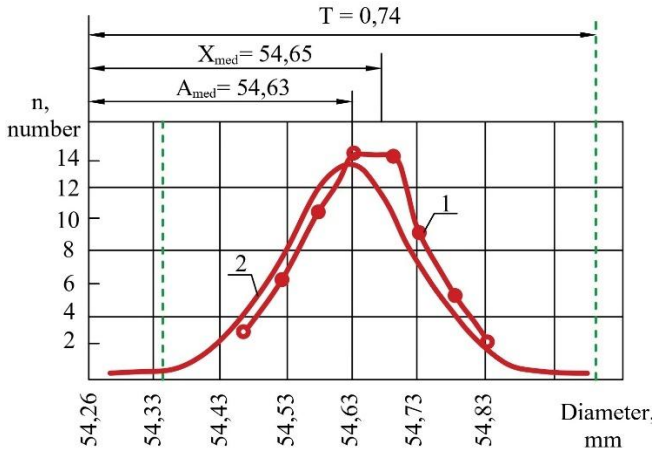

Fig. 7. Graphs of the density of the dimension distribution after the roughing stage of machining dimension Ø55$_{-0,74}$: 1-empirical curve; 2-theoretical curve

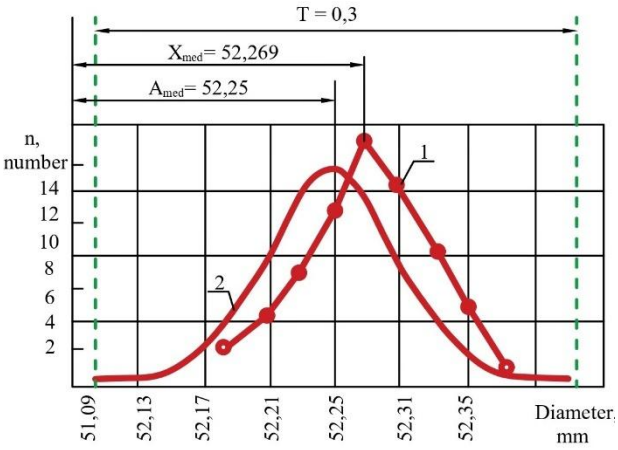

Fig. 8. Graphs of the density of the dimension distribution after the semi-finishing stage of dimension Ø52,4$_{-0,3}$: 1-empirical curve; 2-theoretical curve

An analysis of these statistical data shows that for the roughing stage, the standard deviation of dimensions (σ) is 0.103, and the operation accuracy coefficient (μ_o) is calculated as: $\mu_o = 6\sigma / T = 0.835$, indicating sufficient process accuracy. The adjustment accuracy coefficient (l) is 0.027, while the allowable value of this coefficient under these conditions (l_a) is 0.0825.

For the semi-finishing stage (achieving the dimension Ø52.4-0.3), statistical control of dimensions revealed the following accuracy data: the standard deviation of dimensions is 0.0374, the operation accuracy coefficient is 0.748, the adjustment accuracy coefficient is 0.019, with its allowable value being 0.0378. These data confirm conditions for defect-free work: $\mu_o \leq 1, l \leq l_a$.

The achievement of the final part dimension Ø51.964-0.054 after the finishing stage was studied by the enterprise during a control operation, and the results showed positive outcomes.

Thus, it can be concluded that the new refinement route for the workpiece and the corresponding cutting conditions ensure the required machining accuracy and improve its productivity.

Table 4 provides the machining parameters for the part "Support" made of brass LS-59 (JIC-59) on a 16K20T1 machine tool. The transitions considered include external turning of diameter

Ø23,93-0,14 from a stamped workpiece of Ø27(-0,5)^(+0,8), as well as boring transitions from diameter Ø17_(-0,8)^(+0,5) to Ø20+0,21 and from diameter Ø15_(-0,8)^(+0,5) to Ø18-0,18.

Table 4. Parameters for machining the "Support" part

External turning $Ø23,93_{-0,14}$				
Parameters	Refinement route, grades	Feed rate, mm/rev	Main time, minutes	Time for the complex, min.
Old parameters of machining	16 ↓ 13 ↓ 11	0,15 0,10	0.118 0,18	0,298
New parameters of machining	16 ↓ 11	0,16	0,11	0,11
Labor intensity of the new option as a percentage of the current option.	37%			
Boring $Ø18_{-0,18}$				
Old parameters of machining	16 ↓ 12	0,10	0,10	0,10
New parameters of machining	16 ↓ 12	0,12	0,083	0,083
Labor intensity of the new option as a percentage of the current option.	83%			

The results of the statistical control of dimensions are presented in Figures 9 and 10 as a comparison of empirical and theoretical distribution curves.

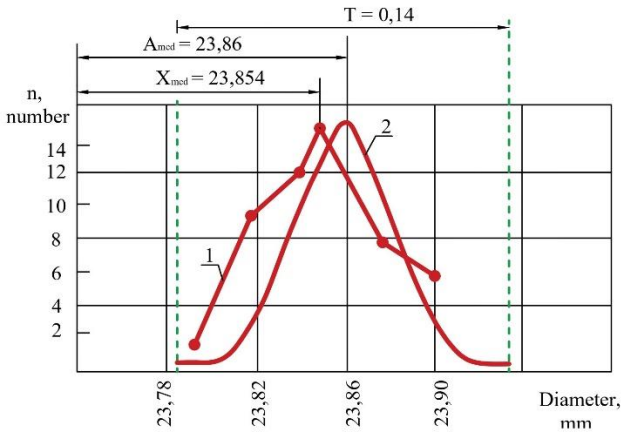

Fig. 9. Graphs of the density of the dimension distribution after the semi-finishing stage $Ø23,93_{0,14}$: 1-empirical curve; 2-theoretical curve

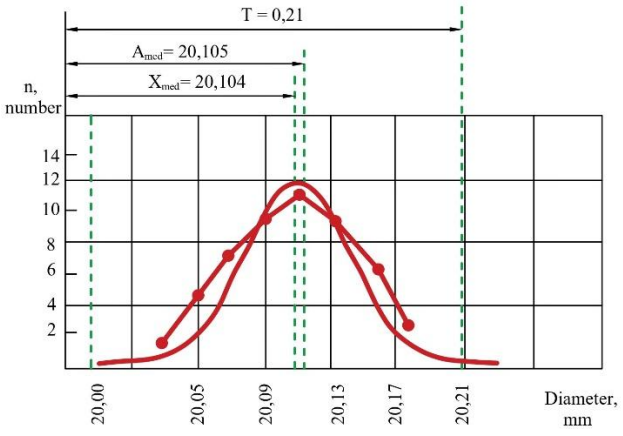

Fig. 10. Graphs of the density of the dimension distribution after the semi-finishing stage $Ø20^{+0,21}$ 1-empirical curve; 2-theoretical curve

For the external turning transition to $Ø23.93_{-0.14}$, the standard deviation was 0.0254, the technological transition accuracy coefficient was 1.0, and the adjustment accuracy coefficient was 0.043, with an allowable value of 0.045. An analysis of this transition shows that the feed rate in the new technological process variant can be reduced (since the labor intensity of the transition in the new variant is 37% of that in the old variant), providing an opportunity to increase the reliability margin for dimensional accuracy in this transition.

For the boring transition to $Ø20^{+0.21}$, the standard deviation is 0.039, the process accuracy

coefficient μ_o is 0.97, and the adjustment accuracy coefficient l is 0.005, with an allowable value l_a of 0.015. Similar results were obtained for thirty other parts from nine different enterprises.

Conclusion. The application of the optimal design methodology allows for a 15-18% increase in the productivity of operations performed in mass production and a 60-70% increase in small-batch and single-item production.

Thus, optimizing the number of machining stages, taking into account rational cutting conditions, enhances machining productivity and reduces the cost of the operation.

Funding Acknowledgements.

This work was supported by the Azerbaijan Science Foundation – **Grant № AEF-MGC-2024-2(50)-16/01/1-M-01**

REFERENCES

[1]. Metelev B. A., Kozlova E. A. *Identification of stages of processing of shaft-type parts in the conditions of a specific enterprise.* Collection of articles. *Nijni Novgorod - Arzamas: NSTU*, 2003, pp. 43-47.

[2]. *General engineering standards for cutting time and conditions for standardizing work performed on universal and multi-purpose machines with numerical control*. Part 2. Cutting mode standards. Moscow, Economica 1990, 472p.

[3]. Method of synthesis in CAD of technological processes. Electronic resource. URL: http://gendocs.ru/v38630/?download=18

[4]. Nguyen V. K. *General methodology for optimizing cutting conditions*. Bulletin of Tula State University. Technical sciences. 2011, iss. 6, vol. 2, pp. 253-263.

[5]. Agapiou J.S. *The optimization of machining operations actions based on a combined criterion*. Part 2: Multipass operations. J. Eng. Ind. Trans. ASME, 1992, no. 114, pp. 508-513.

[6]. Shin Y.C., Joo Y.S. *Optimization of machining conditions with practical constraints*. Intern. J. of Proeducation Research, 1992, vol. 30, no. 12, pp. 2907-2919.

[7]. Adamenko V.M. *Theoretical prerequisites for optimizing the cutting process based on energy-consuming parameters of process equipment*. Mechanical engineering: collection of scientific papers; Minsk: TekhnoPrint, 2001, iss. 17, 398 p.

[8]. Yusubov N.D. Practical applicability matrix model precision processing. Mashinostroitel, 2009, vol.2, pp, 37-40.

[9]. Mrochek Zh.A., Adamenko V.M., Adamenko D.V. *Optimization of surface shaping parameters by cutting based on energy-consuming parameters of process equipment*. Bulletin of the Brest State Technological University, 2007, pp. 54-57.

[10]. Yusubov N.D., Abbasova H.M., Dadashov R.Y. *Theoretical basis for the development of an algorithmic unified complex of mathematical models of cutting forces*. Machine science, 2023, No1, pp.55-60.

[11]. Yusubov N.D., Abbasova H.M., I.Khankishiyev. Development of a planning theory for multi-tool machining with the possibilities of modern CNC machine tools. Forschung im Ingenieurwesen, 2021, vol.85, iss.2, pp. 661-678.

[12]. Sidorchik E.V. *Optimization of the cutting process in automated programming systems for machining on CNC machines*. International Research Journal, 2013, no. 8 (15). URL: https://research-journal.org/archive/8-15-2013-august/optimizaciya-processa-rezaniya-v-sistemax-avtomatizirovannogo-programmirovaniya-dlya-obrabotki-na-stankax-s-chpu

[13]. Davim J. Paulo. *Machining: fundamentals and recent advances*. Springer, 2008, 361 p.

[14]. Nosirov I.S., Belov A.M. *Optimization of cutting process parameters of a CNC lathe using a genetic algorithm*. Bulletin of ETU "LETI" No. 2/2020, pp. 73 – 77.

[15]. Bogatenkov S.A., Sazonova N.S., Guzeev V.I., Yusubov N.D., Abbasova G.M. *Increasing the productivity of multitool machining on automated lathes by optimizing the tool positions*. Russian Engineering Research, 2021, vol.41, iss. 11, pp.1075-1079.

[16]. Cus F., Baltic J. *Optimization of cutting process by GA approach*. Robotics and Computer-Integrated Manufacturing, 2003, no. 19, pp. 113-121.

[17]. Al-Ahmar R., Al-Osaili A. A. *GA-based parameter design for single machine turning process with high volume production.* Computers & Industrial Engineering, 2007, no. 50, pp. 317-337.

[18]. Domnyshev A.A. *Automation of calculation of the cutting mode of external longitudinal turning and drilling by the linear programming method*. Polytechnic Youth Journal, 2019, no. 10, pp. 1–12. http://dx.doi.org/10.18698/2541-8009-2019-10-539

[19]. Gruby S.V. *Optimization of the mechanical processing process and control of process parameters*. Moscow: Publishing House of Moscow State Technical University named after N.E. Bauman, 2014. 149 p.

[20]. Ivaschenko A.P. *Methodology for selecting more efficient cutting modes in metal turning*. Modern problems of science and education, 2014. no. 6. URL: https://science-education.ru/ru/article/view?id=15420

[21]. Shal'skaya E.E., Ivchenko T.G. *Optimization of cutting modes in finish and fine turning by the geometric programming method*. Progressive technologies and systems of mechanical engineering, 2010. iss. 39, pp. 91-95.

[22]. Yusubov N.D. *Matrix models of the accuracy in multitool two-support setup*. Russian Engineering Research, 2009, vol. 29, pp. 268-271. DOI: 10.3103/S1068798X09030125.

[23]. Novik F.S., Arsov Ya.B. *Optimization of metal technology processes by methods of experiment planning*. Moscow: Mechanical Engineering; Sofia: Tekhnika, 1980, 304 p.

[24]. Klocke F. *Manufacturing Processes. Cutting*. Springer, 2011, 500 p.

[25]. Urmanov M.D., Khusainov R.M., Khisamutdinov R.M. *Search for the optimal range of cutting modes based on modeling of cutting tool wear.* Modeling, optimization and information technology, 2021, vol. 9(3). URL: https://moitvivt.ru/ru/journal/pdf?id=965. DOI: 10.26102/2310-6018/2021.34.3.030

[26]. Khusainov R.M., Khisamutdinov R.M., Urmanov M.D. *Methodology for selecting cutting modes based on monitoring the average chip thickness*. Modeling, optimization and information technology, 2023, vol. 11(3), pp. 1 – 10.

Received: 12.09.2024
Accepted: 13.12.2024

MACHINE SCIENCE

ISSN: 2227-6912
E-ISSN: 2790-0479

2024, № 2 Pages 13-28

DESIGN OF REVERSIBLE THYRISTOR FEED DRIVE WITH PROPORTIONAL-INTEGRAL CONTROLLERS

Natalia MOKROVA[1,a], Viktor ARTEMYEV[2,b], Anar HAJIYEV[3,c*]

[1]National University of Science and Technology «MISIS», Moscow, Russia
[2]Plekhanov Russian University of Economics, Moscow, Russia
[3]Department of Machine design and industrial technologies, Azerbaijan Technical University, Baku, Azerbaijan

E-mail: [a]nvmokrova@misis.ru, [b]artemev.VS@rea.ru, [c*]anar_hajiyev_1991@mail.ru

https://doi.org/10.61413/IYNU7656

Abstract: This paper presents a detailed analysis of a reversible thyristor feed drive for industrial metalworking systems, oriented for application in machine tools with position or contour numerical control, as well as in copying and milling machines. The drive under consideration is based on a three-phase zero-reversing scheme, providing a wide dynamic speed control range of the executive motor speed not less than 10000 revolutions, which allows effectively adapting to changes in technological parameters and various production modes. The application of proportional-integral speed and current regulators in the control loop contributes to the accuracy, stability and speed of the system under various mechanical loads and transient modes. The paper offers a comprehensive consideration of structural features, principles of operation and performance characteristics of reversible thyristor feed drive with PI controllers. The obtained results allow to optimize the drive operation in conditions of high precision machining, to expand the functional capabilities of the machine tool equipment, to reduce the influence of external disturbances and to increase the reliability of the industrial system as a whole. The basis of the hardware configuration of the drive consists of thyristor block (BT), control unit (CU), stabilized power supply of control circuits, as well as synchronization transformer, interacting by means of functional blocks: regulator block (RB), phase shifting device (PSD), logic block (BL), stabilized power supply block (SPB) and correction block (BC). The described functional structure simplifies the procedure of initial setting of the drive, tightening the interaction of the system elements and reducing the risk of uneven operation modes. It is possible to use both conventional electric motors with normal inertia-torque ratio and motors with increased torque overload capacity or reduced inertia. An important feature of the proposed solution is a built-in system of protection of power keys against short circuits by using high-speed maximum protection automatics (MPA), which contributes to increased reliability of operation and reduces the risk of failure of expensive elements. Additional stability of thyristor switching process is achieved by using transistor electronic keys, whose operation is synchronized with the supply network due to a special transformer winding, providing fast and accurate transition between positive and negative half-periods.

Keywords: *dynamic programming, mathematical model, object control, system behavior.*

Introduction.

Modern high-precision machine-tool equipment, widely used in a dynamically developing industrial environment, places increased demands on feed and drive systems, which are assigned the functions of precise positioning, contour control and stable operation under the influence of variable loads. In the conditions of tough competition, growing production volumes and rates, as well as the need to optimize operating costs, the development and improvement of power and control systems of

feed drive for numerically controlled machine tools, including positioning and contouring machines, as well as copying and milling systems, is of particular relevance [1].

CNC machines minimize the human factor, ensure the continuity of the production process, increase the accuracy, quality and reproducibility of machining results. To achieve the most efficient operation of such systems is possible only with a harmonious combination of hardware and software components, where a special role is played by feed drives that provide flexible control of speed and position of tools [2]. The use of reversible thyristor feed drives (RTDs) with high dynamic characteristics, an extended speed range, reliable overload protection and the ability to integrate with various types of electric motors opens the way to significant improvements in productivity and the quality of machining complex profiles.

Traditionally, systems with proportional-integral (PI) controllers have been used to control feed drives. Due to their simplicity, stability and predictability, these controllers are widely used in industrial automation. Their use in the thyristor feed drive circuit provides a balance between the accuracy of maintaining the set speed and effective current control, which is especially important for preventing overloads, maintaining stability in transient modes and ensuring long-term trouble-free operation of the equipment [3-6]. Achieving a combination of these goals - stability, accuracy, reliability and a wide control range - is possible through an integrated approach to the design, analysis and experimental debugging of a reversible thyristor drive with PI controllers.

One of the key factors affecting the quality of control is the correct selection and adjustment of the functional units of the actuator. The system under study involves the use of many functional units: regulator unit (RU), phase shifter unit (PSU), logic unit (BL), stabilized power supply unit (SPU) and correction unit (CU). Each of these assemblies contributes to the combined result of optimizing the dynamic and static performance of the actuator. In addition, structurally implemented as a panel with integrated power (thyristor block - BT), control (control unit - CU), as well as additional power supply and synchronization elements, the feed drive can be easily adapted to different operating conditions. The presence of control points in functional blocks simplifies the procedure of initial adjustment, diagnostics and further modernization of the system, providing convenient service and reduced labor intensity of commissioning works.

Another important aspect is to ensure an adequate level of reliability and safety. Under conditions of intensive operation in industrial plants, situations in which there is a risk of short circuits or overloading of power electronics elements inevitably arise. In such cases, the availability of fast-acting maximum protection using high-speed circuit breakers (CBs) becomes critical to prevent the failure of expensive components. The introduction of transistor-controlled electronic keys synchronized to the supply network allows accurate control signals to be generated to the thyristors and increases the overall level of accuracy and consistency of the drive.

Thus, the objective of this study is to present a comprehensive analysis of the design, principles of operation, tuning methodology and performance characteristics of the reversible thyristor feed drive with proportional-integral controllers. The system under consideration is able to provide flexible and reliable speed and torque control, improve the economic performance of production, reduce maintenance costs and increase the stability of the technological process [7]. In the course of the study experimental and theoretical results will be summarized, which allowed to optimize circuit solutions, simplify the procedure of drive integration into existing production lines, as well as to determine the areas of further development and improvement of this class of drive devices.

Formulation of the problem.

Modern reversible thyristor feed drives for controlled metalworking systems require an impact, accurate and safe algorithm of control pulse generation. This task is complicated by the fact that in the course of the drive operation it is necessary to provide correct on switching circuit of several logic blocks, phase shifting device (PSD), logic block (BL), regulator block (RB), as well as transistors, capacitors, diodes and pulse transformers, sequences. for generation and transmission of control signals to thyristors. The problem boils down to the strict fulfillment of a set of conditions allowed by the authorities that at any moment of time only pulses are generated that correspond to the active group of thyristors even or odd, ensuring their simultaneous switching on, as well as providing a smooth transition while ensuring the polarity mismatch. In a controlled reversible thyristor drive, there are a number of input signals, hence nodes and conditions on which the actuation and delivery of pulses that open the corresponding thyristors depend. The task is reduced to the following: in the presence of synchronizing signal from synchronizing signal and transformer, control signal (from regulator unit) and at alternation of polarity of supply voltage, to lead sawtooth voltage correctly, to compare it with control signal, to form control pulses of thyristors and to provide impossibility of continuous voltage. switching on of thyristors from even and odd groups [9]. It is necessary to ensure the correct time order of switching on the keys and prevent simultaneous switching on of thyristors from the even and odd group, which will lead to reliable switching and safe direction of inverting.

When the polarity of the mismatch is transmitted (signal at the input of the FSU), the Schmidt trigger returns to the initial state. At this point, the supply of operating pulses of one group is stopped, but the generation of standby pulses for safe inverting continues for a preset time. Logic and external elements protect the absence of overlapping operation modes of thyristor groups and minimize the risk of simultaneous switching on of all keys. To protect the control circuit of thyristors from noise, diode D7 and capacitor C4 are used to stabilize the shape and level of control pulses. The output signal of the FSU has an amplitude of about 6 V at a load current of 0.5 A, beyond the safe opening of thyristors. The functional diagram of the drive is shown in Fig. 1

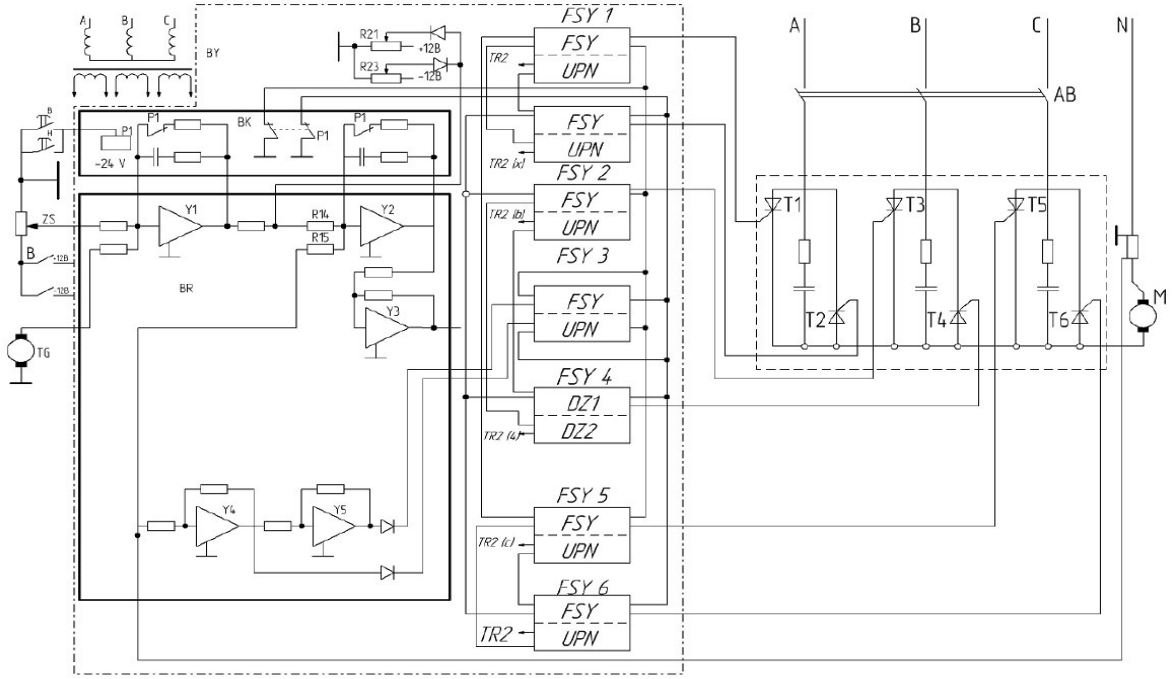

Figure 1. Functional diagram of the actuator

We introduce the following notations and variables:

Synchronization period where T is the period of the line voltage from which half-periods of duration are reached $\frac{T}{2}$.

The voltage is formed on the collector of transistor $T2$ (through the charge and discharge of capacitor $C1$ with a slope regulated by potentiometer $P4$.

Its changes vary according to the law

$$Y = f(\frac{1}{P4C1}T)$$

f - function specifying the line changing in time of increase

The control signal Y - control coming to the input of the phase shifting device (PSD) from the regulator unit (RU). The control signal coming to the input of the DCS (pin 2) is a command that determines the logic of operation of the PI controllers of pulse frequency and current. The input of this control signal makes it possible to adjust the moment of the Schmidt trigger, thereby changing the phase and time of the control pulses to the thyristors. When the difference between the sawtooth and control signals reaches the trigger threshold, the Schmidt trigger (on transistors T4, T5) switches from one state to another, generating a rectangular pulse at its output. This rectangular signal is subsequently differentiated using the circuit. C3, P17, generating the sharp negative pulses required to trigger transistors T6, T7. In this way, an accurate timestamp is applied to output the control pulse thyristor.

The power part of the reversible thyristor drive used in numerical or contour program-controlled machine tools is realized by a three-phase zero-phase scheme, which provides the possibility of smooth, symmetrical and reliable reversal of the electric motor rotation. This configuration not only simplifies the transition from one direction of rotation to another, but also contributes to increased stability of operation during load changes. To protect the thyristor keys from emergency conditions such as short circuits in the load or mains faults, a high-speed maximum protection with circuit breaker (CB) is introduced to prevent overheating and failure of expensive semiconductor components. Formation of control signals for thyristors is based on the operation of an electronic key reacting to the voltage coming from the synchronizing winding of the transformer. In the initial phase of each half-period of negative polarity transistor $T1$ is open, as a result of which capacitor $C1$ is rapidly discharged through open transistor $T1$ and diode $D1$. This process causes a sharp increase in the positive potential on the collector of transistor $T2$, thus forming the initial section of the sawtooth characteristic, which will later be used for comparison with the control signal. In the opposite half-period, when the voltage acquires positive polarity, transistor $T1$ closes, preventing further discharge of $C1$. The capacitor now begins to charge through transistor $T2$, resulting in a gradual decrease in the positive potential at its collector. As this potential decreases, the voltage at the base of transistor T3 also decreases, which begins to close smoothly. As a result, a dynamic sawtooth voltage dependence is created in the reference point 02 U_{02}, repeating the trend of voltage change on the collector of $T2$. An important aspect of setting up the sawtooth voltage generation unit (VGU) is the possibility of regulating the charge current of capacitor $C1$. For this purpose, a potentiometer $R4$ is included in the base circuit of transistor $T2$, which allows changing the sawtooth slope. Thus, by changing the resistance of $R4$ it is possible to fine-tune the dynamics of sawtooth signal formation,

providing the optimal matching of the time characteristics of the system with the requirements of the technological process.

In addition to the basic function of sawtooth signal generation, the UUT performs the role of a source of duty pulses generated by differentiation of rectangular signals coming from the output of transistor $T1$. These duty pulses are fed to contact 11 of the phase shifting device (PSD), operating in counter-phase with this PSD. This signal arrangement optimizes the operation of several DCSs interacting in the same drive system, which is particularly important for reversing or complex operating modes. The phase-shifting device (PSD) has a Schmidt trigger realized on transistors $T4$ and $T5$, a differentiating circuit ($C3$, $R17$), and a power amplifier on transistors $T6$, $T7$. In the absence of an input control voltage, transistor $T4$ is closed and $T5$ is open, creating the initial steady state of the trigger. Since $T6$ and $T7$ are also closed, the output stage of the device is in the ready state without generating control pulses. The resulting sleep mode ensures that parasitic triggering is minimized and protects the thyristors from unnecessary excitation.

The input of transistor $T4$ receives the sawtooth voltage from transistor $T3$ and the control signal from the regulator block (RB), which is fed to pin 2 of the FSU. Here the key comparison takes place: when the difference between the sawtooth voltage and the control signal reaches the threshold value, the Schmidt trigger switches over. At this point, a sharp voltage change occurs on the collector of $T5$ (reference point 03), which corresponds to the formation of a rectangular pulse. The magnitude of the control signal determines the moment at which the trigger switches, thereby setting the phase shift and time reference of the pulses with respect to the line voltage. The rectangular pulses generated by the Schmidt trigger are differentiated using the circuit $C3$, $R17$. At its output appear short negative pulses, which serve as “triggers” to turn on transistor T6, provided there is no prohibition signal from the logic block on pin 6 of the FSU. In parallel, the duty pulses from pin 11, generated by the UUT, are also received here; transistor T6 can be opened either by the operating pulses or by the duty pulses, depending on the current system logic.

In the presence of an enable signal (pin 12 from the logic block), any incoming pulses can turn on transistor T6, which together with $T7$ forms a power amplifier. The load of the amplifier is the pulse matching transformer T_p1. When transistor $T7$ is triggered, a positive pulse of the specified shape and amplitude (about 6 V at 0.5 A load) is induced in the secondary winding of the transformer. This pulse is fed through diode $D6$ to the control electrode of the thyristor, and a clear and fast control signal is formed for the power key, which is necessary for stable and predictable control of the drive. Under conditions of polarity mismatch change of the control signal, the Schmidt trigger returns to the initial state ($T4$ closed, $T5$ open), which leads to the cessation of operating pulses. At this point, the system does not remain “blind”: the duty pulses continue to flow for a certain time delay set by the logic block to avoid sudden inversion in the absence of clear transients and, therefore, prevents emergencies. To reduce noise in the thyristor control circuit, diode D7 and capacitor C4 are used to stabilize the shape and level of the signal. The logic block ensures that under no circumstances the control impulses to the even and odd groups of thyristors can be supplied simultaneously. Consisting of two identical logic circuits LE1 and LE2, the logic block ensures that the thyristors of one group can be started only after the thyristors of the other group are completely extinguished. The input of LE1 receives negative pulses from the odd group of FSU, and the input of LE2 receives negative pulses from the even group. These signals form conditions for charging and discharging of capacitors associated with transistors $T2$ ($T12$), preventing the level required to trigger transistors $T3$ ($T13$) and $T4$ ($T14$).

As a result, transistors $T3$ ($T13$) and $T4$ ($T14$) remain closed, while T5 ($T15$) remains open and saturated. Closed transistors $T4$ and $T14$ provide an enable signal to the corresponding "AND" inputs pin 12 of FSU1, FSU3, FSU5 (for odd-numbered group) or FSU2, FSU4, FSU6 (for even-numbered group). Open transistors $T5$ ($T15$), included in parallel to the differentiating circuit $C3$, $R17$ at the input of transistors T6 of the corresponding groups, provide the formation of the prohibition signal, which guarantees a clear separation of logic and excludes the simultaneous appearance of pulses that can cause simultaneous opening of thyristors of even and odd groups. At the moment the odd group of the FSU is operating, and pulses from transistors $T6$ of this group arrive at the input LE1. Closed transistor $T4$ of LE1 gives an enable signal to the odd group U_{09}, If there is a need to switch to the even group, the logic will block the odd group, wait for the complete cessation of its working pulses, and then let the pulses to the even group. This step-by-step switching logic, which relies on negative and standby pulses, ensures safe and reliable reversal of the motor rotation direction, minimizing the risk of equipment damage [10].

The described functionality ensures a high level of reliability and accuracy of the thyristor reversing drive control system. The combination of elements - from the boosters and phase shifters to logic blocks and power amplifiers - forms a coherent mechanism that reacts to changes in input signals and external conditions. This realization allows to accurately dose the moment of thyristors switching on, to prevent the appearance of "conflict" modes of operation and to form stable transients at direction inversion. All this determines high performance, adaptability and safety of the drive operation in the conditions of complex industrial tasks. Since the previously discussed theoretical provisions and structural control schemes of the reversible thyristor drive are much easier to understand when visualized, it is reasonable to proceed to the illustration of these regularities with the help of graphs. The construction of graphical dependencies reflecting the change of the sawtooth signal, control signal and trigger threshold will make it much easier to understand the internal logic of the system operation. For this purpose, below is a sample program code, which, based on the specified parameters, will create a visual graph in the Python environment. xTo analyze the interaction of signals in automatic control systems, a model of a pilot signal accompanied by a control input is often used. This approach provides a clear visualization of signal dynamics and helps identify key threshold values for trigger activation. The presented graph, titled, Fig.2. illustrates the sawtooth pilot signal, control signal, and trigger activation threshold.

```
import numpy as np
import matplotlib.pyplot as plt

# Time parameters
t_end = 0.02  # 20 ms
dt = 1e-5
t = np.arange(0, t_end, dt)

# Parameters for the sawtooth (pilot) signal
f_line = 50
half_period = 1/(2*f_line)
pilot_signal = np.zeros_like(t)
for i, time_val in enumerate(t):
    phi = (time_val % half_period) / half_period
    pilot_signal[i] = phi

# Control signal
U_control_level = 0.5
U_control = np.ones_like(t) * U_control_level

# Trigger threshold
threshold = 0.2
threshold_line = U_control_level + threshold

# Plotting
plt.figure(figsize=(10,5))
plt.plot(t, pilot_signal, label='Sawtooth signal U_pilot', lw=2)
plt.plot(t, U_control, label='Control signal U_control', lw=2)
plt.axhline(threshold_line, color='r', linestyle='--', label='Trigger threshold')
plt.xlabel('Time, s')
plt.ylabel('Voltage, arbitrary units')
plt.title('Sawtooth and control signals with trigger threshold')
plt.legend()
plt.grid(True)
plt.show()
```

Figure 2. Analysis of pilot and control signals with trigger threshold

After plotting, we observe the sawtooth signal gradually increases and crosses the period of the control level, and then with the trigger threshold stability when the trigger transitions from one state to another, which leads to accurate parameter selection to achieve stable and inexpensive operation of the driving system, to better understand the prediction.

The chart depicts the voltage versus time for both a sawtooth signal U_{pilot} and a control signal U_{pilot}. The red line corresponds to the sawtooth signal U_{pilot}, which exhibits alternating positive and negative peaks. In contrast, the blue line represents the control signal $U_{control}$, which remains relatively constant throughout the measurement period. The horizontal axis is labeled as "Time, s," indicating the time interval, while the vertical axis is marked as "Voltage, arbitrary units," showing the magnitude of the voltage Fig. 3.

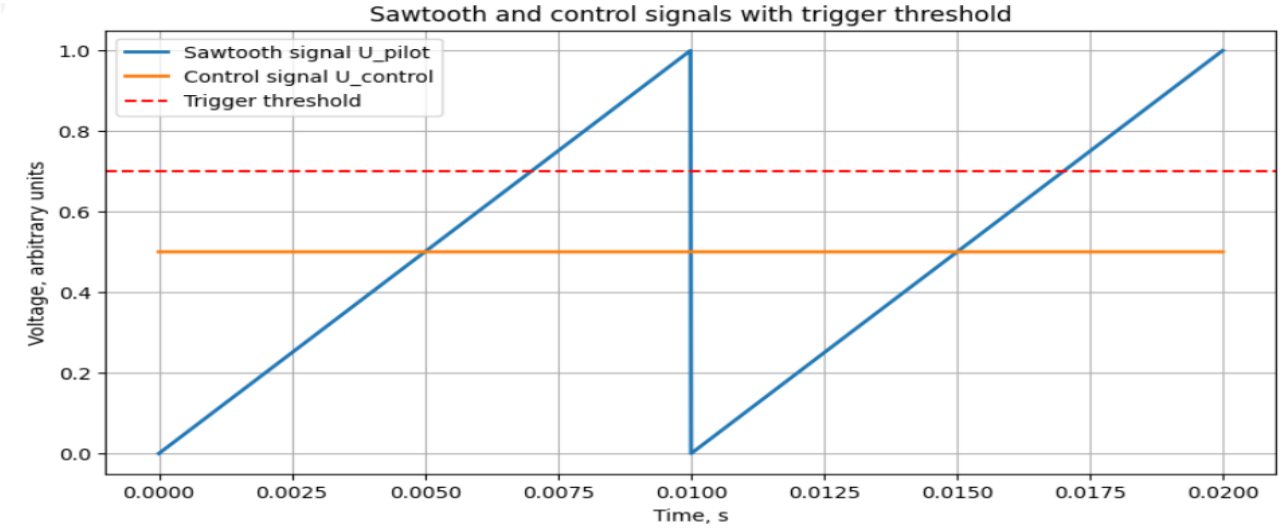

Figure 3. Sawtooth and control signals with trigger threshold

The abscissa axis specifies the time in seconds, e.g. from 0 to 0.02 s (20 ms). The start point is 0 s and the end point is 0.02 s. The time step is so small that the curve looks smooth and continuous. In the graph there is a curve going from points (0, 0) in low voltage mode to point (0.01, 1), that is, for half of the period (about 10 ms) the voltage line increases from 0 to 1. Then, starting at 10 ms, the signal drops back to 0 as the sawtooth signal repeats every half-periodic portion of time. The graph looks like the “teeth of a sawtooth”: it angles upward, reaches a maximum (1), and then abruptly zeroes out to 0, forming this rising line. If we consider only one half-period - it is just a line growing from left to right.

Since we are only looking at 20 ms (and at 50 Hz the half-period is ~10 ms), we see two saw teeth:

1. From 0 to 10 ms: the line rises smoothly from 0 to 1.
2. At around 10 ms, the signal returns to 0 again.
3. From 10 to 20 ms it grows from 0 to 1 again.

On the same chart there is a horizontal straight line at the level of 0.5 on the ordinate axis, a vertical axis, a flat line (without slope) is drawn along the entire time interval, at half height of the chart, dividing the visual chart field approximately in half vertically.

Another horizontal dashed or indicating line, for example the color red, is drawn at the level of 0.7 is 0.5 ± 0.2, where 0.5 is the level of the control signal, and 0.2 is the threshold. What is above the control signal line. It remains at 0.7 continuously throughout the time interval.

- X-axis: time from 0 to 0.02 s.

- Y-axis: voltage from 0 to just above 1 (to move the 0.7 threshold line and sawtooth signal to 1).
- At the bottom of the graph is a toothy rising signal (sawtooth) that goes from 0 to 1 in 10 ms.
- Just below the height is the control line $Ucontrol = 0.5$.
- Even higher is the dotted line of the trigger threshold at 0.7.

Between 0 and 10 ms the sawtooth signal (the line going up horizontally) crosses the control signal level (0.5) at about dawn, the threshold line 0.7 a little later, we can see the sawtooth rising and at a certain point the threshold turns, which corresponds to the trigger time.

As a result, there are three main elements in one graph: the rising sawtooth signal, the horizontal line of the control signal and the horizontal line of the threshold we can see the relationship between the sawtooth voltage waveform, the level of the control signal and the trigger threshold.

Solution of the problem

To ensure stable, accurate and safe operation of reversible thyristor feed drive with regard to the inclusion of "creeping" speed, to preserve the output voltage in the stable power supply unit (SPU), as well as to prevent unauthorized inclusion of thyristors in the same group at a signal at the input, a complex system is proposed. It is based on the generator frequency regulator, current, inverter, logic elements and stabilized power supply unit.

At normal closing of the contacts of the interlock relay R1 is shunted feedback circuits of amplifiers U1 and U2, as well as the outputs of logic elements LE1 and LE2. Due to this, even minimal control signals in the actuator are blocked in the absence of applied setpoint voltage, e.g. when direction relays "B" or "H" are not switched on. This measure ensures that the actuator does not tend to accelerate to a creeping speed without additional operator or control program assignment.

Formally, we can represent the state of the creeping velocity state through the system.

Let

$$Y(m) = 0,\ \forall m \notin [m_0, m_1],$$

where $Y(m)$ - setpoint voltage at the drive input. The interlocking is then ensured:

$$Y(m) \approx 0,\ \forall m \notin [m_0, m_1],$$

detection of the occurrence of non-zero output torque or speed.

The stabilized power supply employs two identical stabilizers that function by using compound transistors (e.g., T8, T2) as a variable resistor. This approach keeps the output voltage constant, regardless of load or input voltage fluctuations. The reference circuitry within the regulator analyzes the difference between the reference voltage (generated by stabilizer D6) and the actual output voltage taken from dividers R7, R8, R9.

Let

$$Y = const$$

is set by stabilizer D6. Output voltage of the stabilizer:

$$Y = Y\frac{P_8 + P_9}{P_8}$$

provided that the resistances R7, R8, R9 are selected accordingly. If for some reason $Y_{\max}$ of the set level, it increases the voltage across the divider, consequently, the input signal on the base of transistor T3 increases:

$$Y_{base}(T3) = F(Y) > Y_{base}$$

This leads to an increase in its collector current:

$$R_C(T3) = K_{T3}(Y_{base}(T3) - Y_{base})$$

where K_{T3} is the gain of transistor T3.

The rising current of T3 partially locks the composite transistor T8, T2, increasing its differential resistance P

$$P_{T8.T2}(m) = P_{T8,T2}^{\min} + \Delta R\ (R_C(T3)),$$

which leads to voltage drop on T8, T2 and restoration of equilibrium:

$$Y\ (m) \to Y\ = const$$

In this way, the system automatically restores the output voltage to the specified customer in case of any disturbance.

The current level limits in the drive are set by potentiometers R21, R23, the possibility of switching between different potentiometers with the machine node selection switch provides flexible adaptation of the drive under the motor of different power. Formally it can be described as follows:

Let ΔUC be the control voltage increment for current limitation, αP be the adjustment factor of the potentiometer. Then:

$$R_{\lim} = R\ (\frac{Y\ \pm \Delta U_C}{Y})\alpha p$$

where $R_{\lim}$ - level of the new current limitation after adjustment with the potentiometer.

By selecting the switching relay, it is possible to change αp, adjusting to a different motor power, thus saving time and simplifying the integration of different units.

The amplifier block ($Y1$ - frequency controller, $Y2$ - current controller, $Y3$ - inverter, $Y4$ - current amplifier, $Y5$ - current inverter) at least integral amplifiers with a transfer coefficient 10^5 large input impedances ($\geq 10^5 \Omega$) are used, which allows minimizing losses and restoring the signal. The low temperature drift of no more than $10mcV / C°$ ensures the stability of the system operation in various temperature regimes. Conditional balanced mode for one of the amplifiers under consideration:

$$Y\ = A \cdot (Y_v^+ - Y_v^-)$$

where

A - coefficient transfer, Y_v^+, Y_v^- - input signals.

At $A \to 10^5$, even a small difference between the inputs results in a significant output signal, which improves the control accuracy. The temperature drift ΔU can be estimated as follows:

$$\Delta U\ \approx 10mcV / C°$$

which, under the right operating conditions, is very small.

Let's move on to plotting the graphs to illustrate how these processes and settings are reflected over time or when parameters are changed.

The graph below depicts Fig.4 the blocking of minimum control signals when there is no setpoint. It shows the relationship between signal output and time for two different conditions: without blocking and with $R1$ lock no creep speed. This is a crucial tool for analyzing safety system performance, helping to understand how various parameters affect device operation in real-world scenarios.

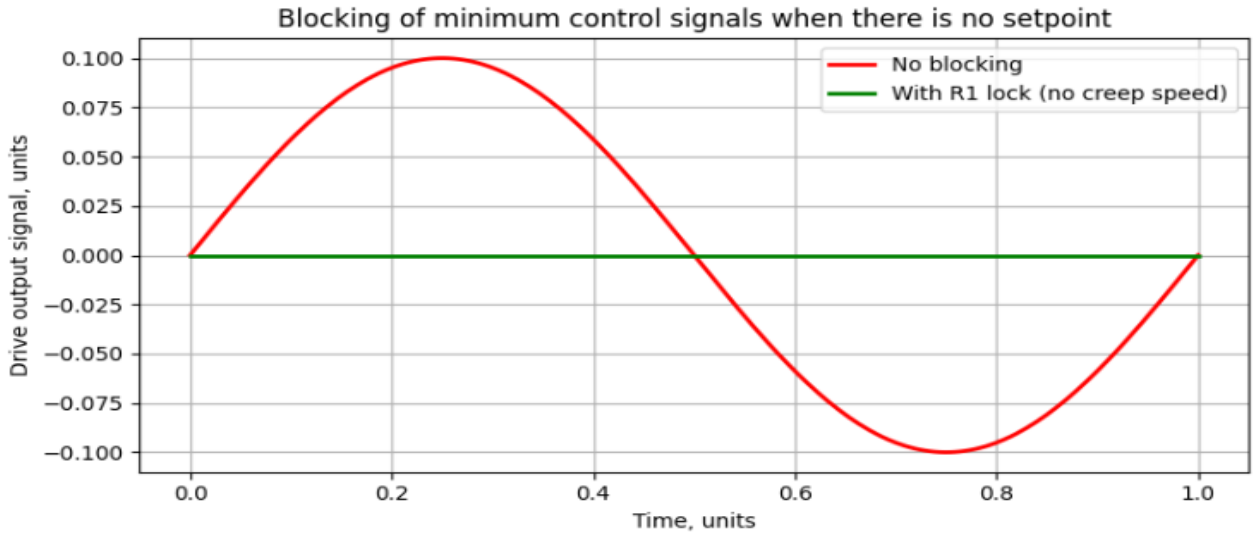

Figure 4.Blocking the «creeping» speed

This graph demonstrates the difference between the operation of the actuator with interlocking. In the absence of setpoint voltage, normal operation of the interlock relay R1 ensures that there are no even minimal control signals - the output signal remains at zero. Without interlocking, small oscillations can be seen, which could cause the mechanism to "creep". This comparison clearly shows the effectiveness of interlocking in preventing unwanted actuator movement in the absence of a command. On the previous slide, we examined the theoretical foundations of voltage stabilization under load conditions, including the impact of various factors such as signal frequency and amplitude. Now let's move on to a practical example shown in Fig.5.

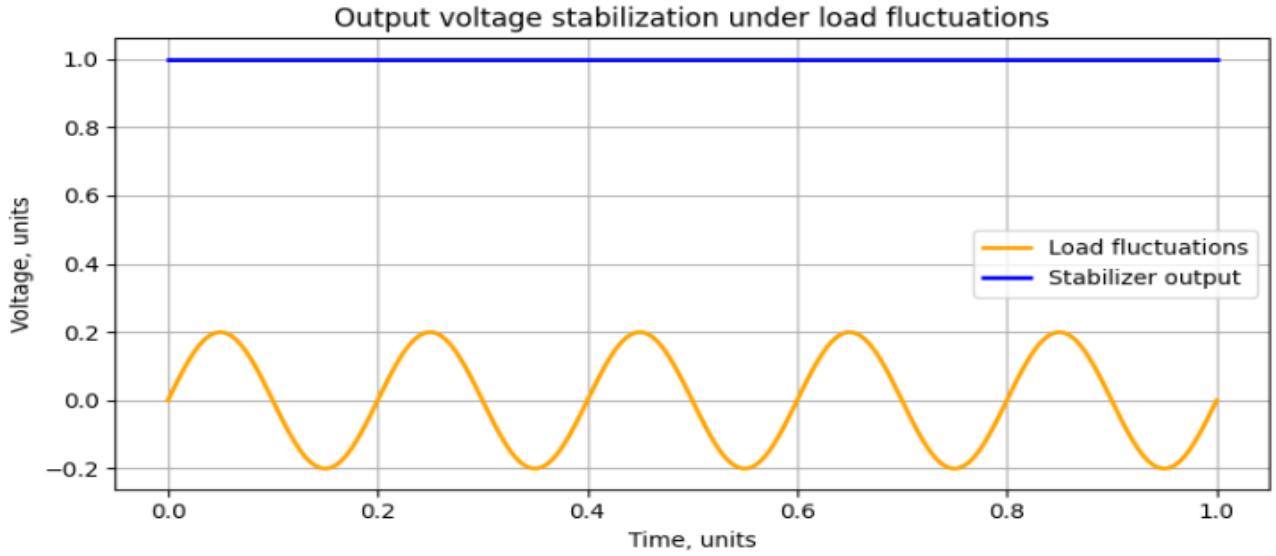

Figure 5. Output voltage stabilization

Here we see the behaviour of the stabiliser despite load fluctuations, the output voltage remains constant, the stabiliser successfully smooths out any fluctuations, ensuring stable operation of the drive units and control electronics, regardless of changing output conditions. Now let's move on to the practical application of these concepts using this graph. This graph shows the effect of changing parameter α_R at the current limit level Fig.6.

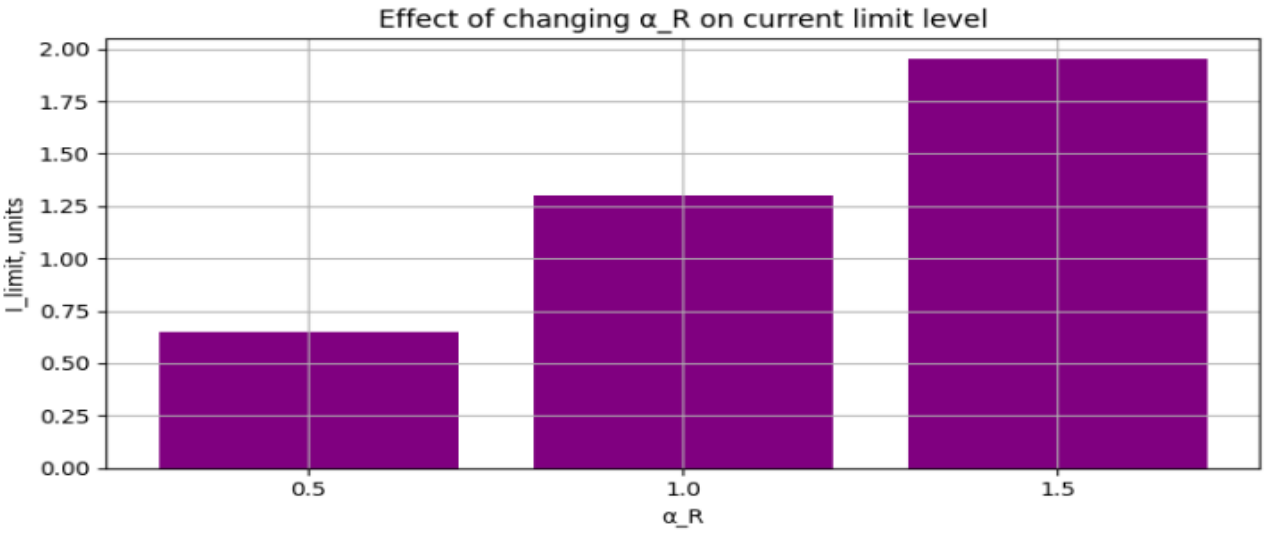

Figure 6. Flexibility of setting the current limit via α_R

Changing the coefficient α_R affects the level of current limitation. A higher α_R increases the maximum permissible current and a lower α_R reduces it, as it allows the drive to be adapted to different motors varying in power and requirements by simply switching potentiometers and selection relays.

All amplifiers are fitted with oscillating circuits. Zero balancing circuits are provided in amplifiers U1, U4.

The correction circuits of amplifiers U1 and U2 are located in the correction block (BC). The level of current limitation is set by potentiometers R21, R23, installed outside the block, and is determined by the formula:

$$I_{T0} = \frac{1}{K_T} \times \frac{R15}{R14} U_{y1}$$

where I_{T0} is the level of current limitation;

K_T - current feedback coefficient equal to the shunt transfer coefficient $1.5 \cdot 10^{-3} V \cdot A$ - for 50 A shunt, 75 mV;

U_{y1} is the maximum output voltage of the amplifier U1, coming to the input of U2, i.e. the voltage determined by resistors R21, R23.

Let's try to map the X-axis in time for several signals:

Enable signal for the odd group of DCFs, up to the moment t_1 the group is active, then when the sign of the control voltage on the side of U3 changes, the access is switched off after a pause Δt_1 . Enable signal for even-numbered group of DCFs: it is enabled only after an additional pause Δt_2, ensuring a smooth transition. Armature current I_y, during odd group operation the current is maintained at a certain level, then when the operating pulses are stopped and only duty pulses are applied during Δt_2 the current drops rapidly to zero. Events in time, where moment t_1 - change of sign of voltage U3, beginning of pauses, moments of removing and setting permissions.

Let's say:

- $t_1 = 0.01$ s - change of sign of voltage at the output of U3.
- $\Delta t_1 = 0.003$ s - pause during which the current decreases.

- $\Delta t_2 = 0.002$ s - pause before switching on the even group after Δt_1.

In load distribution control systems, particular attention is paid to the algorithms responsible for enabling and disabling different groups of components. These algorithms ensure balanced load distribution and minimize delays during switching operations. The graph below provides a detailed depiction of the timing of activation signals for the odd and even groups labeled as odd group and Even group during the control process. Key moments are highlighted on the graph, such as the sign change of the output signal $U3$ denoted as t_1, the end of the pause for the odd group $t_1 + dt_1$, and the activation of the even group $t_1 + dt_1 + dt_2$. These events are visually distinguished using color-coded markers to simplify identification and analysis.

This visualization helps evaluate the efficiency of switching between groups and identify potential areas for optimization, such as minimizing pause durations or improving synchronization. Let us now examine the graph titled Fig. 7 for a more detailed analysis of the system's behavior.

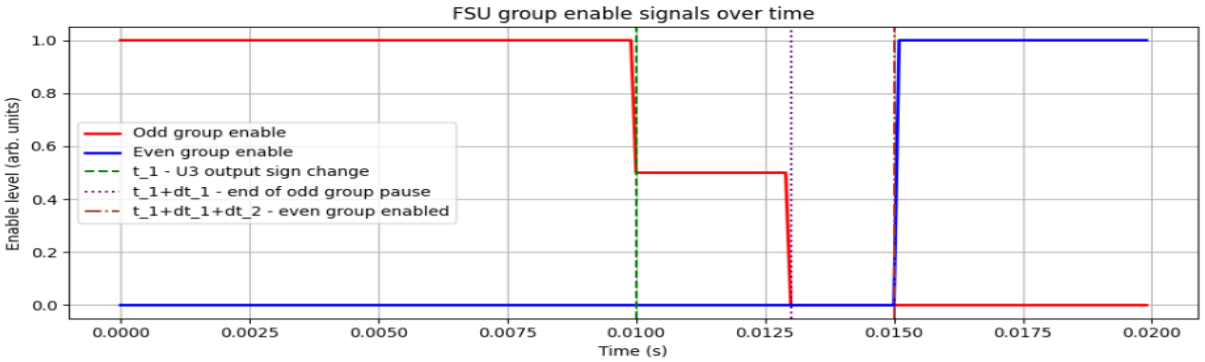

Figure 7. FSU group enable signals over time

At time t_1, when the sign of the voltage at the output of U3 changes, the resolution for the odd group is gradually removed. At first, only duty pulses are applied during Δt_1, then the permission disappears completely. Only after an additional pause of Δt_2 does the resolution change to the even group. This visual representation underlines the organised sequence of actions aimed at preventing the impulses of the two thyristor groups from overlapping and guaranteeing safe switching.

The behavior of the armature current I_y over time plays a crucial role in understanding the dynamics of the load distribution system. This parameter is directly influenced by the enabling signals of the odd and even groups, as well as the timing of the system's switching operations. By analyzing the graph, we can observe how I_y responds to these control actions, providing insights into system performance and stability.

The graph titled Fig. 8 armature current I_y over time illustrates the temporal evolution of the current. Key moments are marked for clarity, including the signal sign change t_1 and the end of the odd group's pause $t_1 + dt_1$. These points signify critical transitions in the control process, directly impacting I_y. The visual representation highlights the decrease in armature current after t_1, reflecting the system's response to the control algorithm. This data is vital for assessing how efficiently the system handles load transitions and identifying potential improvements in current regulation mechanisms.

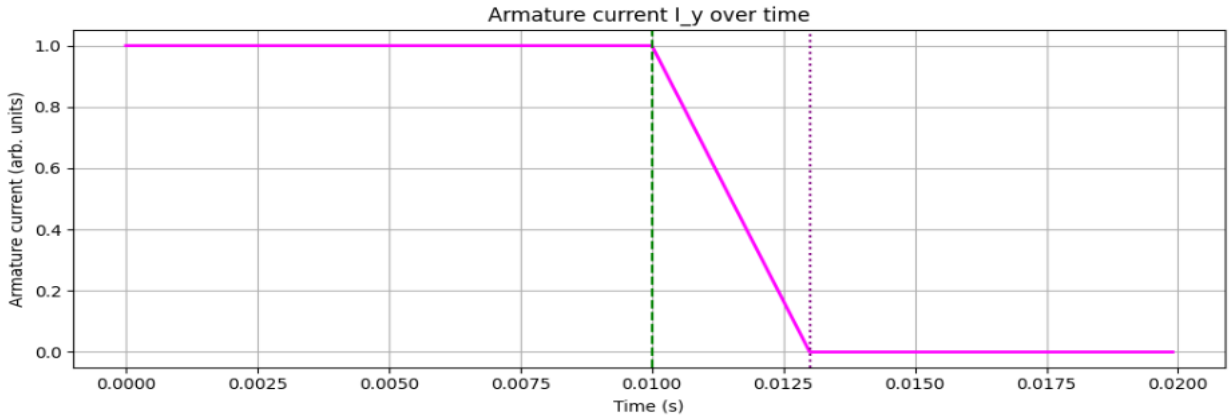

Figure 8. Armature current I_y over time

The armature current I_y is maintained at a stable level until t_1. At the moment t_1, the current is rapidly discharged by means of duty pulses only. During the time Δt_1, the current drops rapidly to zero, which prevents dangerous transients and guarantees a soft termination of one of the groups.

The dynamics of the pilot signal are instrumental in regulating the system during critical operational phases, such as pauses and threshold evaluations. The graph titled Fig. 9 pilot signal during the pause and threshold level, provides a detailed view of the voltage variations of the pilot signal sawtooth-like in comparison to the threshold U_{08}.

This representation shows the behavior of the pilot signal, characterized by its sawtooth waveform, alongside the fixed threshold level, marked as a red dashed line. Notably, the intersection between the pilot signal and the threshold signifies critical triggering points, essential for initiating specific control actions within the system. From the graph, we observe the periodic nature of the pilot signal and its ability to reset upon reaching the threshold, which ensures synchronization and stability in the control process. Analyzing these interactions helps evaluate the system's responsiveness and the effectiveness of the set threshold in maintaining desired operational conditions. This graphical insight lays the foundation for optimizing signal configurations and refining system control strategies.

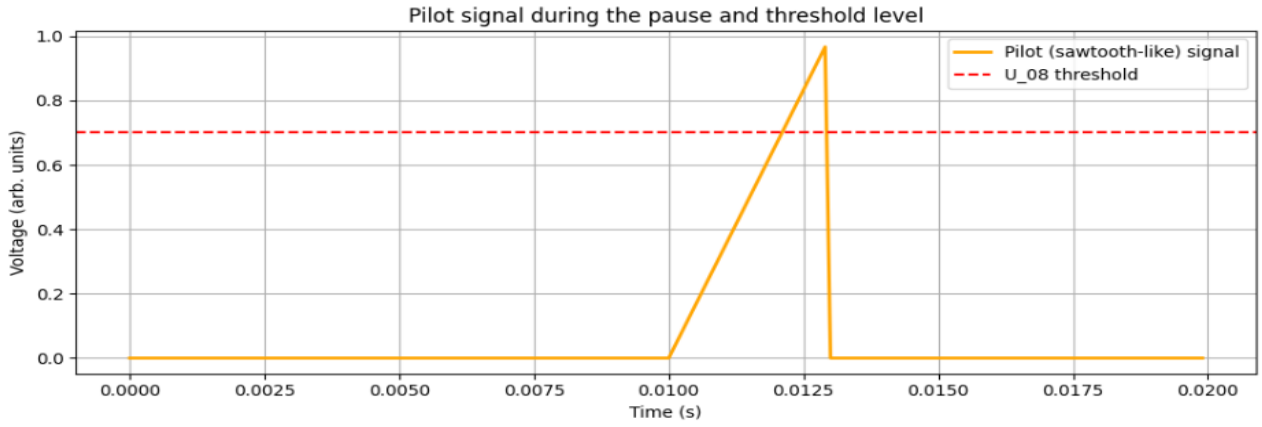

Figure 9. Pilot signal during the pause and threshold level

Limiting the maximum level of the control voltage applied to the phase-shifting devices (PSDs) is carried out by stabiliser D2, which ensures that the amplitude of the input signal does not exceed the maximum permissible values.

If the system is used in a single motor configuration, a standard jumper is connected between pins 16-17 of connector Ш2 on the external side. If the drive serves several motors with different

power characteristics, external current limiting potentiometers are connected to pins 16-17 via the machine unit selection relay. The important prerequisite is the sequence of operation. The voltage sawtooth device (VDU) and the associated phase-shifting device are placed on a single printed circuit board, ensuring compactness and reducing noise sensitivity. The VVM consists of an electronic key on transistor T1, a current stabiliser on transistor T2 and an emitter repeater on transistor T3. The sawtooth signal is formed during the charging of capacitor C1, and the charging current is set by the base bias determined by the ratio of resistances R3 and R4. A stable sawtooth slope required for accurate phase p is provided.

The circuits of logic elements provide modes of mutual blocking and delay of permissive signals. Thus, open transistor T5 of the LE1 circuit shunts the input of transistor T6 of the even group of FSU, and also short-circuits the LE2 input on terminals 18-20, forming the prohibition signal U_{04} for the even group of FSU. Suppose that at time t_1 at the output of the amplifier U3 of the regulator block, BR changes the sign of the voltage, as a result of which the working impulses from the odd-numbered group of DCF cease to arrive at the input LE1. As a result, transistor T2 of the LE1 circuit closes, and capacitor C1 during the pause Δt_1 is charged to the triggering voltage of transistor T3 U_{08}. The pause Δt_1 is determined by the time constant of the circuit R4C1, as well as by the level of the signal proportional to the armature current coming from the output of the inverter of the current amplifier U5 of the BR unit. During this time interval Δt_1, only duty pulses are supplied to the thyristors of the odd group, accelerating the armature current reduction to an acceptable low level. After the pause Δt_1, transistor T4 opens, removing the permission from the odd group of DCFs, and the duty pulses are no longer supplied to the corresponding thyristors. C Δt_2, determined by the time constant of the C2R8 circuit. This time delay Δt_2 is critical to guarantee that the current in the previously operating group is reduced to zero.

At the end of the pause Δt_2, the logic circuit LE2 transfers control to the even group of DCFs. The operating pulses of this group start to flow from transistors T5 of the even branch to the input of LE2, forming the signal U_{04}. When the first pulse in LE2 discharges capacitor C11, and without any additional delay, the prohibition signal is fed to the odd group of DCF, because the transistor T15, opening, shunts the input of transistors T6 of the odd group.

The closing of transistor T14 at this moment gives an enable signal for the even group of DCSs. The operating and standby pulses are fed back to the thyristors of the even group, ensuring a smooth and safe control transition as well as synchronisation of the drive operating modes during reversing or changing load conditions.

Results and conclusions.

The use of specialised correction blocks, potentiometers for setting current limiting levels and machine node selection relays makes the drive extremely flexible. The use of proportional-integral controllers, amplifiers with high gain of the order of 10^5. makes it possible to achieve stable and accurate maintenance of the set parameters. This results in stabilisation of the speed of rotation, accurate holding of the allowable current and maintenance of the required accuracy in the control loop even under significant changes in load or external conditions. The inclusion of an interlock relay and logic element circuit, as well as the correct organisation of the operating and standby pulses applied to the thyristors of both groups of DCFs, ensures that the drive will not spontaneously reach minimum speed in the absence of a setpoint signal. Implementation in the stabilised power supply

unit of comparison circuits with reference stabilitron and use of compound transistors as variable resistance ensures constant level of output voltage in case of load fluctuations or changes in input parameters.

The logic of delays (Δt_1 , Δt_2), duty and working pulses, as well as the sawtooth voltage control ensures a smooth transition between odd and even groups of DCFs during reversing. Transients are controlled predictably, armature current has time to decrease to a safe level, after which another group is connected without the risk of overlapping or simultaneous switching on of thyristors of different branches. This approach minimises the risk of damage, overheating and unwanted mechanical shocks in the drive. Low temperature drift of integrated amplifiers, optimal selection of resistors, stabilisers and transistors in stabilisation and correction circuits allow to guarantee stability of control parameters in a wide range of temperatures and external conditions. As a result, the reliability and durability of the drive is increased, and the need for frequent adjustments and readjustments is reduced. All these aspects form a complete, integrated control system for reversible thyristor drive, characterised by high accuracy, safety, adaptability and stability

REFERENCES

[1]. Timofeev A. *Synthetically generated convection-diffusion type differential equations with integral boundary condition.* J. Appl. Math. computer, 2009, pp. 79-86.

[2]. Timofeev A. *Third order differential equation with sinusoidal perturbing function and integral boundary condition*. J. Appl. Math. Comput., 2010, pp. 99-110.

[3]. Gorodenskaya O.Yu., Gobareva Y.L., Medovarov A.V. *Constructing financial markets with the help of a composite neural network*. Problems of Economics and Applied Mathematics. 2021, Vol. 17, No. 3. pp. 65-72.

[4]. Timofeev A. *A difference scheme for a third-order differential equation with sinusoidal perturbations in a domain with an integral boundary condition*. Journal of Computational Mathematics and Mathematical Physics, 2007, vol. 47, no. 6, pp. 73-86.

[5]. Selivanov, L. A. and Ramnajam, N. *Parametric difference scheme for differential perturbation of the problem of three-dimensional magnetic field propagation of a toroidal coil in a conducting medium.* Izvestiya vysshee obrazovaniya vysshee obrazovaniya. Physics, 2017, No. 296, pp. 101-115.

[6]. Amirkhanov G.M., Amirkhanova I.G. and Mustafaeva K.Ch. *Numerical solution of differential equations with singular perturbations and integral boundary conditions,* Applied Mathematics and Informatics, 2007, vol. 19, no. 4, pp. 548-574.

[7]. Mokrova N.V., Volodin V.M. Justification for the choice of methods for solving the problem of optimal control of complex processes. Bulletin of TSTU, 2006. Volume 12. 22-28 p. ISSN 0136-5835.

[8]. Bellman R. *Dynamic programming* . Transl. from English – M.: Izdatinlit, 1960. – 400 p.

[9]. Hu Wen-Tsen., Umbetov U. *Decentralized control of multidimensional objects with decomposition by situations.* News of the National Academy of Sciences of the Republic of Kazakhstan, Physics and Mathematics Series, 2007, No. 1, pp. 82 – 85.

[10]. Volodin V.M., Guseva A.Yu. *Optimal control of multi-stage processes with complex flow structures.* Chemical and petroleum engineering. No. 3. 1997. pp. 20 – 21.

[11]. Wilco van Harselaar, Niels Schreuders, Theo Hofman, Stephan Rinderknecht. *Improved Implementation of Dynamic Programming on the Example of Hybrid Electric Vehicle Control*, IFAC-PapersOnLine, Volume 52, Issue 5, 2019, Pages 147-152, ISSN 2405-8963,

doi.org/10.1016/j.ifacol.2019.09.024.

[12]. Artemyev, V. Theoretical and practical aspects of the application of the dynamic programming method in optimal control problems / V. Artemyev, N. Mokrova, A. Hajiyev // Machine Science. – 2024. – Vol. 13, No. 1. – P. 46-57. – DOI 10.61413/GIPV6858.

[13]. A. S. Maksimov, S. D. Savostin, V. S. Artemyev. *SCADA systems* . – Kursk: Closed Joint Stock Company "University Book", 2023. – 127 p. – ISBN 978-5-907776-95-1.

[14]. V. Artemyev, A. Medvedev, V. Yaroshevich. *Investigation of optimal control of variable systems in the dynamic spectrum.* Machine Science. – 2023. – Vol. 12, No. 1. – P. 68-75.

[15]. V. Artemyev, S. Mokrushin, S. Savostin [et al.].*Processing of time signals in a discrete time domain.* Machine Science. – 2023. – Vol. 12, No. 1. – P. 46-54.

[16]. V. S. Artemyev, M. N. Makhiboroda, S. L. Yablochnikov [et al.]. *Implementation of Adaptive Control with Parametric Uncertainty*. Intelligent Technologies and Electronic Devices in Vehicle and Road Transport Complex (TIRVED), Moscow, 10–11 november 2022. – Moscow: IEEE, 2022. – P. 9965505. – DOI 10.1109/TIRVED56496.2022.9965505.

[17]. A. Haag, M. Bargende, P. Antony, F. Panik. *Iterative refinement of the discretization of the dynamic programming state grid*. In 16. Int. Stuttgarter Symposium, Springer (2016), pp. 145-154.

Received: 06.02.2024
Accepted: 22.07.2024

MACHINE SCIENCE
ISSN: 2227-6912
E-ISSN: 2790-0479
2024, № 2 Pages 29 – 34

KINETOSTATIC ANALYSIS OF A FIVE-LINK FLAT MECHANISM

Isa KHALILOV[1,a], Savalan KERIMOV[1,b], Semaye BAGIROVA[1,c]

[1]Department of Machine Building Technology, Azerbaijan Technical University, Baku, Azerbaijan

E-mail: [a*]khalilov@aztu.edu.az, [b]savalan.kerimov@aztu.edu.az, [c]semaye.bagirova@aztu.edu.az

https://doi.org/10.61413/NXAU2793

Abstract: The article considers the first problem of dynamics. With a known law of motion of a five-link flat mechanism, which also includes a higher kinematic pair, unknown forces are determined. The reaction forces in kinematic pairs and the balancing force applied to the input link of the mechanism are determined by the graphoanalytical method.

Keywords: *kinetostatics, degree of freedom, reaction forces, Assur group, kinematic pair.*

Introduction.

Kinetostatic analysis of a mechanical system refers to the first problem of dynamics. In this problem, unknown forces are determined for a known law of motion of a mechanical system. Kinetostatic analysis of flat lever mechanisms has been considered in sufficient detail at present. However, it should be noted that flat mechanisms, which also include higher kinematic pairs, have not been studied enough.

For example, in [1] flat tensegrity mechanisms with three linear springs are analyzed in detail. Kinetostatic equations are derived and solved under several load conditions and geometric conditions. The paper [2] is devoted to the method of numerical solution of a 5-link vehicle suspension mechanism. The multidimensional Newton method and regularization are used as the mathematical apparatus. The paper [3] studies a flat tensegrity manipulator consisting of two X-mechanisms connected in series. Unlike the classical 2-R-linkage, the proposed architecture does not contain elements subject to bending. The papers [4, 5] consider a vector method for solving one of the important problems of dynamic analysis of flat lever mechanisms with lower kinematic pairs, which consists in determining reactions in kinematic pairs and balancing the moment (force) on the driving link for a given law of motion of the mechanism. In the article [6], the main attention is paid to determining the force or torque acting on a flat mechanism using a numerical method, when the acceleration and dynamic properties of the joints are known. The article [7] developed an analytical interpretation of an approximate method for calculating forces in kinematic pairs taking into account friction forces for the Assur group of the second class with three rotational pairs. In the paper [8], dynamic equations of motion are used for kinetic analysis. Vector/scalar equations are solved using the MathCAD software. The results are verified using the Working Model 2D software. The paper [9] proposes a new design of a lifting mechanism, the peculiarity of which is that in its structure it belongs to the Assur group of a high class, which determines the ease of operation and reliability of the design. For this design, a synthesis of the mechanism was carried out. The work [10] is devoted to the kinetostatic analysis of the ratchet mechanism acting on the conveyor, which is part of the MGL-3 solid organic fertilizer spreader, namely, the reactions in the kinematic connections, as well as the torque in the drive clutch of the mechanism, are determined.

The conducted literature review shows that despite the numerous works devoted to the kinetostatic analysis of various mechanisms, a five-link flat mechanism, which has one higher kinematic pair in its structure, has not been studied.

Formulation and solution of the problem. This paper examines the kinetostatic analysis of a flat five-link mechanism, which, in addition to the lower ones, includes one higher kinematic pair (Fig. 1).

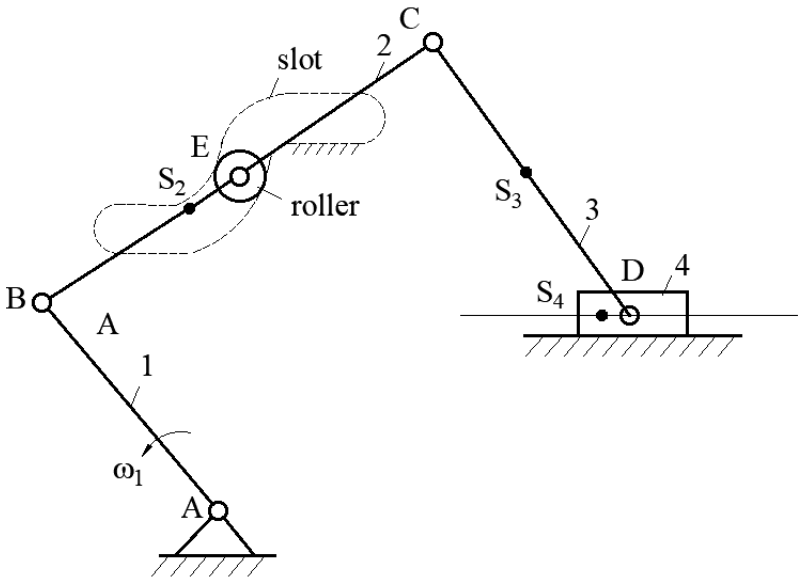

Figure 1. Five-link flat mechanism with one higher kinematic pair.

It is known that a five-link flat-lever mechanism has two degrees of freedom. If a known point of this mechanism moves along a certain trajectory, then this mechanism turns into a mechanism with one degree of freedom. For example, if a roller is placed at point C and forced to move along the trajectory shown in Fig. 1 by a dashed line (slot), then the mechanism will have one degree of freedom. To do this, a slot is made in the fixed post of the mechanism, into which the roller mounted at point C is placed. Then, when the crank AB rotates, point C will move along this slot, and point D will perform the required movement. The synthesis and kinematic analysis of this mechanism are considered in [11].

Here we consider the kinetostatic analysis of the mechanism shown in Fig. 1. It is known that in kinetostatic analysis, unknown forces are determined with a known law of motion of the mechanism. In this case, the reaction forces in kinematic pairs and the balancing force applied to the leading link AB are determined.

In kinetostatic analysis, the resistance forces or driving forces, masses, moments of inertia and the center of mass of the links are specified. According to the known law of motion of the mechanism, the inertial forces and moments of inertial forces of the links are determined. In the force analysis of mechanisms, the d'Alembert principle is used. In this case, the inertial forces of the links are added to the real forces and the problems of dynamics are solved using the equations of statics.

It is known that if the degree of freedom of a kinematic chain is zero, then this chain is statically determinate. A kinematic chain with zero mobility, which is part of a mechanism, is an Assur group. Therefore, in a kinetostatic analysis, the mechanism is divided into structural Assur groups and a primary mechanism. We emphasize that with such a division of the mechanism in the force loading of each structural group, only the reaction forces in the kinematic pairs will be unknown. In the composition of the mechanism under consideration (Fig. 1), in addition to the primary mechanism -

the input link AB with the support, there are two Assur groups. The 4th link - the slider, with the 3rd link - the connecting rod make up the Assur group of the second class. The 2nd link with the roller is called a "monad". Its degree of mobility is zero and is statically determinate:

$$W = 3n - 2p_1 - p_2 = 3 \cdot 1 - 2 \cdot 1 - 1 = 0 \quad (1)$$

First, we consider the force analysis of the structural group consisting of the 4th and 3rd links, which is connected to the last mechanism (Fig.2).

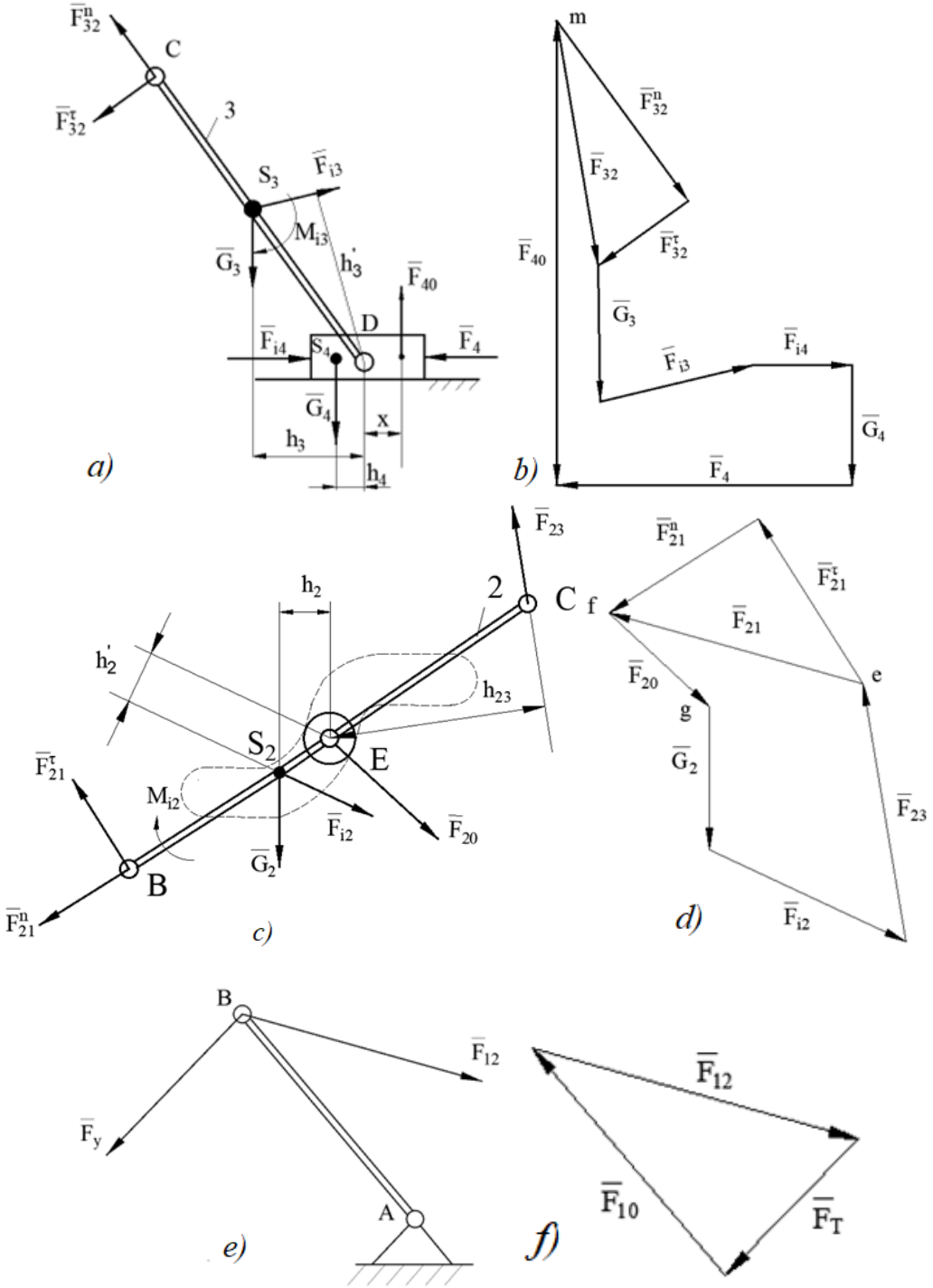

Figure 2. Kinetostatic analysis of a five-link flat mechanism with one higher kinematic pair.

The production resistance force F_4, the gravity force G_4, and the inertial forces of this link F_{i4} acting on the output link – the slider are known (Fig.2*a*). In particular, the gravity force of the 3rd

link G_3, the inertial force F_{i3}, and the moment of inertia M_{i3} are known. The reaction force from the support to the slider $\bar{F}_{40}$ is known in direction. This force is directed normally relative to the motion of the slider, its value and the point of application *x* are unknown. In a single-motion rotational kinematic pair located at point *C*, the point of application of the reaction force $\bar{F}_{23} = -\bar{F}_{32}$ arising in it is known. The direction and modulus are unknown. We will decompose the reaction force $\bar{F}_{32}$ into two components, normal and tangential, known in direction but unknown in value: $\bar{F}_{32} = \bar{F}_{32}^{n} + \bar{F}_{32}^{\tau}$. The reaction force $\bar{F}_{32}^{n}$ is directed along the link *CD*, $\bar{F}_{32}^{\tau}$ is perpendicular to the link *CD*.

To determine the reaction force of the structural group consisting of the 3rd and 4th links, we will use the graphoanalytical method. To do this, we first draw up an equation for the moments of forces acting on the 3rd link relative to point *D*:

$$\sum M_D = F_{32}^{\tau} \cdot CD \cdot \mu_l + G_3 \cdot h_3 \cdot \mu_l - F_{i3} \cdot h_3' \cdot \mu_l - M_{i3} = 0 \qquad (2)$$

From here:

$$F_{32}^{\tau} = \frac{F_{i3} \cdot h_3' + M_{i3} \cdot \frac{1}{\mu_l} - G_3 \cdot h_3}{CD}$$

where μ_l - is the scale of the position plan.

To determine the values of $\bar{F}_{40}$ and $\bar{F}_{32}$ based on the selected force scales, we construct a force polygon (Fig.2*b*). When constructing a force polygon, the direction of one of the unknown forces is first noted, for example: $\bar{F}_{32}^{n}$ ends with the directions of the other unknowns - $\bar{F}_{40}$. To construct a force polygon, you can use the following vector equation:

$$\bar{F}_{32}^{n} + \bar{F}_{32}^{\tau} + \bar{G}_3 + \bar{F}_{i3} + \bar{F}_{i4} + \bar{G}_4 + \bar{F}_4 + \bar{F}_{40} = 0 \qquad (3)$$

After constructing the force polygon, the values of the unknown forces are determined:

$$\bar{F}_{32} = mn \cdot \mu_F, \ \bar{F}_{40} = mk \cdot \mu_F,$$

where μ_F is the scale of the force plan.

From the condition of the slider equilibrium, the points of application of the reaction force $\bar{F}_{40}$. are determined. To do this, we compose the equations of the moments of forces acting on the slider:

$G_4 \cdot h_4 - F_{40} \cdot x = 0,$

$$x = \frac{G_4 \cdot h_4}{F_{40}}$$

Reaction forces from the 3rd link to the 2nd link

$$\bar{F}_{23} = -\bar{F}_{32}, \ \ \bar{F}_{32} = \bar{F}_{32}^{n} + \bar{F}_{32}^{\tau}, \quad F_{32} = mp \cdot \mu_F.$$

The next stage of the force analysis will be the force analysis of the "monad" - the second link with the roller (Fig.2*c*). Since the roller with the fixed link make up a kinematic pair, the reaction force from the fixed link to the roller $\bar{F}_{20}$ will be normal to the elements of the kinematic pair, that is, normal to the trajectory of point *E*. Then the point of application and the direction of $\bar{F}_{20}$ are known. The reaction force $\bar{F}_{21}$, arising at point B from the leading link to the second link is decomposed into two components:

$$\bar{F}_{21} = \bar{F}_{21}^{n} + \bar{F}_{21}^{\tau}.$$

To determine $\bar{F}_{21}^{\tau}$, we will compose an equation of moments of forces relative to point *E*.

$$\sum M_E = -F_{21}^{\tau} \cdot EB + F_{,2} \cdot h_2' + G_2 \cdot h_2 + F_{23} \cdot h_{23} - M_{i2} \cdot \frac{1}{\mu_l} = 0 \qquad (4)$$

Hence,

$$F_{21}^{\tau} = \frac{F_{i2} \cdot h_2' + G_2 \cdot h_2 + F_{23} \cdot h_{23} - M_{i2} \cdot \frac{1}{\mu_l}}{EB}$$

The values of the reaction forces $\bar{F}_{20}$ and $\bar{F}_{21}^{n}$ are determined by constructing a force polygon (Fig.2*d*). To do this, we use the following vector equation:

$$\bar{F}_{20} + \bar{G}_2 + \bar{F}_{i2} + \bar{F}_{23} + \bar{F}_{21}^{\tau} + \bar{F}_{21}^{n} = 0 \quad (5)$$

After constructing the force polygon, we find:

$$F_{20} = fg \cdot \mu_F. \quad F_{21} = ef \cdot \mu_F.$$

At the end of the kinetostatic analysis, the force analysis of the primary mechanism is considered, i.e. the leading link *AB* with the support (Fig.2*d*). From the analysis of this system, the balancing force $\bar{F}_{\text{y}}$, the reaction force $\bar{F}_{01}$ arising in the kinematic pair between the support and the link *AB* are determined. $\bar{F}_{\text{y}}$ – the balancing force is conditionally applied to point *B* perpendicular to link *AB*. The mass and moment of inertia of the input link *AB* are not taken into account. Then the forces acting on the primary mechanism $\bar{F}_{01}$, $\bar{F}_{21}$ and $\bar{F}_{\text{y}}$ intersect at one point. The values of $\bar{F}_{01}$ and $\bar{F}_{\text{y}}$ are determined by constructing a force triangle (Fig.2*f*).

Conclusion.

Based on the above, the following conclusions can be made:

1. A kinetostatic analysis of a five-link flat mechanism, which in addition to the lower ones includes one higher kinematic pair, was carried out using the graphoanalytical method;

2. Adding one higher kinematic pair to a flat lever mechanism with two degrees of freedom turns it into a mechanism with one degree of freedom;

3. Using the d'Alembert principle, the reaction forces arising in kinematic pairs were determined;

4. A force analysis of the primary mechanism was considered and the balancing force was determined.

REFERENCES

[1]. Philippe Wenger, Damien Chablat. *Kinetostatic Analysis and Solution Classification of a Planar Tensegrity Mechanism. Computational Kinematics*., Mechanisms and Machine Science, 50, Springer, Cham, 2017.

[2]. Kreinin, G.V., Misyurin, S.Y. & Nelyubin, A.P. *Numerical solution of problems on the position of a five-link mechanism of an automobile suspension. J. Mach. Manuf. Reliab.* 43, 255–260 2014.

[3]. Furet, Matthieu, and Philippe Wenger. *Kinetostatic analysis and actuation strategy of a planar tensegrity 2-X manipulator. Journal of Mechanisms and Robotics* 11, no. 6 (2019):

[4]. Jomartov, A., Tuleshov, A. *Vector method for kinetostatic analysis of planar linkages. J Braz. Soc. Mech. Sci. Eng.* 40, 56 (2018).

[5]. Abduraimov, A., Yuriy Drakunov, Bolat Espaev, and Tatyana Zmeikova. *Kinetostatic Analysis of the Mechanism of 5-Th Class by Using Vector Method Applied Mechanics and Materials.* Trans Tech Publications, Ltd., August 2013.

[6]. Thanh Nhan Phan. (2024). Dynamic Analysis of Planar Mechanism in Numerical Methods. *Journal of Technical Education Science, 19*(SI03), 50–58.

[7]. Sebastián Durango; Gabriel Calle. Oscar Ruiz. *Analytical method for the kinetostatic analysis of the second-class RRR Assur group allowing for friction in the kinematic pairs.* Technical Papers • J. Braz. Soc. Mech. Sci. & Eng. 32(3), Sept 2010

[8]. Ahmet Shala and Mirlind Bruqi/ Kinetostatic Analysis of Six-Bar Mechanism Using Vector *Loops*

and the Verification of Results Using Working Model 2D, International Journal of Mechanical Engineering and Technology 8(8), 2017,

[9]. Abdrakhimov, U. T., & Akimkhanova, A. A. *Kinetostatic calculation of a high class lifting mechanism (by assur classification) of a technological load-lifting machine. Journal of Mathematics, Mechanics and Computer Science*, *118*(2), 57–63.

[10]. Lucretia Popa , Luciana Dudici, Ancuta Nedelcu, Andreea Catalina Cristescu, Daniel Dumitru. *Kinetostatic analysis of ratchet mechanism that acts on conveyor of manure spreading machine.* Engineering for rural development jelgava, 23.-25.05.2018.

[11]. Khalilov I.A., Kerimov S.Kh., Rzaeva H.M. *A method for synthesizing a lever mechanism that ensures a given law of motion*. Vestnik mashinostroyeniya, Moscow, No. 3, 2017, pp. 3-5.

Received:.14.08.2024
Accepted: 19.11.2024

MACHINE SCIENCE

ISSN: 2227-6912
E-ISSN: 2790-0479

2024, № 2 Pages 35 – 41

PRACTICAL APPLICABILITY OF MATRIX MODELS FOR ACCURACY IN MULTI-TOOL MACHINING ON AUTOMATIC LATHES

Nizami YUSUBOV [1a], Heyran ABBASOVA[1b*]

[1] *Department of Machine Building Technology, Azerbaijan Technical University, Baku, Azerbaijan*

E-mail:[a]nizami.yusubov@aztu.edu.az, [b] abbasova.heyran@aztu.edu.az*

https://doi.org/10.61413/IBAL4228

Abstract: Features and challenges of multi-tool turning operations are proposed: equipment for multi-tool turning; the level of utilization of the technological potential of multi-tool machining in mechanical engineering; achievable machining accuracy; statistics on machining parts with predominant dimensions; statistics on multi-tool configurations; dimensional-accuracy theory of multi-tool machining. Therefore, the objectives of developing a design theory for multi-tool machining, considering the capabilities of modern CNC machines, are substantiated. The article provides information on the development of matrix models for machining error in multi-tool setups with spatially arranged tools, taking into account the simultaneous effect of all cutting forces from all tools in the setup and the elastic deformations of the technological system in all coordinate directions. It is noted that these models were developed both for dimensional distortion models and scatter field models. The developed full-factorial dimensional distortion model for a dual-carriage setup allows consideration not only of planar-parallel movements of technological subsystems but also their angular displacements around reference points. The theoretical solutions obtained were tested and refined directly in the practice of machine-building plants across various industries. The results of this refinement included various methodological and regulatory recommendations, as well as the development of a methodology for determining the comprehensive compliance characteristics of the technological system — the coordinate compliance matrix and the angular compliance matrix.

Keywords: *multi-tool machining, matrix accuracy models, CNC metal-cutting machines, automatic and semi-automatic lathes, operation concentration, achievable machining accuracy, multi-tool machining accuracy theory, comprehensive compliance characteristics of the technological system.*

Introduction.

Equipment for Multi-Tool Turning Operations. One of the most important factors in improving the productivity of the technological process is the concentration of operations. The highest efficiency of operation concentration is achieved through its implementation in multi-tool setups [1-5]. A wide range of specialized equipment is currently being produced for organizing multi-tool setups. The most prominent in this regard is the group of turning machines, as turning operations offer the richest possibilities for organizing multi-tool setups.

The Utilization Level of the Technological Potential of Multi-Tool Machining in Machine Building. To determine the actual level of utilization of the potential capabilities of multi-tool automatic turning, N.D. Yusubov [2-4] conducted a special survey of 85 factories across 13 different branches of machine building. This survey was carried out through the “Manufacturing Technology” department of South Ural State University using documentation provided by the Central Bureau of Labor Standards of the Russian Federation (CBLS). It should be noted that this statistical data pertains to cam-controlled machines. Unfortunately, conducting a similar statistical survey for CNC machines was not feasible. The survey and subsequent analysis were conducted in two directions [2-4, 7-8]:

-the achievable level of operation concentration;

-the attainable machining accuracy.

Achievable machining accuracy. Statistics on machining accuracy on turret lathes (TL) for major types of work at leading machine-building plants [6] show a wide variation in the achievable accuracy on TLs. For example, when turning external grooves at the Volgograd Tractor Plant (VGTZ), the accuracy achieved is no higher than grade 13, while at the Minsk Automobile Plant (MAZ), the accuracy is grade 11.

The achievable accuracy level on turret lathes (TL) is limited to grade 11. However, the most common accuracy for nearly all types of work is grade 13-12.

As follows from the consolidated statistics on machining accuracy for the main types of automatic lathes across various branches of machine-building, turret lathes (TL) primarily operate within the range of grades 14-12. Grade 9 accuracy accounts for 1% of setups, and only the instrument-making industry provides 5% of setups for grade 9 accuracy. The chemical engineering industry, on the other hand, does not achieve accuracy higher than grade 12.

Figure 1 shows a diagram of the consolidated statistics on the achievable machining accuracy on turret lathes (TL).

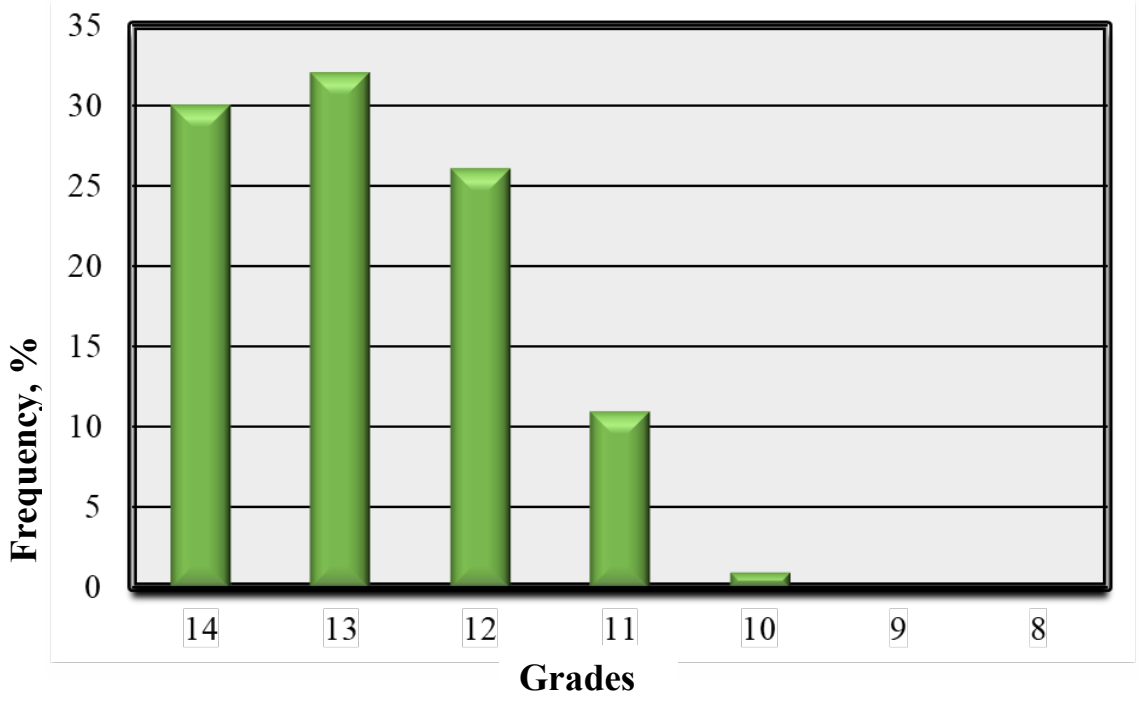

Fig. 1. Consolidated Statistics on Machining Accuracy on Turret Lathes

As can be seen from the diagram (Figure 1), turret lathes can typically achieve grade 10 accuracy, although the majority of the statistics fall within the 14-12 grade range. The analysis indicates that the potential capabilities of turret lathes are utilized to no more than half of their capacity.

Statistics on Machining Parts with Predominant Dimensions.

One of the tasks of the analysis was to determine the extent to which the capabilities of machining parts with predominant dimensions (L ≥3d) are utilized. Figure 2 presents the data from the statistical analysis of machining parts with different ratios of coordinate dimensions – lengths L and diameters D [2-4, 7-8].

The constructed diagrams show that machining parts with predominant dimensions is quite common, reaching up to 42% of cases (Figure 2) in turret lathe machining at leading machine-building plants and across major industries.

As can be seen from the diagrams, machining parts with predominant dimensions (L≥3d) is quite common. This is important for the formation of machining errors. In this case, even small rotational (angular) deformations of the part, which always occur during the cutting process, can cause noticeable distortions in the diametrical or linear dimensions.

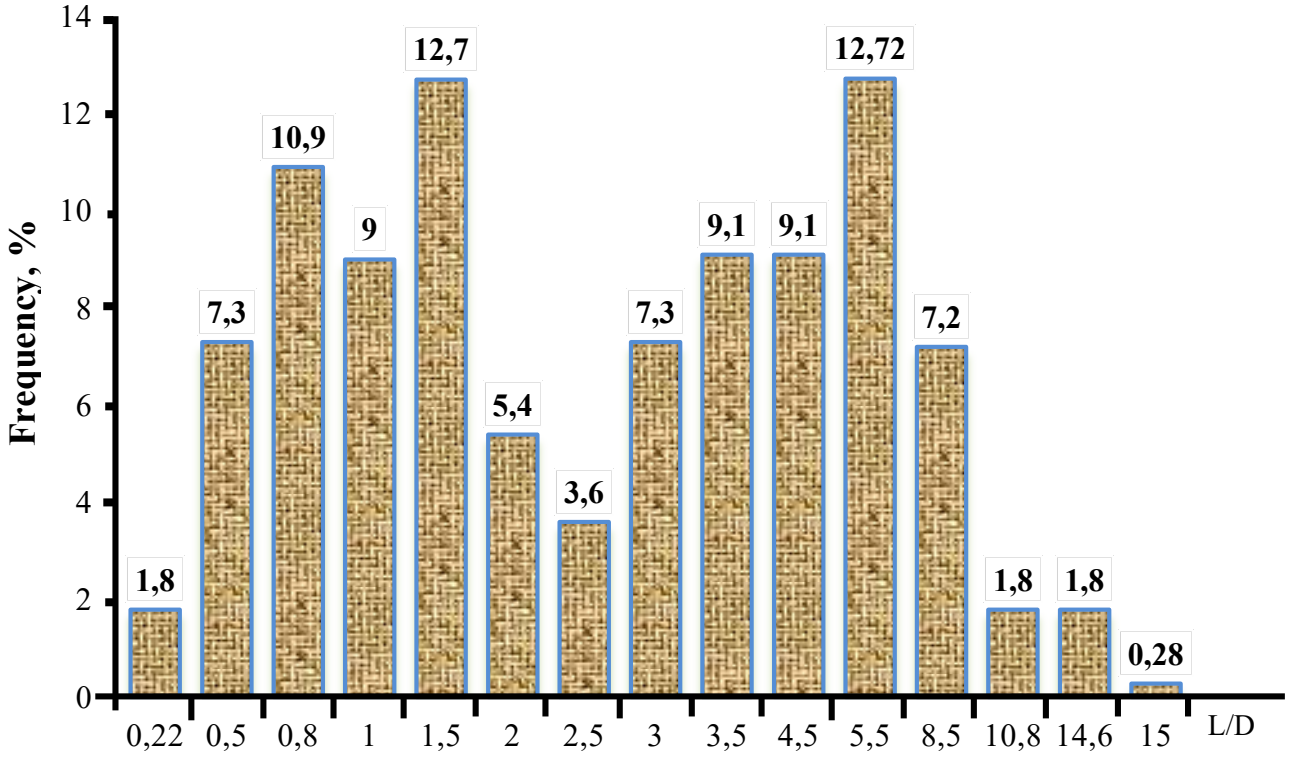

Fig. 2. Relative Frequency of Machining Parts on Turret Lathes with Different Length-to-Diameter Ratios [2-4, 7-8]

Statistics on multi-tooling. Multi-tool setups implemented on automatic and semi-automatic lathes can be divided into two types: single-carriage and dual-carriage setups [1-8].

In the first type of setup, several tools are positioned on a single carriage. In the second type of setup, one or more tools are placed on each position of the cross and longitudinal carriages.

When designing multi-tool setups, it is necessary to consider the organizational and force interactions between the tools in the setup. Modern cutting condition standards for turret lathe operations [9] take into account 11 types of multi-tool setups. However, in practice, there are many more types of multi-tool setups. As a result, most multi-tool setups are designed without regulatory support, based on subjective decisions. For scientifically substantiated design of multi-tool setups, it is necessary to include a comprehensive list of the types of multi-tool setups used in the cutting standards.

For this purpose, a statistical analysis of the frequency of using multi-tool setups was conducted. The analysis considered setups for single-spindle automatic lathes (of nearly all brands) across various machine building enterprises within the Commonwealth of Independent States (CIS). The analysis of the frequency of single-carriage multi-tool setups was performed on 978 single-carriage setups. Multi-tool setups accounted for 26%. Following the approach of A.A. Koshin [1], it is proposed to divide all single-carriage multi-tool setups into elementary and combined types. Elementary setups have two tools on the carriage, while combined setups have more than two tools. Among single-carriage multi-tool setups, the usage frequency of elementary setups is 98.4%, and combined setups account for 1.6%. A total of 38 types of elementary setups can be identified. Among combined single-carriage multi-tool setups, the following 19 types are frequently used. In the overall statistical analysis of multi-tool setups, dual-carriage setups accounted for 44%. Here as well, it is proposed to divide all dual-carriage setups into elementary and combined types. In elementary setups,

one tool is placed on each carriage, while in combined setups, more than two tools are used. Among dual-carriage setups, the usage frequency of elementary setups was 74%, and combined setups accounted for 26%. Based on the analysis conducted, it is proposed to identify 49 types of elementary dual-carriage setups.

Thus, the analysis showed that machining parts with predominant dimensions is quite common, where the load from the cutting tool in the form of a moment of forces applied to the part becomes significant. For example, grooving on the end face with longitudinal feed or facing the end face with longitudinal feed. In such cases, the moment generated by the cutting force significantly affects the magnitude of the part's radial displacement.

Moreover, setups frequently involve the simultaneous operation of an axial tool and another cutting tool. The axial tool serves as an additional support, ultimately increasing the part's resistance to displacement. Therefore, the calculation model should account not only for coordinate stiffness but also for rotational stiffness.

Dimensional-accuracy theory of multi-tool machining: Turret lathes, semi-automatic lathes, and especially modern CNC machines possess significant technological potential, both in terms of transition concentration and machining accuracy. Machines with turret heads or tool magazines allow the concentration of up to 20 transitions within a single turret-lathe operation. Multi-spindle machines can increase the transition concentration level to 30. Modern CNC machines in multi-tool setups can achieve machining accuracy up to the 8th grade [2-4].

However, the analysis of the utilization level of the extensive technological capabilities of multi-tool turret lathes revealed that the actual usage level for transition concentration is 63%, with machining accuracy remaining at the 14th–12th grades, and the number of tools in a multi-tool setup not exceeding four [2-4].

An even more challenging situation is observed with modern CNC machines. Multi-tool machining is only found in setups designed by the machine manufacturer during its delivery [2-4].

The extremely low utilization of the technological potential of modern CNC equipment is due to the complete lack of normative guidelines for designing multi-tool setups and assigning cutting conditions for such setups on this equipment. The 1989 normative reference book on cutting conditions for multi-tool turret lathe machining [9], developed under the guidance of A.A. Koshin, covers only traditional cam-operated lathes. The general engineering normative cutting conditions for CNC machines published in 1990 [10], under the guidance of V.I. Guzeev, address only single-tool setups.

There are no regulatory guidelines for multi-tool machining on CNC machines. Currently, the design of multi-tool setups on CNC machines relies on the intuition of the setup operator, and technologists often avoid such complex setups, failing to utilize the vast technological potential of modern CNC machines.

Thus, the primary prerequisite for solving this issue is the development of a design theory for multi-tool machining that takes into account the capabilities of modern CNC machines.

The foundations of the theory for designing and optimizing multi-tool machining, based on accounting for the force interaction of tools in a multi-tool setup, were laid in the works of A.A. Koshin [1]. However, he only considered two classes of the simplest planar multi-tool setups implemented on cam-controlled automatic machines.

The design aspects of machining on CNC machines for contour trajectory machining are explored in the works of V.I. Guzeev [11]. However, these works are dedicated solely to single-tool machining.

The theory for designing multi-tool machining on modern multi-carriage and multi-spindle CNC machines must be based on balancing the force interactions of tools in the setup. This includes accounting for the possibility of tool movements along curved trajectories and the arbitrary spatial arrangement of tools in the setup. Thus, the development of error models for machining in multi-tool setups with spatial tool arrangements is crucial. These models must consider the simultaneous effects of all components of cutting forces from all tools in the setup and the elastic deformations of the

technological system in all coordinate directions. For this purpose, the apparatus of analytical mechanics, which describes the elastic force interactions of a system of bodies in space and is based on matrix theory, proves to be convenient. Consequently, there is a need to develop a matrix theory of accuracy for multi-tool machining.

The development of a general theory of multi-tool machining is required, one that incorporates the setup structure at the level of initial data. It is this theory that should form the basis of the algorithmic support for technological design systems for modern CNC turning machines and their onboard computers.

To this end, a matrix theory of accuracy for multi-tool machining on modern multi-carriage and multi-spindle CNC turning machines has been developed, where for the first time a unified algorithmic model of machining errors has been created for the entire set of spatial multi-tool setups, taking into account the compliance of the technological system in all coordinate directions [2-4]. A unified generalized model has been proposed for distortions of performed dimensions, covering the entire range of multi-tool setups specified in the classification. A class of multi-tool setups is identified for scatter fields—homogeneous setups that allow an analytical representation of the model. For the first time, two different mechanisms for forming scatter fields within the class of homogeneous spatial multi-tool setups have been identified: opposite and co-positioned setups [2]. A full-factor model of dimensional distortion has been proposed for the first time, accounting for the compliance of the technological system across all six degrees of freedom, thereby enabling consideration of angular displacements in the technological system [2-4, 12-21]. For the first time, a stochastic simulation model of scatter fields in multi-carriage multi-tool machining has been proposed. This model reflects the probabilistic nature of error formation processes and encompasses the entire range of multi-tool setups, including non-homogeneous ones [2-4, 22]. Additionally, a comprehensive characteristic of the technological system's compliance has been introduced for the first time-each subsystem is represented by a set of two matrices [2-4, 23-24]:

- A coordinate compliance matrix, characterizing the subsystem's compliance along coordinate axes and their mutual influence;
- An angular compliance matrix, characterizing the resistance to rotations around coordinate axes and their mutual influence.

The description of a multi-tool setup using a system of loading vectors made it possible to define the structure of the setup at the level of the model's input data. This is fundamentally important for modern CNC machines, where the diversity of structures is difficult to classify.

Conclusions.

1. The foundation of the theory of accuracy in multi-tool machining consists of mathematical models of dimensional accuracy achieved by the tools in a multi-tool setup. Therefore, the current state of mathematical models for dimensional error formation in multi-tool setups is of particular interest.
2. Structural models of accuracy in multi-tool machining, reflecting the structure of the multi-tool setup and accounting for all major influencing factors, can serve as the foundation for a computational design theory of multi-tool machining.
3. Matrix models of accuracy in multi-tool machining on automatic lathes enable the prediction of machining accuracy under specified conditions (setup structure, properties of the technological system, machining conditions), thereby establishing a methodological basis for CAD systems in multi-tool turning operations.
4. The practical application of matrix models of accuracy in multi-tool machining on automatic lathes is reflected in the management and development of recommendations for cutting conditions, taking into account the setup structure for a range of standard multi-tool setups.

Funding Acknowledgements.

This work was supported by the Azerbaijan Science Foundation – **Grant № AEF-MGC-2024-2(50)-16/01/1-M-01**

REFERENCES

[1]. *Koshin* A.A. *The theory of accuracy and optimization of multi-tool turning operations*. Abstract of the dissertation Doctor of Technical Sciences, Chelyabinsk, 1997.
[2]. Yusubov N.D. *Improving the efficiency of multi-tool processing on automatic lathes*. Abstract of the dissertation Doctor of Technical Sciences, Baku, 2009.
[3]. Yusubov, N.D. *Multi-tool machining on automatic lathes (Matrix theory of multi-tool machining accuracy on modern CNC lathes).* AV Akademikerverlag Gmbh & Co. KG / LAP LAMBERT Academic Publishing, Saarbrücken, 2013.
[4]. Yusubov, N.D. *Fundamentals of matrix theory of accuracy of multi-tool turning. (Principles and structure of the theory, design and management of multi-tool machining processes).* AV Akademikerverlag Gmbh & Co. KG / LAP LAMBERT Academic Publishing, Saarbrücken, 2013.
[5]. Yusubov N.D. O*ptimization of multi-pass machining based on the productivity criterion.* Monograph. Omni Scriptum GmbH & Co. KG / LAP LAMBERT Academic Publishing, Saarbrücken, 2014.
[6]. Koshin A.A. *Computational design of optimal turning automatic operations* // Automated Design of Turning Automatic Operations. Restricted, Chelyabinsk, 1987.- pp. 14-16.
[7]. Yusubov N.D., Bogatenkov S.A., Badalova B.B. *Features and Challenges of Multi-Tool Turning*. Proceedings of the 2nd International Scientific and Technical Conference "Problems of Metallurgy and Materials Science", 28-30 November, 2017, Baku, AzTU, pp. 340 - 346.
[8]. Yusubov N.D., Bogatenkov S.A., Badalova B.B. *Study of Technological Capabilities of Multi-Tool Turning on CNC Lathes*. Proceedings of the International Scientific and Technical Conference on "Measurement and Quality: Problems and Perspectives". 2018, Baku, AzTU, November 21-23, pp. 128- 134.
[9]. *General engineering standards for cutting time and modes for automatic turning operations*. Part I-II., CBNT, Publishing House Economy, 1989.
[10]. *General engineering standards for cutting time and modes for standardizing work performed on universal and multi-purpose machines with numerical program control*. Part I-II. CBNT, Publishing House Economy, 1990.
[11]. Guzeev V.I. T*heory and methodology for calculating the productivity of contour machining of parts with various accuracies on CNC turning and milling machines*: Abstract of the dissertation … Doctor of Technical Sciences, Chelyabinsk, 1994.
[12]. Yusubov N.D. *Algorithmization of analytical model of dimensions stray field, executed in multi-tool multi-carriage adjustments.* Bulletin of Mechanical Engineering. 2008. No 2, pp. 54-56.
[13]. Yusubov N.D. *Matrix full-factor model of dimensional distortions in multi-tool setups*. Mechanical Engineering Technology, 2008, No 1, pp. 36-39.
[14]. Yusubov N.D., Abbasova H.M. *The fundamental principles of the mechanism for forming the scatter field of dimensions in dual-support setups*. Proceedings of the 2nd International Scientific and Technical Conference "Problems of Metallurgy and Materials Science", 28-30 November 2017, Baku, AzTU, pp. 375-380.
[15]. Yusubov N.D., Abbasova H.M. *The basic principles of the mechanism for the formation of scattering areas in the two-carriage adjustments*. / Machine science, Baku, 2018, vol. 7, No1, pp. 57-61
[16].Yusubov N.D., Abbasova H.M. *Generalized Segmented-Matrix Model of Multi-Tool Machining Accuracy*. Scientific works AzTU, No 4, 2018, pp. 16-22
[17]. Yusubov, N., & Abbasova, H. (2020). Models for Machining Accuracy in Multi-Tool Adjustment. International Journal of Automotive and Mechanical Engineering, 17(3), pp. 8067–8085. https://doi.org/10.15282/ijame.17.3.2020.01.0605
[18].S. A. Bogatenkov, N. S. Sazonova, V. I. Guzeev, N. D. Yusubov, and G. M. Abbasova. Increasing the Productivity of Multitool Machining on Automated Lathes by Optimizing the

Tool Positions. Russian Engineering Research, 2021, Vol. 41, No11, pp. 1075-1079.
[19]. Yusubov N.D., Abbasova H.M. Full-factor matrix model of accuracy of dimensions performed on multi-purpose CNC machines. Obrabotka metallov (tekhnologiya, oborudovanie, instrumenty) = Metal Working and Material Science, 2021, Vol. 23, No. 4, pp. 6-20. DOI: 10.17212/1994-6309-2021-23.4-6-20.
[20]. Nizami Yusubov, Heyran Abbasova. *Model of machining process control on multi-tool single-carriage adjustments*. Machine science, 2023, No 1, pp. 22-27
[21]. Nizami Yusubov, Heyran Abbasova. Models of cutting forces in the matrix theory of multitool machining accuracy. Key Engineering Materials, 2024, Vol. 979, pp. 27-38.
[22].Koshin A.A., Yusubov N.D. *Imitative stochastic model of fields of dissipation of the sizes executed in multi pockets of multi tool plate settings up adjustments*. Scientific works AzTU, 2007, No 1, pp. 32-35.
[23].Yusubov N.D. *Experimental determination of the static matrix characteristic of the compliance of a technological system*. Machine Builder, 2007, No 10, pp. 39-41.
[24].Yusubov N.D. *Statistical evaluation of the comprehensive compliance characteristic of a technological system*. Mechanical Engineering Technology, 2007, No 4, pp. 70-73.

Received: 27.10.2024
Accepted: 12.12.2024

MACHINE SCIENCE

ISSN: 2227-6912
E-ISSN: 2790-0479

2024, № 2 Pages 42– 49

AZERBAIJAN METALLURGICAL INDUSTRY: CURRENT SITUATION AND NEW GOALS

Arif MAMEDOV[1,a], Agil BABAYEV[1,b], Mukhtar HUSEYNOV[1,c], Beture MUSURZAYEVA[1,d], Nizami ISMAILOV[2,e], Anatolii VERKHOVLIUK[3,f]

[1]*Azerbaijan Technical University*

[2]*Azerbaijan State Maritime Academy*

[3]*Physico-technological Institute of Metals and Alloys National Academy of Science of Ukraine*

E-mail: [a]*arif.memmedov@aztu.edu.az, [b]aqil.babayev@aztu.edu.az, [c]muxtar.huseynov@aztu.edu.az, [e]nizism@mail.ru, [d]beture.musurzayeva@aztu.edu.az, [f]anatoliiverkhovliuk@gmail.com

https://doi.org/10.61413/FBID1194

Abstract: The article analyzes the current situation and upcoming tasks of the Azerbaijan metallurgical industry. The activities of enterprises producing metal products in the country are assessed. It is noted that for the dynamic development of the metallurgical industry, a deep study of the mineral resource base existing in the territory of the Republic of Azerbaijan is required and it should be put into operation. In the near future, for the accelerated development of the metallurgical industry of the country, there is a mineral resource base, energy reserves, material and technical base, engineering and scientific and pedagogical potential. The tasks arising from the orders of the President of the country, stimulating the development of the metallurgical industry are shown and promising directions in this area are presented. The need to use local resources for the accelerated development of the metallurgical industry is noted. The industrial capacities of operating companies and plants are assessed, new goals are presented for them. At the same time, the article notes the acceleration of gold mining in the country and shows the ways of using their locations, liberated from the occupation of the Karabakh region. In recent years, in contact with the development of the non-oil sector, the order of the President of the country on the establishment of a steel production complex in Azerbaijan will determine the concept of sustainable development of the metallurgical industry. The article also provides information showing the dynamics of growth in the production of steel pipes, construction reinforcement and other products of ferrous metallurgy. A diagram is presented in the aspect of the prospective development of the ferrous metallurgy industry in Azerbaijan. The indicators of import and export in the Republic of Azerbaijan for ferrous metallurgy in 2002-2022 are given. It is noted that the metallurgical industry of the country will experience a new stage of development and in order to achieve new successes in this area, the development and implementation of innovative technologies are of great importance.

Keywords: *metallurgy, steel, ferroalloy, mineral resource deposits, new intentions.*

Introduction.

The state and development prospects of the metallurgical industry of Azerbaijan are always in the center of attention of specialists and the scientific and technical community of this industry. This, of course, is due to the important role of the metallurgical industry in the country's economy.

For example, in article [1], the metallurgical industry is characterized as one of the most profitable, dynamically developing sectors of the Azerbaijani economy.

The article analyzes the activities of the flagship enterprises of the metallurgical industry of Azerbaijan - Baku Steel Company LLC (BSC), Dashkasan Dashkesan ore enrichment OJSC, and also notes the great potential of industrial potential in Ganja and Sumgait. The capabilities of the Sumgait

Technological and Chemical Industrial Parks for the production of metal products are assessed. It is noted that at present, the main attention is paid to increasing the quantitative and qualitative indicators of the production of metallurgical products.

The article assesses the mineral resource base of the country, including the reserves of the territories liberated from occupation. It is noted that in the first half of 2023, Azerbaijan exported more than 90 thousand tons of ferrous metals and products made of them, and imported more than 600 thousand tons. The cost of imported metal products is 700 million US dollars. more than dollars. This indicator confirms that the development of high-quality steel and ferroalloy production by the country's metallurgical industry is a pressing scientific and technical task and can bring great technical, economic and social benefits.

In the article "Metallurgy is a priority direction of the Azerbaijani industry" [2] attention was paid to the issues of training metallurgical personnel in the country. It is shown that the metallurgical faculty has been operating at AzTU since the 60s of the last century. The article characterizes with irrefutable facts the fact that metallurgical production in Azerbaijan has an ancient history.

The authors associate the development of the metallurgical industry in Azerbaijan with the efforts of the national leader H. Aliyev. Within the framework of the comprehensive program for the development of the metallurgical industry of Azerbaijan, large production areas have been created in Sumgait, Ganja, Dashkasan and Gadabay. Thanks to the initiative of H. Aliyev, the huge plant "Baku Steel Company" began operating in 2001; this plant is the largest industrial enterprise in the Transcaucasus.

It is shown that the President of the country Ilham Aliyev pays great attention to the development of the metallurgical industry in the country. In recent years, the Sumgait Technopark, Chemical-Technological Park, Industrial Parks and microdistricts have begun to operate in the regions, turning the production of metal products into the leading direction of the non-oil sector. The article notes that the country has all the necessary factors for the rapid development of the metallurgical industry: mineral resource base, energy resources, material and technical base, engineering and scientific-pedagogical personnel potential.

Current status and goals of the metallurgical industry of Azerbaijan.

The metallurgical complex, which is planned to be built in the Ganja region, envisages the processing of 5 million tons of ore and the production of 1 million tons of high-quality steel based on Dashkasan iron ore. It is expected that 2500 people will work at this enterprise, and this will be a great contribution to the development of the regions.

At the same time, the Azerbaijan Technical University and the Metallurgical Faculty face important tasks to ensure the sustainable development of the metallurgical industry.

In the article entitled [3] - Metallurgical industry of Azerbaijan: achievements, problems and future development paths, it is noted that at present there are good opportunities for the development of the metallurgical industry of Azerbaijan. The author emphasizes that the metallurgical industry of Azerbaijan has a rich history, and in support of his opinion, he mentions the exceptional role of Azerbaijani Chingiz Yildirim in the construction of the Magnitogorsk Iron and Steel Works in Russia.

The author notes that the development of the metallurgical industry in Azerbaijan in modern times is closely connected with the company "BSC", Founded by the National Leader G. Aliyev. It should be noted that at present this enterprise produces up to 800 thousand tons of metal products and meets almost all the needs of the country's construction sector.

Currently, the author points to the decree of the president of the country on the establishment

of the "Azerbaijan Steel Production Complex" as a factor that will give a great impetus to the development of the metallurgical industry of the country [4]. According to this decree, the development of metallurgy is associated with the launch of the Dashkesan Oil Refinery OJSC, the start of operations of AzerGold CJSC, as well as the planning of the design and construction of a steel production facility with a capacity of 1 million tons in Ganja.

Aluminum plants in Ganja and Sumgait, the Sumgait Technological Park, the Chemical-Technological Park and other enterprises producing metal structures confirm that the country's metallurgy has great potential and development prospects.

In his work [3] he identifies 10 areas that will ensure the future development of the metallurgical industry:

- create production of non-metallic products and special alloys;
- create production of hard alloys and superhard materials to meet the republic's needs for various tools;
- create production of lightweight and durable composite and ceramic materials using SPS and injection molding technologies;
- reconstruct foundries and workshops in the republic using special casting methods to improve productivity and quality;
- create technological processes that improve the quality of alunite ore to meet the needs of the aluminum plants in Ganja and Sumgait;
- create a special independent organization engaged in the research and application of nanotechnology and functional coatings;
- build a new plant for the production of abrasive materials and products made from them to meet the needs of the republic;
- create a special scientific and technical center dealing with the problems of the metallurgical industry;
- in connection with the rapid development of the gold mining industry, to accept students in the specialty "Jewelry" at AzTU;
- develop a technology for the synthesis of nanosized aluminides, borides and hard alloys using the IPS method.

According to the author, the solution of the above-mentioned problems will allow achieving real technical and economic efficiency and developing innovative metallurgical technologies and materials science in our country.

Article [5] is devoted to the metallurgical industry of Azerbaijan and its development prospects.

The article states that the country has enough raw materials, equipment and engineering potential for the development of the metallurgical industry. Iron ore in Dashkesan, non-ferrous metals in Filizchay, Katekh, Kashdag, Mehmanly and Nakhchivan - deposits of aluminum, cobalt, copper, zinc, lead, as well as bentonite clay deposits in Dashsalahly are striking proof of this.

Then, article [5] examines the historical past of metallurgical industrial enterprises of Azerbaijan and assesses the potential opportunities of today. It is noted that Baku Steel Company (BSC), which produced 100000 tons in 2001, 250000 tons in 2008, 400000 tons in 2010 and 800000 tons in 2020, is currently expanding its production capacity. It is planned to increase it to 1. million tons. It is shown that at the time of the launch of BSC in 2001, it employed 400 people, and today MMK employs up to 3000 people.

The article notes that President Ilham Aliyev pays great attention to the non-oil sector,

especially the rapid development of the metallurgical industry as a priority. In one of his speeches, the President stated: "**... the creation of a powerful metallurgical industry is on our agenda, and we will do it.**"

The article estimates the reserves of Dashkasan ore deposits at 350 million tons, and the reconstruction of the Dashkasan Mining and Processing Plant and direct recovery of iron from ore are assessed as priority tasks. By the way, the non-ferrous metals and ferroalloys plant, commissioned in 2014, creates broad opportunities for the sustainable development of the country's metallurgy.

Sources [6,7,8] explain some information about the activities of AzerGold CJSC, established according to Decree No. 1047 of the country's President Ilham

Aliyev dated February 11. 2015.

It is shown that AzerGold JSC began gold mining in 2009 at the Gadabay deposit, in 2013 it was mined at Gosh, in 2015 at Kadyr, in 2017 at the Ugur deposit. In 2016, gold mining began at the Chovdar deposit. In 2017, the company produced 6390.8 kg of gold, worth $77340 million. In the first half of 2018, gold production was 2081.7 kg, up 20% from the previous year. In 2019, production was approximately $20 million.

These sources indicate that since 2009, AzerGold has been increasing gold production by approximately 18-20% annually. Such growth rates confirm that the mineral resource base of the country's non-ferrous metallurgy has quite a strong potential. [6] The largest metallurgical enterprises of Azerbaijan are listed: Sumgait Aluminum Plant (SAP), DetAluminium LLC, Ganja Clay Plant, Baku Steel Casting JSC, Baku Steel Company LLC, Azerboru JSC, Global Construction JSC, Atahan Demir Industry JSC, Dashkasan Ore. Affinage OJSC, ElMetal OJSC, Non-Ferrous Metals and Ferroalloys Plant, etc.

The Internet resource [8] entitled “Metallurgy in Azerbaijan” (15.06.2010) notes that there are broad opportunities for the development of the metallurgical industry in the country:

1. Availability of an abundant and diverse base of raw materials and metal waste.
2. Local energy resources – availability of oil and natural gas.
3. Availability of industrial and construction sites with high metal capacity.
4. Availability of experienced personnel and labor resources.
5. Possibility of creating new production areas based on the existing material and technical base.

Thus, the issues of development of ferrous and non-ferrous metallurgy industry in Azerbaijan are constantly discussed in the country's press, periodical scientific and technical sources and Internet resources, which confirms the relevance and practical significance of the problem under study.

The information we received from Internet sources was briefly explained in articles [9-14]. Scientific article [15] ("Ferrous Metallurgy Industry in Azerbaijan: Development Stages and Prospects" (i.e. "Azerbaijan Tax Journal of Professor Hajizade E.M.", No. 2, 2014) is a study that requires special attention. Let us comment on its main points.

[15] confirms that the ferrous metallurgy industry occupies a leading position in the economy of all countries. Azerbaijan's ferrous metallurgy is also important in this sense and has a certain history, traditions and great potential.

In the context of the development of the non-oil sector in recent years, the article highly appreciates the Decree of the President of the country on the establishment of the Azerbaijan Steel Complex [16]. It is noted that the Dashkasan iron ore reserves with a reserve of 230 million tons are the basis of the concept of sustainable development of the metallurgical industry.

The article analyzes the historical aspects and production characteristics of the ferrous metallurgy industry for the first time. It is shown that out of more than 110 known chemical elements, up to 80 are metals. Iron is the 4th most common element on earth, iron ore reserves in the world are estimated at more than 200 billion tons. About 90% of all metal-based materials are iron alloys (steel and cast iron).

The article shows that in the 20th century, the ferrous metallurgy industry has undergone great technical progress and currently has successful development prospects. Then, the main trends in the development of the global ferrous metallurgy industry are examined. It was noted that according to statistics, 2 billion people currently live in the world. tons of steel are produced, and 1 billion tons of it. More than a ton comes from the People's Republic of China.

According to the author, a number of trends have formed in the development of the ferrous metallurgy industry in the world:

1. Transfer of metallurgical production to coastal areas - this is aimed at increasing the efficiency of transportation.

2. Transfer of steel production to developing countries - here cheap raw materials, human resources and environmental factors are taken into account.

3. Application of new methods of steel production - electrometallurgy and direct reduction of iron from ore - in order to increase the efficiency of production.

4. Creation of metallurgical enterprises of small production capacity (up to 1 million tons) - enterprises that mainly use recycled ferrous metal waste have more flexible technologies.

5. Increased demand for ferrous metal products.

6. Growing demand for special quality steels and alloys.

The article further analyzes the organization of the ferrous metallurgy industry of Azerbaijan and its modern development directions. The production activities and types of metal products of the Dashkesan Oil Refinery, Binagadi Steel Plant, Central Electrofoundry, Baku Metallurgical Company, Azertechnoline, non-ferrous metals and ferroalloys plants and other large metallurgical enterprises are studied. [17]-a graph is provided reflecting the dynamics of production of steel pipes and construction reinforcement in Azerbaijan in 2003-2022 (Figure 1).

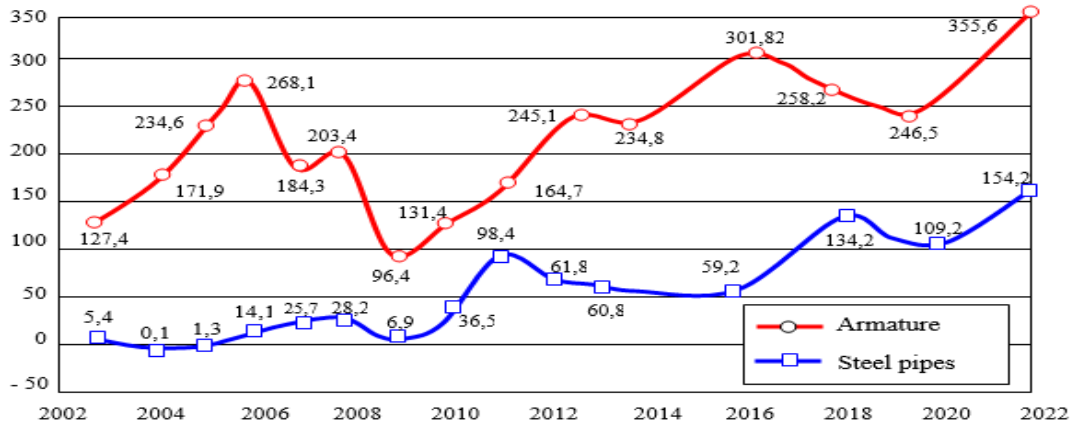

Figure 1. *Production of steel pipes and construction fittings in 2003-2022 (thousand tons)*

Table 1 below shows the production dynamics of other ferrous metallurgical products in Azerbaijan during that period.

Table 1. Production dynamics of other ferrous metallurgy products in Azerbaijan in 2012-2022.

Products	Unit of measure	2012	2014	2016	2018	2020	2022
Steel castings	thousand tons	256,4	286,1	306,5	379,1	444,2	552,4
Ferrous metal wire and coils	tons	483,6	499,8	501,7	598,8	523,2	584
Carbon steel cold-rolled profiles	tons	8891,7	10380,3	11875	11982	12839	21801,6
Various cold-worked stainless steel profiles	tons	0,0	0,0	9153,3	10732,1	17824,8	19034,3
Cast iron castings	tons	9631,7	11166,2	21836,5	23692	31631,2	41972,6

Taking into account the above, the author proposed the perspective development scheme of the ferrous metallurgy industry in Azerbaijan as follows (Figure 2).

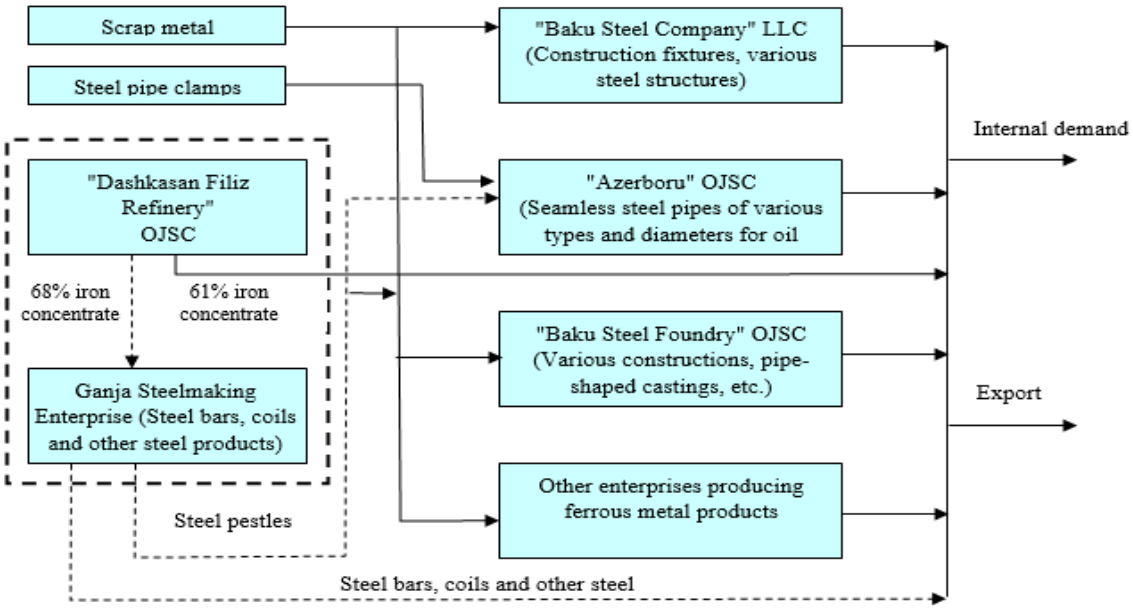

Figure 2. Prospective development scheme of ferrous metallurgy industry in Azerbaijan

3. The level of import and export of metal products of the country

It should be noted that the Baku Shipyard, which is currently working at full capacity, creates an important basis for the development of the production of steel sheets. Thus, the plant consumes about 25-30 thousand tons of steel sheets per year to fulfill shipbuilding orders, and this amount of steel products is imported only from abroad.

In general, referring to the website of the State Statistics Committee of the Republic of Azerbaijan, it can be shown that during the year, 200 names, the total value of which is 1 billion. ferrous metal products are imported over USD. Table 2 provides statistical data on import and export of ferrous metallurgy products in the Republic of Azerbaijan during 2012-2022 [18].

In conclusion, it can be noted that the ferrous metallurgy industry in our country is experiencing a new stage of development. Ferrous metallurgy, being a real production sector of the country's economy, has the opportunity to increase its potential many times in the near future.

Table 2. Import and export indicators of ferrous metallurgy in the Republic of Azerbaijan in 2012-2022, tons.

Years	Products	Import	Export
2012	Ferrous metals	580900	512
	Ferrous metal products	497644	6152
2014	Ferrous metals	688 971	54 785
	Ferrous metal products	415 838	55 253
2016	Ferrous metals	652 544	264 232
	Ferrous metal products	237 661	9894
2018	Ferrous metals	861 857	307 120
	Ferrous metal products	560 544	203 920
2020	Ferrous metals	827 580	21 081
	Ferrous metal products	564 650	62 583
2022	Ferrous metals	976 859	63 203
	Ferrous metal products	519 220	62 561

4. Conclusions

1. A number of positive trends were observed in the development of the country's ferrous metallurgy. In the context of the development of the non-oil sector, the important role of the Decree of the President of the country on the establishment of the Azerbaijan Steel Production Complex was noted. Based on the concept of sustainable development of the metallurgical industry, the importance of launching the Dashkasan Mining and Processing Plant, which has rich mineral resources, was substantiated.

2. The main directions of development of the metallurgical industry with low metal intensity in the country were determined: production of non-metallic and special alloys, hard alloys and superhard materials; made of light and durable composite and ceramic materials; widespread use of special casting methods; application of deep ore enrichment processes; application of nanotechnology and functional coatings; production of abrasive materials and products, synthesis of nanosized aluminides, borides and hard alloys, etc.

3. It was determined that the country has ample opportunities for sustainable development of the metallurgical industry. Various raw material base and metal waste, local energy resources, large metal-intensive industries and construction sites, experienced personnel and labor resources, the possibility of creating new industries based on the existing material and technical base were assessed.

Acknowledgment

This work was supported by the Azerbaijan Science Foundation - **Grant No. AEF-MCG-2023-1(43)-13/01/1-M-01**

REFERENCES

[1] G. Huseynli. *What is the situation in the metallurgical industry of Azerbaijan, banco.az site // 17.10.23*

[2] H. Mammadov, S. Namazov, *Metallurgy is a priority area of Azerbaijani industry // Azerbaijan newspaper,* 2011, July 31, p. 4

[3] A. Mammadov, *Azerbaijan's metallurgical industry: achievements, problems and future development paths* // January 24, 2020.

[4] Decree of the President of the Republic of Azerbaijan on the establishment of the Azerbaijan Steel Production Complex, April 23, 2013 (No. 2875)
[5] R. Mammadov. *Metallurgical industry of Azerbaijan and its development prospects* // Xalq kazeti, 16.06.2012
[6] Wikipedia. *Black metallurgy. Nonferrous metallurgy. Gold mining.*
[7] Decree of the President of the Republic of Azerbaijan on the establishment of AzerGold Closed Joint Stock Company, February 11, 2015 (No. 1047).
[8] *Metallurgy in Azerbaijan*. 15.06.2010
[9] *Black metallurgy of Azerbaijan* (Russian d.). World of Science. ru, 2018.07.18
[10] "Home" (ing). www.bakusteel.com 2017-06-03
[11] "Azerbaijan: homepage" (eng). azerbaijans.com, 2018-07-15
[12] T. Huseynzade. *Independent Azerbaijan* (eng.). Republic.- preslib.az.
[13] "About AzerGold CJSC", azergold.az. 2018-07-17
[14] "Azerbaijan. Metallurgy, mining industry". polpred.com. 2018-07-18
[15] E. Hajizadeh. *Ferrous metallurgical industry in Azerbaijan: development stages and perspectives* // Azerbaijan Tax Magazine, No. 2, 2014, 1.2 ch.
[16] Official website of the President of the Republic of Azerbaijan - http://www.president.az
[17] Website of the State Statistics Committee of the Republic of Azerbaijan - http://www.azstat.org
[18] The website of Baku Steel Company LLC - http://www.bakusteel.com

Received: 19.09.2024
Accepted: 13.11.2024

MACHINE SCIENCE
ISSN: 2227-6912
E-ISSN: 2790-0479
2024, № 2 Pages 50– 58

FAILURES IN CENTRIFUGAL COMPRESSORS

Jamaladdin ASLANOV[1,a*], Tarlan FARAJOV[2,b]

[1]Research İnstitute"Geotechnological Problems of Oil , Gas and Chermistry"Azerbaijan State Oil and Industry University
[2] PhD Azerbaijan State Oil and Industry University, Baku, Azerbaijan

E-mail: [a*]tribo72@mail.ru, [b]tarlan.farajov@hotmail.com

https://doi.org/10.61413/FCBE3989

Abstract: Centrifugal flash gas compressors are mechanisms that convert the kinetic energy of gas into pressure energy, playing a crucial role in compressing and transporting associated gases in the oil and gas industry. These compressors operate on the principle of centrifugal force and are widely used in key industrial sectors. They are considered essential equipment for compressing and transporting gases in fields such as the oil and gas industry, chemical production, power generation, and cooling systems. Capable of handling high flow rates and large volumes, centrifugal compressors use impellers to increase the gas velocity, while the diffuser converts this velocity into pressure. As a result, gas compression occurs within the compressor, ensuring the continuous operation of industrial processes. Although centrifugal compressors offer high performance and durability, they can fail under certain conditions due to various reasons. Failures and breakdowns can lead to serious production issues, significant financial losses, and even safety risks. Let's now examine the causes of these compressor failures.

Keywords: *compressor, failures, wear, abrasion, corrosion, surge, dry gas seal, buffer gas.*

Failures and Breakdowns in Centrifugal Compressors

Centrifugal flash compressors are used to increase the pressure of gases and liquids through high-speed rotating rotors. Dynamic machines make use of rapidly rotating impellers to accelerate the gas to high speed. By changing the direction and decelerating the gas much of its kinetic energy is converted to pressure energy [2].

Centrifugal compressors use the same operating principle as centrifugal pumps. They can be single stage or multiple stages. A casing can have multiple rotors, but the casing can be one stage in a multi-stage process. The word "stage" usually refers to the stage in a process. The part of the centrifugal compressor that moves the gas is the impeller. The gas enters through the eye of the impeller and the rotating impeller accelerates the gas towards the outer rim. When the gas reaches the tip of the impeller blades it is at its maximum velocity and possesses the maximum amount of energy. As the gas leaves the impeller it is pushed into passageways called diffusers. The flow area in the diffuser is larger than that in the impeller so the velocity of the gas begins to decrease. This causes the gas pressure to increase. The diffuser converts the kinetic energy of the gas to increased pressure.

These compressors are highly efficient and have a wide range of applications, but certain failures (malfunctions) can occur in their operation. The main types of failures include [1]:

Wear and Erosion – Wear is one of the most common causes of failure in centrifugal compressors. High-speed rotating impellers and other mechanical parts are subjected to wear over time. This leads to reduced equipment efficiency, increased energy consumption, and eventually the need for extensive repairs. Erosion, on the other hand, results in material loss from parts that come into contact with the gas passing through the compressor. During the compression process, gas particles can erode the surfaces of the impeller and diffuser, which diminishes the compressor's

operational capability. (Fig. 1).

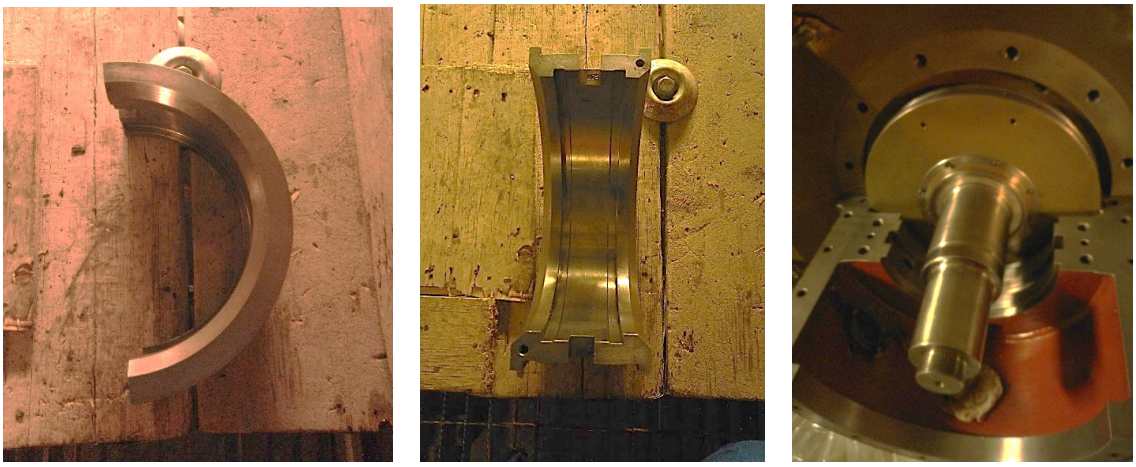

Figure 1. Friction Bearing Pads and Shaft

Failure of Bearings and Sealing System – Bearings used in compressors can fail over time due to high speed and loading conditions. Bearing malfunction leads to the disruption of the equipment's rotational balance and the formation of vibrations. This can also cause improper functioning of the impellers. A lack of lubrication, wear, or mechanical damage in the bearings can result in the compressor stopping. When the bearings do not function properly, the rotor becomes unstable, which can lead to serious malfunctions. [1]

Bearings: Describe different types of bearings (e.g., ball bearings, roller bearings) and their functions.

Sealing Systems: Explain types of seals (e.g., mechanical seals, O-rings) and their purpose in preventing contamination and fluid leakage.

Causes of Failure -Wear and Tear: Explain how prolonged use can lead to failure.

Contamination: Discuss how dirt, moisture, or foreign particles can damage the bearings and seals.

Improper Lubrication: Explain the effects of insufficient or excess lubrication.

Misalignment: How misalignment of components can increase wear and lead to failure.

Thermal Issues: Discuss the impact of excessive heat on bearing and seal performance.

Seals are crucial for preventing gas leakage. When seals fail, gas leakage can occur, leading to reduced efficiency, compromised safety, environmental pollution, and energy losses. Leaks in the sealing elements, valves, or pipes in the compressor system can result in pressure loss and decreased performance, which in turn also creates safety risks(Fig. 2).

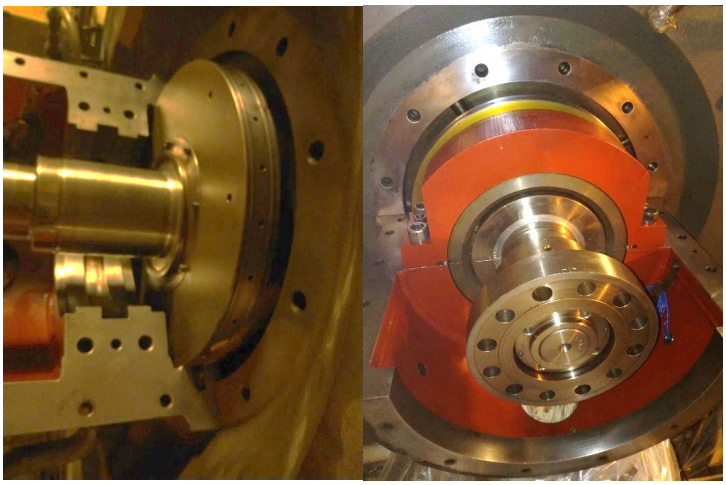

Figure 2. Dry Gas Mechanical Seals

Surge Instabilities and Resonance – If unstable flow conditions develop inside the compressor, this can impose additional load on the impellers. During hydrodynamic resonance, a mismatch occurs between the rotational speed and the flow velocity, which can lead to severe vibrations and malfunction of the mechanism. These issues often arise from design flaws or incorrect operating conditions.

Centrifugal compressors can enter a condition known as stall or surging under certain flow conditions. During stall, the flow stops in a specific part of the compressor, causing vibration and performance loss. Surging, on the other hand, is a malfunction characterized by periodic fluctuations in pressure during compressor operation, and it can cause significant damage to the compressor [2,3]

Vibration and Imbalance – Imbalance and vibration in high-speed rotating impellers are common issues. Vibrations can cause significant damage to the mechanical parts of the equipment, which not only reduces operational continuity but also increases repair costs. Imbalance typically arises from improper assembly of the impellers, material defects, or erosion. Disruption of rotor balance leads to vibrations in the compressor, which can damage both the compressor and the piping system. This situation occurs due to changes in the rotor's center of gravity, wear, or fractures. If the filtration systems are malfunctioning, dust or other contaminants can accumulate on the rotor blades. This results in rotor imbalance and reduced performance. High vibration can occur due to rotor imbalance, bearing issues, or resonance, which can damage mechanical components and cause the equipment to be out of 0 peration (Fig. 3).

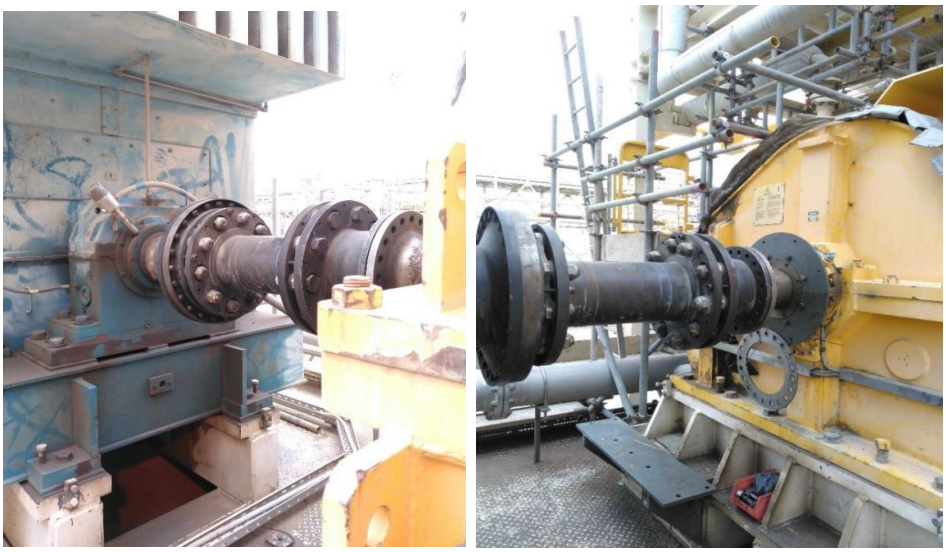

Figure 3. Gearbox and Compressor Shaft Transmission Coupling

Thermal Fatigue and Disruption of Thermal Balance – When centrifugal compressors operate at high temperatures, the thermal expansion of components may occur unevenly, leading to material fractures, cracking, or deformation. If a fault occurs in the compressor's cooling system, the temperature will rise, resulting in thermal fatigue. Thermal fatigue develops due to the repeated effect of high temperatures on components, which reduces the strength of the metal. [4,5]

Lubrication System Failures – Any malfunction in the compressor's lubrication system can have disastrous consequences for the bearings, rings, and other mechanical components. Without proper lubrication, friction increases, leading to the rapid failure of components and causing the equipment to stop(Fig. 4).

Figure 4. Lubrication System Failures

Preventive Measures:

Regularly monitor vibration levels, temperature, and pressure.

Perform routine maintenance and inspections for bearings, mechanical seals, and rotors.

Ensure proper filtration to prevent contamination.

Implement control systems to protect against surge damage resulting from sudden gas flow reduction.

Check and properly balance rotating components.

By implementing a strong maintenance strategy and utilizing condition monitoring systems, most of these failures can be detected early, preventing significant damage.

In this regard, the power consumed is determined by the characteristic optimal mode of the compressor unit, that is, the efficiency, temperature, nominal power and pressure distribution in stages, in accordance with the manufacturer's instructions. In this case, the degree of compression of the gas in the compressor cylinders in stages becomes normal, the consumed nominal power increases to 1350 hp. and the efficiency increases by maintaining the number of crankshaft revolutions at the level of 300 rpm. In practice, the operation of the GMC should be constant in such a mode, and in this case, the efficiency can be increased to 95÷100% in accordance with the technical instructions. At the same time, it should be taken into account that if the operation of the GMC in such a mode is constantly continued in gas lift and gas transportation systems, the wear limit in the friction areas of nodes and parts will be normal, premature wear will be eliminated and the unit's repair time will be extended. When the technical-technological-thermodynamic regime is violated in the operation of the compressor unit, the economic and energy regime of the unit is seriously violated, see table 5.

It is more clear from table 5 that if the clearance in the friction areas of the main nodes and details of the compressor unit exceeds the permissible clearance according to the manufacturer's instructions, the technical and economic indicators of that unit decrease. Of course, in such an operating mode, if the technical parameters of the lubrication system of the compressor unit do not comply with the manufacturer's instructions, wear increases and the number of idle stops increases in the event of an accident.

Therefore, engineers and technicians operating the compressor unit must constantly take into account that as the permissible clearances in the friction areas of nodes and details increase, the most important economic parameters of the units decrease significantly. This means that the reliability and efficiency of the compressor unit decreases, productivity decreases, and the cost of compressed gas

increases. It is known from mining practice that compressor units in GKS and SKS are often operated with changing loads. As a result, it can be said that frequent changes in the pressures of low-pressure side oil gas entering the compressor cylinders and high-pressure compressed gas at the outlet lead to a corresponding change in the number of crankshaft revolutions. As a result, difficulties arise in regulating the power and compressor cylinders, and ultimately, dynamic forces increase [6,7,8]. Therefore, as a result of the increase in dynamic forces in the compressor and power cylinders, the thermodynamic process in the cylinders is disrupted, and, accordingly, the normal operation of pistons, piston rings and valves is seriously changed. Therefore, as a result of the influence of dynamic forces in the compressor and power cylinders, the clearances in their nodes and details increase, and the probability of an accident increases. Therefore, the main technical and technological parameters of the operated compressor units must be maintained in accordance with the manufacturer's instructions, and a comparison of the distances that can be left in the wear areas of the nodes and details in the manufacturer's technical instructions with the practically measured distances is shown in Table 1 (several nodes and details are listed as examples):

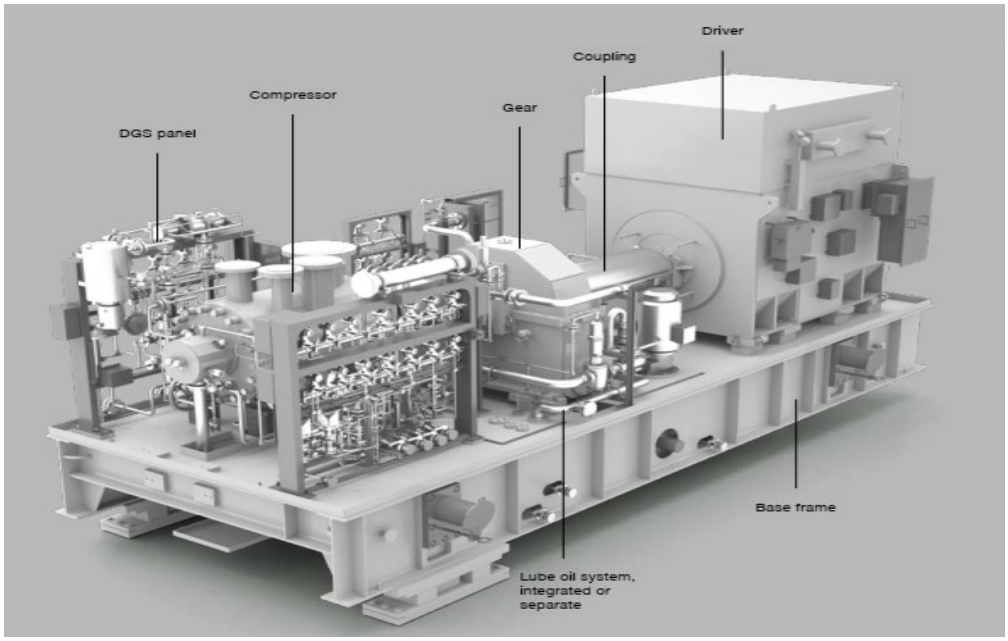

Figure 4. General Diagram of a Centrifugal Compressor

Table 1

№	Names of components and details	Allowable diametrical clearance, mm (normal)	Practical diametrical measured clearance	As a result of wea	
				Nominal power	Productivity
11	Distance between cylinder and piston of power cylinders	1,5	2÷2,5	8÷10% reduces	12÷15% reduces
22	Distance between cylinder and piston of 1st stage compressor	1,0÷12%	1,5÷1,8	10÷12% reduces	1,5÷1,8 reduces

Based on the conducted studies, it can be concluded that the selection of risers and their effective operation in wells depends on three main factors:

1) Despite the theoretical calculation, in production, the energy in the well is determined by a practical method, in addition to the correct and effective working agent (compressed high-pressure associated petroleum gas), and in the best case, with the help of oil to be produced according to the technological regulations;

2) The diameter of the risers should fully correspond to the maximum power of the protected oil production;

3) The depth of the compressor risers in the well should be as great as possible, and for this it is possible to install the f.i.e. of the risers.

It is known that the most widespread risers in the OGPD consist of two-row pipes:

1) Injection of compressed high-pressure gas;

2) Formation of the liquid with compressed gas. This also occurs with the main energy of the gas rising upwards.

The main reason for this is that the compressed high-pressure gas injected into the riser moves in the direction of the lowest pressure, that is, from the shoe to the wellhead.

During the movement of the gas-liquid mixture in the riser pipes to the wellhead, the pressure of the mixture must be such that it both overcomes friction in the distance from the point of formation of the mixture to the wellhead, and also overcomes any movement in front of it during its movement. At the same time, it is necessary to obtain that there is no exact calculation of the riser pipes in the central gas lift system.

During the operation of gas lift wells, small diameter pipes are selected to have a large annular area. Through these pipes, the injection of compressed oil-pressured associated gas is ensured at the gas lift compressor station. However, the diameter of the pipes cannot be reduced too much, as a very large pressure loss may occur. In mining practice, this is achieved by selecting the diameter of the riser pipes according to the operating column.

For this purpose, the dimensions of the riser pipes are taken depending on the diameter of the operating column and the depth of discharge. If the operating diameter is 203.2mm (8″), then the pipe for shallow penetration is 76.2mm (3″), for deeper penetration, 63.5mm (2.5″) or 50.8mm (2″), 1.4mm (6″) diameter increases the effect of only 50.8 (2″) pipes on gas lift wells. Now, for example, to ensure the optimal productivity of a gas lift well and the pressure in the well bottom zone in accordance with this productivity, the length of the riser pipes, the length of the riser pipes, the required daily supply of compressed high-pressure gas (working agent).

It is known in mining practice that when the gas factor of the formation decreases, it becomes very difficult to lift the fluid to be produced to the wellhead, and in this case, high-pressure associated oil gas compressed in an additional gas lift compressor station is injected from the wellhead to the bottom zone, and then, starting from the bottom zone, artificial oil production in the well passes into the fountain form.

As a result, the operating conditions in the gas lift riser pipes become the same as those of the fountain method, and this can be determined by the following formula [2,9]:

$$Q_{ef'} + R_{0.v.r.} \geq R_0 \text{„}$$

(1)

Here $Q_{e.f.}$ is the effective gas factor; $R_{0v.r}$ is the specific consumption of gas injected to the bottom of the well; R_0 is the specific consumption of the required gas.

The total efficiency of the compressor gas lift system is equal to the product of the total energy

of this system and the energy distributed in individual areas of the system [2]:

$$\eta_{k.q.s.} = \eta_{q.m.} \cdot \eta_{p.k.} \cdot \eta_{m.q.x.} \cdot \eta_{q.b.} \cdot \eta_{p.q.x.} \cdot \eta_{q.} \quad (2)$$

where $\eta_{k.q.s.}$ – efficiency of the compressor gas lift system; $\eta_{q.m.}$ – efficiency of the gas engine; $\eta_{p.k.}$ – efficiency of the piston compressors in the oil well; $\eta_{m.q.x.}$ – efficiency of the high-pressure main gas line in the field; $\eta_{q.b.}$ – efficiency of the battery distributing h_{igh}-pressure gas to the wells; $\eta_{p.q.x.}$ – efficiency of the gas distribution lines to the wells; $\eta_{q.}$ – efficiency of the gas lift unit.

For this, we assume the following data: well depth $H = 1470m$; formation pressure $P_1 = 66atm$, productivity factor $K = 6t/day \cdot \leftarrow atm$; allowable depression pressure, ΔP=16atm; diameter of the production casing $D = 7''$ (177.8mm); percentage of water with oil from the formation is 20%; specific gravity of oil $\gamma_h = 0.9$; relative specific gravity of water $\gamma_h = 1$; natural gas factor $G_0 = 50m^3/ton$; gas solubility coefficient corresponding to 1atm pressure, $a = 0.53m/t.atm$; gas working pressure $P_{i.t.} = 37.5atm$; P_y at the wellhead.

Using the data, let's determine the optimal productivity of the gas lift well [4,10]:

$$Q_{opt} = K \cdot \Delta p = 6 \cdot 16 = 96m/day \quad (3)$$

Knowing the optimal productivity of the well, we determine the pressure in the well bottom zone.

$$P_{q.d.} = P_1 - \Delta p = 66 - 16 = 50atm \quad (4)$$

Considering that the pressure in the well bottom zone is greater than the working pressure, then the length of the riser pipes is calculated not according to the depth of the well, but only according to the working pressure.

In this case, the length of the riser pipes is determined according to the working pressure as follows.

$$L = H - \frac{10(P_{i.t.} - P_b)}{\gamma} \quad (5)$$

Here, first, let's determine the pressure in the shoe (P_b). For this, it is known from mining practice that the pressure loss in the pipes, taking into account the assumption of $P_1 = 4atm$, should be subtracted.

Then, knowing the pressure loss, we determine the pressure in the shoe:

$$P_b = P_{i.t.} - P_1 \quad (6)$$

Then we determine the average specific gravity of the liquid mixture between the wellbore zone and the shoe of the riser pipes.

$$\gamma = \frac{\gamma_{q.d.} + \gamma_1}{2} \quad (7)$$

It should be noted that in the formula - is the specific gravity of the liquid, and we determine it as follows.

$$\gamma = \frac{80_\gamma + 20\gamma_b}{100} = \frac{80 \cdot 0{,}9 + 20 \cdot 1}{100} = 0{,}92$$

However, knowing that it is 20% water, the yield is found based on the liquid.

The diameter of the riser pipes is calculated as follows for the optimal well productivity regime:

$$d = 0.235\sqrt{\frac{1}{\varepsilon}} \cdot \sqrt[3]{\frac{Q}{(1-\varepsilon)\cdot\gamma}} \tag{9}$$

In this case, taking into account that gas is dissolved in oil and that oil contains 20% water, we determine the specific consumption of compressed high-pressure associated oil gas required to lift one ton of oil.

$$R_{0_{su}} = R_0 - \left[G_0^1 - \frac{a}{\gamma}\left(\frac{P_b + P_y}{2} - 1 \right) \right] \left(1 - \frac{\pi_b}{100} \right) \tag{10}$$

We determine the dynamic level that can be generated in the well, corresponding to the daily gas consumption:

$$h_0 = h - \frac{10(P_b - P_y)}{\gamma} = 1285 - \frac{10(34.5 - 1.2)}{0.92} = 923m$$

The report once again shows that other required parameters can be calculated in advance for each gas lift well in accordance with the technological regime predetermined by the geological and well development departments of the OGPD.

It is known from mining practice that the amount of product extracted from a gas lift well depends largely on the volume and pressure of compressed high-pressure associated petroleum gas injected into the well. This dependence varies depending on the depth of the risers, the depth of the pipes, the diameter of the pipes and the back pressure in the well discharge line.

Conclusions

Failures that occur during the operation of centrifugal compressors can lead to serious problems. Various mechanical, thermal, and hydrodynamic causes result in faults and breakdowns in compressor performance. Regular maintenance, balancing, and the application of proper operating conditions help prevent these issues.

Taking into account the above, in order to ensure the operation of compressor units in accordance with the instructions of the manufacturer, to improve their economic indicators and increase their reliability, it is proposed to carry out the following innovative technical and technological works at the N. Narimanov Oil and Gas Production Department's GKS and SKS:

1. By improving the low-pressure associated oil gas collection system, maintain the gas pressure directed to the GKS and SKS at a constant level of 4.2÷4.5 atm;

2. Deeply clean the internal surface and gas cleaning parts (metal meshes and plates) of the separator head units installed in the GKS and SKS once a year;

3. By fully restoring the operation of the separator head units, cleaning the low-pressure associated oil gas entering the 1st stage compressor cylinders from mechanical impurities, especially sand particles and large and medium-sized liquid hydrocarbon particles, it is possible to structurally protect the surface of the inner mirror part of the cylinder from deep scratches and abrasions;

4. Taking an oil sample from each operating GMC every two months and solving the issue of changing the oil in the crankcase by checking the mechanical mixture, water and at least its color change in the laboratory (if it is darkened);

5. Eliminating serious technical malfunctions that may occur by ensuring the distribution of gas pressures in the compressor cylinders in accordance with the manufacturer's instructions;

6. Maintaining the permissible clearances in the friction areas of the GMC, especially in the engine section, by constantly monitoring the lubrication pressure and oil temperature in accordance with the manufacturer's instructions;

7. At the intake of the 1st stage compressor cylinders of the gas turbine, by maintaining the pressure of the low-pressure associated oil gas at 4.2÷4.5 atm, ensure the overall productivity of the compressor unit in accordance with the manufacturer's instructions;

8. When the number of revolutions of the crankshaft in the gas turbine is less than the manufacturer's instructions, i.e. 260÷270 revolutions/min., the clearance in the friction areas of the nodes and details is 1.5÷2 times greater than the permissible norm. To prevent this, maintaining the number of revolutions of the crankshaft in accordance with the instructions (300 revolutions/min) increases productivity and is very profitable.

9. By maintaining the technical-technological-thermodynamic parameters of the gas turbine in operation in accordance with the instructions, it is possible to reduce the number of operating compressor units. As a result, the cost of compressed gas can be reduced.

REFERENCES

[1] Compressor site operating procedures, Man turbo manufacturer data sheet , https://www.man-es.com/oil-gas/products/compressors/centrifugal

[2] International Journal on Technical and Physical Problems of Engineering, 2023, 15(3), pp. 247–255

[3] The Influence of the Addition of Nickel on the Structure and Mechanical Properties of Aluminium Bronze Alloy

[4] J.N. Aslanov , T.U. Khankishiyeva , L.T. Huseynova, *"Study of physical processes created by sand grains in the working nodes of adjustable throttle",* Journal of Technical and Physical Problems of Engineering, Issue 1, Vol. 15, pp. 171–177, - Romania, 2023

[5] J.N. Aslanov, A.B. Sultanova, Z.S. Huseynli, F.F. Mustafayev, *"Determination of Radial Strains in Sealing Elements with Rubber Matrix Based on Fuzzy Sets"*, Conference of Theory and Application of Soft Computing, Vol. 362, pp. 765–773, Dorval, Canada, 2022.

[6] J.N. AslanovM. Mehdizade Z. Huseynli G. Hasanov L.Ibayeva G.Ağayeva *"Increasing the wear resistance of the impellers of electrical centrifugal submersible pumps through repair",* RGSA – Revista de Gestão Social e Ambiental vol.18.№11.pp1-20.2024

[7] Babanlı M.B., Mamedov G.A, Aslanov J.N.(2017). *Increasing Reliability of The Improved Machines and Equipment. Determination Of Productivity Criteria.* Bulletin of Environment, Pharmacology and Life Sciences journal, 5(12): 2277-1808

[8] O.S.Əsədov, V.İ.Əliyev, V.V.Makarov. *Новый научный подход к определению реальной производительности поршневых компрессоров в системах газлифта и транспорта газа.* – М.: издательства «Спутник» 2011, 240с.

[9] А.И.Акулсин, В.С.Бойко, Я.А.Зарубин, В.М.Дорошенко. *Эксплуатация нефтяных и газовых скважин.* – М.: «Недра», 1989, 474с.

Received: 24.07.2024
Accepted: 12.10.2024

MACHINE SCIENCE

ISSN: 2227-6912
E-ISSN: 2790-0479

2024, № 2 Pages 59-64

IMPROVING SURFACE QUALITY IN FLAT GRINDING OPERATIONS USING MODERN TECHNOLOGICAL METHODS

Sarvan AZIZ

Department of Machine Building, Azerbaijan Technical University, Baku, Azerbaijan

E-mail: sarvan.aziz@aztu.edu.az

https://doi.org/10.61413/XTTO3306

Abstract: The article analyzes general aspects of the flat grinding process, analyzes the main features, provides a technological solution to the issues of surface and surface layer formation, dimensional and shape accuracy. The main input parameters affecting quality are machine parameters, processing methods, grinding wheel and abrasive grain characteristics, cutting mode elements, etc. The degree of influence of factors, as well as strength and hardness indicators obtained from the physical and mechanical properties of the part material, in general, is analyzed and the pattern of quality formation is determined. Similarities and differences in operations performed on the side and periphery of the grinding wheel during flat grinding, as well as functional dependencies of productivity and quality indicators are determined. It is determined that to select optimal processing modes for flat grinding operations, it is considered necessary to control process parameters, use machines controlled by a modern digital program, and modernize other process equipment in terms of increasing quality. In the article, the general aspects of the flat grinding process are analyzed, the main features are analyzed, the technological solution of the issues of surface and surface layer quality formation, size and shape accuracy is given.

Keywords: *grinding, abrasive grain, hardness, roughness. dimensional accuracy, productivity*

Introduction.

In all areas of modern machine engineering, there is a high demand for parts with precise accuracy and quality. Achieving this quality requires the application of advanced technological processes, which is of particular importance. In this regard, abrasive machining operations, as a finishing process, ensure the required quality of machine parts. High-quality indicators not only involve improving the design, metallurgical, and metrological parameters, but also depend on the proper implementation of technological processes themselves. It should be noted that the demands of time are constantly increasing, and manufacturers are required to adopt more advanced machining methods, achieve high productivity, and ensure the profitability and competitiveness of enterprises, as well as meet environmental, occupational safety, and other conditions.

For many machine engineering companies, the grinding operation is considered the final finishing process. Through the application of this operation, high-precision machine parts with circular, flat, and complex surfaces are processed, and both dimensional and shape accuracy, as well as surface layer quality, can be brought to the required level.

Recently, more attention is being given to the grinding operation, and its technological capabilities are continuously being improved. The main aspect of this process is the possibility of automating and mechanizing these operations. In most manufacturing industries, especially in precision machining, the quality application of functional connections on planar surfaces, in line with the demands of time, is being increasingly utilized [1, 2]. However, there are still several

shortcomings in the grinding process, which is used to obtain precision planar surfaces with high accuracy, both in terms of micro-geometrical parameters and the high physical-mechanical properties of the surface and its layers. These shortcomings include problems related to the delivery of coolant-lubricant fluids to the contact zone, the uneven effect of abrasive particles on the surface, the generation of high heat during cutting, the removal of chips from the cutting zone, the clogging of the grinding wheel, etc. These undesirable factors remain unresolved aspects of the process. The listed issues negatively affect both the enhancement of the micro-geometrical parameters of the surfaces and the improvement of their physical-mechanical properties [3, 4, 5]. The complete elimination or significant reduction of these problems requires substantial scientific and research efforts.

The flat grinding process can be performed along the wheel's side and peripheral surface, each method having its own distinct advantages and disadvantages. Peripheral grinding is of higher quality compared to side grinding but is somewhat less productive. Depending on the geometric dimensions of the machine part, its configuration, the accuracy and quality requirements for the main working surface, as well as the type of machine and its technological capabilities, the operation can be performed either on the side or the peripheral surface.

Side grinding is applied for processing harder materials, while peripheral grinding is more suitable for processing softer parts. In general, it can be stated that the highest precision and surface quality are achieved in peripheral grinding [6, 7, 8]. The figure illustrates the impact scheme of the grinding wheel on the workpiece surface during a peripheral grinding operation. As shown in the diagram, abrasive particles have various physical interaction possibilities with the surface, and these interactions continuously change throughout the machining process.

The technological capabilities of modern CNC grinding machines have been significantly expanded, and the main kinematic parameters that define the fundamental motion scheme of flat grinding are as follows: the primary motion (rotation of the grinding wheel around its axis), the main feed motion (longitudinal movement of the grinding head), vertical feed motion or cutting depth (motion perpendicular to the grinding wheel surface), and lateral feed motion (movement of the grinding wheel parallel to the processed surface).

In addition to the machine specifications, the grinding wheels must also meet various requirements, such as high hardness, heat resistance, wear (fragmentation) resistance, impact resistance, multi-purpose use, and others [9, 10]. The abrasive materials used can be natural (quartz, corundum, etc.) or synthetic (electro corundum, boron carbide, nitrides, silicon carbide, etc.), and they are selected based on the machining method and the type of workpiece material.

As seen, the formation of the geometric parameters of the high-precision surfaces of the parts has a complex structure and must be carried out throughout the entire technological process. Compared to side grinding, peripheral grinding has a smaller contact area between the grinding wheel and the workpiece, which helps prevent excessive heat generation. Although the lower heat may complicate chip removal, it is considered a positive factor in terms of maintaining dimensional accuracy and machine settings.

Formulation of the problem. One of the key issues in ensuring quality in grinding is related to the process of grinding wheel conditioning. In this regard, modern, computer-controlled machines play a prominent role. The abrasive particles on the cutting surface of the grinding wheel have arbitrary shapes and placements, which, by creating different cutting angles, generate micro-cutting effects. In this context, each abrasive particle penetrates the surface to different depths; larger particles experience higher loads, while smaller particles are less loaded [11, 12]. As a result, microscopic observations of the chips show that their size and shape vary. Some abrasive particles are unable to

perform cutting; instead, they only cause plastic deformation of the surface, while very small particles do not make contact at all. Figure 1 illustrates the chip formation scheme during peripheral flat grinding [13, 14, 15]. As shown in the diagram, the thickness of the contact layer and the length of the contact result in the formation of chips in a "comma" shape.

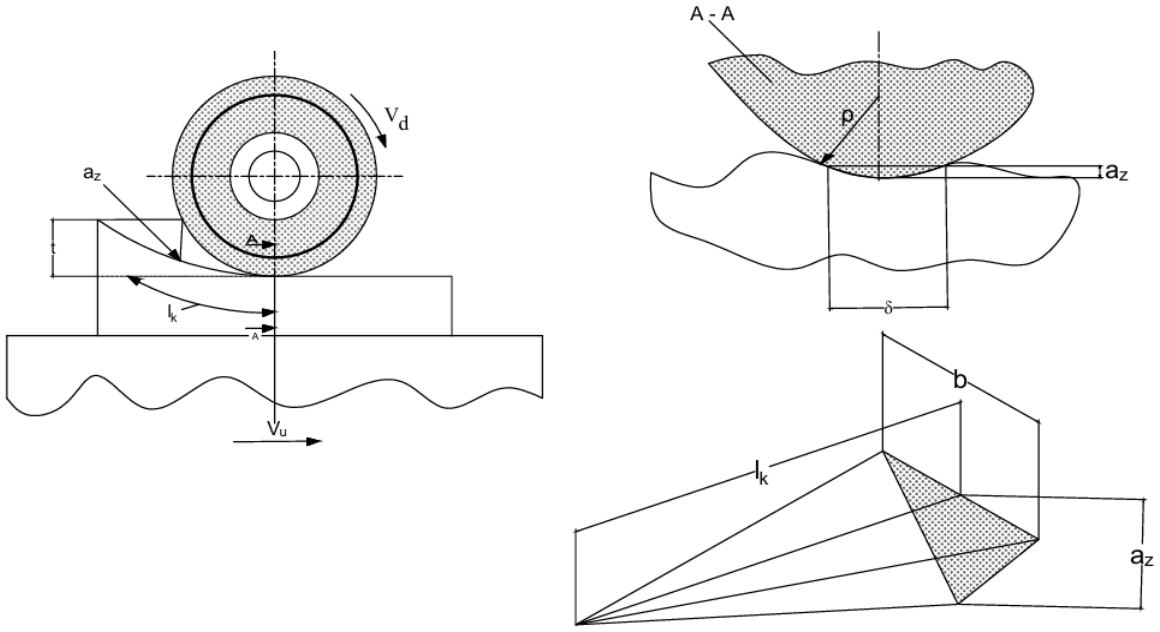

Figure 1. Chip formation scheme in peripheral flat grinding.

In flat grinding, the length of the contact between the workpiece and the abrasive wheel, denoted as l_k, is determined by the following expression:

$$l_k = \sqrt{Da_x} \tag{1}$$

Here, D is the external diameter of the grinding wheel (in mm), and a_z is the thickness of the cut layer (in mm).

If we simplify the "comma" shaped chip by approximating it as a pyramid with a triangular base, where the height is equal to the contact length lk, then the volume of the chip can be considered as the volume of the pyramid.

$$\omega y' = \frac{1}{3} a_z^2 \sqrt{2\rho D} \tag{2}$$

Here, ρ is the radius of the abrasive particle's apex (in mm).

The volume of the chip obtained from this expression can be used to determine the volume of material removed from the metal surface per minute, denoted as Q. This volume is related to the number of active abrasive particles (N_m) passing through the grinding zone and participating in chip removal during that time period. Thus, the material removal rate per minute is given by the ratio of the chip volume to the number of active abrasive particles involved in the cutting process.

$$\omega y' = \frac{Q}{N_m} \tag{3}$$

The minute material removal rate (Q) can be expressed in terms of the specific minute material removal rate (Q_{yd}), and the number of abrasive particles' apexes in a unit surface area of the circle

(N_z) as follows:

$$\omega y' = \frac{Q_{yd} H}{6 \cdot 10^4 N_g H V_d} = \frac{Q_{yd}}{6 \cdot 10^4 N_g V_d} \quad (4)$$

Here, V_d is the rotation speed of the wheel, in mm/min, and Hd is the width of the grinding wheel, in mm.

Assuming $\omega y = \omega y'$ (i.e., the angular velocity of the grinding wheel is constant), the final expression for the cutting thickness a_z (assuming it's small) would be as follows:

$$a_z = 33 \sqrt{\frac{Q_{yd}}{N_z V_d}} \cdot \sqrt[4]{\frac{1}{D\rho}} \quad (5)$$

Here:

Q_{yd} is the specific minute material removal rate (in mm^3/mm),

N_z is the number of active cutting tips of the abrasive particles per 1 mm^3 of the working surface of the wheel (in count),

D is the diameter of the wheel (in mm),

ρ is the radius of the abrasive particle's apex (in micrometers).

The graph shows the distribution of nonlinearity and non-flatness parameters formed during the processing of 33CrMoV12-9 steel using a CNC surface grinding machine model SGS-1632 AHD on a PP-250x20x76 machine with a typical 25A25PJM17K5P grinding wheel.

In surface grinding, the processing accuracy is characterized by the indicators of non-linearity (W_m) and non-parallelism (W_d). The theoretical and experimental results showing the dependency of non-linearity and non-parallelism (W_m, W_d) on the cutting depth (t) are presented in Figure 2.

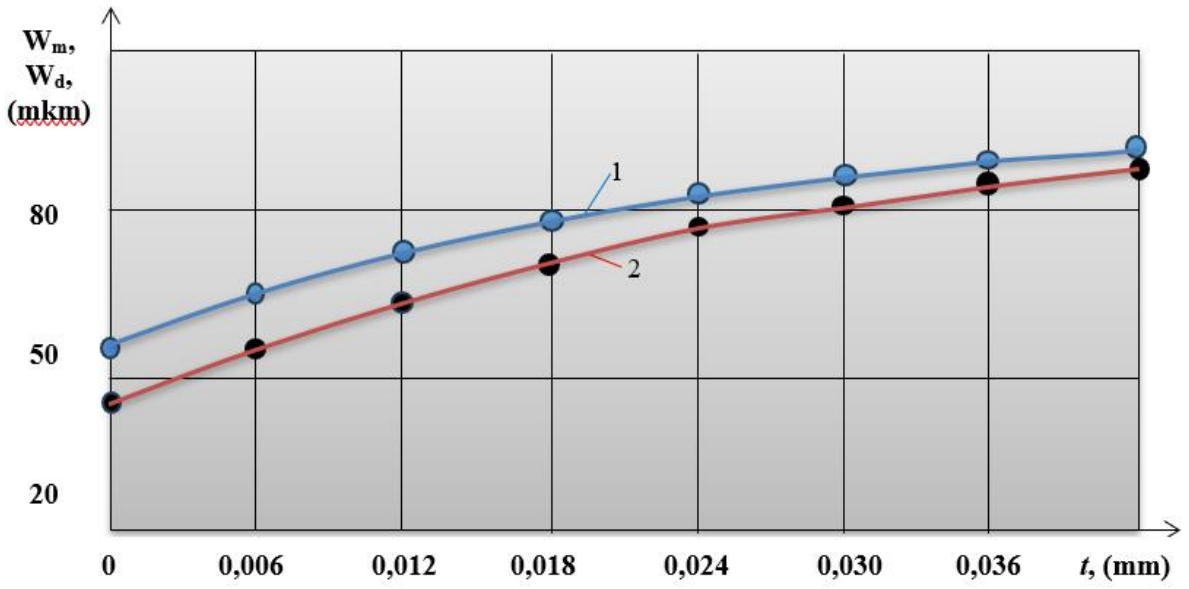

Figur 2. Graph of dependence of nonlinearity-1 and nonflatness-2 (W_m, W_d) on the cutting depth (t);

As with all mechanical machining processes, the cutting force in planar grinding depends on the physical and mechanical properties of the workpiece, primarily its hardness, the cutting parameters (such as cutting depth and feed rate), and other factors. As the cutting depth and feed rate increase, the cutting force also increases. However, when the cutting speed increases, the cutting force

decreases because the thickness of the material being cut by each individual abrasive particle decreases. Additionally, the type of grinding wheel and its technological characteristics have a significant impact on the cutting force.

The productivity of the operation Q (mm³/min) characterizes the working capacity of the grinding wheel. In the peripheral surface grinding process, the non-parallelism of the surface is influenced by the cutting regime elements. The empirical model for this dependency is as follows:

$$W_m = 144,32t^{0,65}V_1^{0,39}S_w^{0,51} \quad (6)$$

For the SGS-1632 AHD model CNC flat surface grinding machine, using 33CrMoV12-9 steel (Annealed HB Max.229) as per UNI EN ISO 4957:2002 standards (ISO 4957, developed by ISO/TC 17, Steel, Subcommittee SC 4), the following cutting conditions are applied during the machining of the workpieces:

- cutting depth - t=(0.006÷0.042) mm;
- longitudinal feed – V_l=(6÷18) m/min;
- lateral feed – S_w=(1.45÷6.25) mm/d.w.

The empirical model for the formation of surface non-parallelism in the peripheral flat surface grinding process, based on the cutting regime elements, has been derived from studies on grinding with a PP250x20x76-form grinding wheel of type 25A25PSM17K5P and grinding a 33CrMoV12-9 steel plate and the research has shown that the primary factor affecting non-parallelism is the value of the cutting depth.

$$W_d = 141,41t^{0,59}V_1^{0,41}S_w^{0,48} \quad (7)$$

It should be noted that the choice of grinding wheel characteristics is of particular importance:

- although a soft wheel has high cutting properties, the intensity of eating is also high;
- a solid wheel is poorly eaten, but quickly becomes dull and loses the ability to cut;
- for a hard tool, it is more advisable to use diamond and elbor wheels than electrocorundum-silicon carbide wheels.

Results and Conclusions. Based on numerous theoretical and experimental studies, it can be concluded that the surface quality in the planar grinding process depends on many factors that are functionally interconnected. There are various approaches to quality control, among which the most important are the application of modern technological methods and the use of next-generation technological equipment. To achieve a surface topography that is as close as possible to a plane after flat grinding, the elastic displacements of the system in both the width and length directions of the machining should be kept stable. Geometric shape errors typically manifest significantly in transverse cuts, especially at the zones where the grinding wheel makes contact with and exits the workpiece. The variation in the contact area at the entry and exit zones of the contact creates elastic displacements, resulting in non-linearity and non-planarity in the surface profile.

REFERENCES

[1]. Aziz S. Sh. *Characterıstıcs of qualıty formatıon ın processıng of 32CrMoV12-10 steel by honıng*, 2nd International Scientific-Practical Conference "Machine Building and Energy: New Concepts and Technologies", December 4-5, 2023, AzTU -Baku, Azerbaijan

[2]. Eziz, S. Sh. *Kinematic features of the lapping process and determination of its basic parameters* // − Moskow: Computational Nanotechnology, − 2020. №3 (Vol.7), − p. 11-16

[3]. Eziz, S. Sh. *Theoretical studies of the dynamic characteristics of the internal lapping process* // − Magnitogorsk: Vestnik of Nosov Magnitogorsk State Technical University, − 2020. №2 (Vol.18), − p. 30-37.

[4]. Gostimirović, M., Rodić, D., Kovač, P., Jesić, D., Kulundžic N., *Investigation of the cutting forces in creep-feed surface grinding process*, JPE (2015), Vol.18 (2),

[5]. Huseynov Hasan, *The Elaboratıon of system of the dıgıtal programmed control of grındıng process accuracy*. International Journal of Advances in Engineering & Technology, April., 2020. ©IJAET ISSN: 22311963Vol. 13, Issue 2, pp. 24-41

[6]. Mammadov A.S., Aziz S.Sh. *Study of the shape error of surfaces obtained after the plane polishing process*, SDU - Abstracts of the 49th scientific and technical conference, Sumgayit, 2006, 3 p.

[7]. Mamedov A.S., Aziz S.S., *Ways to improve accuracy in the process of flat polishing*, Baku: AzTU, -2006, pp.13-15.

[8]. Umid Yusif, Khalilov A.H., *Fundamentals of mechanical engineering technology*, Baku-1987, p.137

[9]. Yusubov N.D., Abbasova H.M. *Full-factor matrix model of accuracy of dimensions performed on multi-purpose CNC machines*. Obrabotka metallov (tekhnologiya, oborudovanie, instrumenty) = Metal Working and Material Science, 2021, vol. 23, no. 4, pp. 6–20. DOI: 10.17212/1994-6309-2021-23.4-6-20. (In Russian).

[10]. Yusubov N.D., Abbasova H.M. *Model of machining process control on multi-tool single-carriage adjustments* // MACHINE SCIENCE. - 2023.- № 1 – P. 22-27

[11]. Yusubov N.D., Abbasova H.M. *Models of Machining Accuracy in Multi-Tool Adjustments. International Journal of Automotive and Mechanical Engineering (IJAME)*. vol. 17, no. 3, pp. 8067-8085, Oct. 2020. Malaysia.

[12]. Yusubov N.D., Abbasova H.M., Dadashov R.Y. *Theoretical basis for the development of an algorithmic unified complex of mathematical models of cutting forces*// Machine Science. - 2023.- № 1 – p. 55-60.

[13]. Yaschiritsyn P.I., *Improving the quality of ground surfaces and cutting properties of abrasive diamond tools* / P.I. Yaschiritsyn, A.Q. Zaychev. – Minsk: Science and Technology, − 2012. – p. 210.

[14]. Filiminov L.N., *Flat grinding*, v-6, L-1999, p. 110

[15]. Rasulov N.M, Nadirov U.M, Alakbarov M.Z. *Improving the efficiency of grinding teeth by copyıng with the control of dynamic technological connections*. / SOCAR Proceedings. Special Issue 1 (2022) 029-035. DOI: 10.5510/OGP2022SI100697.

Received: 06.09.2024
Accepted: 22.11.2024

MACHINE SCIENCE

ISSN: 2227-6912
E-ISSN: 2790-0479

2024, № 2 Pages 65-76

MODELLING OF AUTOMATIC CONTROL SYSTEM ON AN ELECTRONIC MODEL

Alexey GRIGORIEV[1,a], Beyali AHMEDOV[2,b*], Viktor ARTEMYEV [3,c], Huseyin KAYA[4,d]

[1]Federal State Budgetary Educational Institution of Higher Education «Chuvash State Agrarian University», Chuvashia, Russia
[2]Azerbaijan Technical University, Baku, Azerbaijan
[3]Plekhanov Russian University of Economics, Moscow, Russia
[4]Bartin University, Bartin, Türkiye

E-mail: [a]grinjaa111@rambler.ru, [b*]ahmedov.beyali@aztu.edu.az, [c]artemev.vs@rea.ru, [d]hkaya@bartin.edu.tr

https://doi.org/10.61413/RSGZ7710

Abstract: This paper presents a detailed analysis of the dynamics of an automatic temperature control system using an electronic model based on a cascade representation of control objects in the form of aperiodic links. The system under consideration includes several stages of signal conversion an actuator, whose inertial link determines the rate of temperature change; and a thermocouple, which has its own inertia, affecting the accuracy and delay of the feedback signal. To stabilise the temperature, a proportional controller is provided, which ensures the adjustment of the control action depending on the deviation of the actual temperature from the set temperature. The authors of the paper consistently derive a high-order differential equation describing the dynamic behaviour of the entire system. It is based on the physical parameters of time constants and gain coefficients responsible for the inertia of the links and the relationships between them. By substituting specific numerical values for time constants T_1, T_2, T_3 and coefficients k_1, k_2, k_3, k_4, as well as for the given initial conditions initial temperature deviation and its derivatives, the final equation of motion is formed, which allows to evaluate the nature of the transient process. The nature of transient processes arising at sudden change of system parameters or at initial deviation of temperature from the desired level is determined. The analysis of the obtained equation and its solutions makes it possible to predict the monotonicity and oscillation of the transient process, to estimate the maximum temperature deviations and the time of reaching the steady-state mode.

Keywords: *control algorithms, simulation system dynamics, digital modeling, feedback management, optimization*

Introduction.

Modern industrial processes place high demands on the accuracy, stability and cost-effectiveness of automatic control systems. Temperature control of industrial furnaces is one of the key aspects of product quality assurance, requiring the use of advanced approaches to the design and tuning of control loops [1-2]. The increasing complexity of technological processes, the use of new materials and energy saving methods make it necessary not only to classically analyse the dynamics of such objects, but also to use more complex models including inertia, time delays and non-linear effects. With the increasing automation of production lines and the introduction of Smart Factory principles, it is becoming increasingly important to develop mathematical and electronic models that allow to study the behaviour of control systems without direct intervention in the

production cycle. This approach reduces the risks associated with the piloting of equipment, reduces time costs and speeds up the process of improving existing solutions [4]. The study of the dynamics of control objects is the representation of them as a cascade of standard links, each of which is characterised by certain parameters, time constants, gain and inertia coefficients, as well as possible delays. Decomposition significantly simplifies the modelling process, facilitating the choice of the controller structure and tuning of its parameters. The use of aperiodic links allows to take into account the key features of the object, the inertial response to changes in fuel supply, the furnace's own thermal inertia response to changes in the heating mode, as well as the inertia of the measuring sensor - thermocouple, which determines the accuracy and speed of providing information about the current temperature [5].

The aim of this paper is to carry out a detailed mathematical modelling of the automatic temperature control system of a furnace with a proportional controller, using a cascade representation of the object and analyzing transients under different initial conditions. In the process of research, it is proposed to obtain the final high order differential equation reflecting the dynamics of the system, and then, on the basis of its numerical parameters and solutions, to evaluate the nature of the transient process - to determine its monotonicity or the presence of oscillatory modes, to estimate the maximum temperature deviations, as well as the time of the system's exit to steady state.

An important stage in the consideration of such objects is the choice of an adequate mathematical model that allows to adequately reflect real physical processes, using aperiodic links with different time constants and transfer coefficients, each of which corresponds to a certain physical stage of energy conversion in the system. The first link reflects the dynamics of the actuator that regulates the fuel supply, the second - the reaction of the furnace to changes in the incoming energy, and the third - the inertia and time delay of the measuring device that provides temperature feedback [6-9]. The proportional controller is considered, which, despite its simplicity, is often used in practice due to its ease of adjustment and sufficient level of reliability. By adjusting the controller gain, it is possible to change the nature of transient processes, achieving a faster output of the system to a given temperature level while minimizing deviations and oscillations. The analysis uses fundamental methods of automatic control theory to transform the initial equations into canonical forms and to identify the key parameters that determine the dynamics of the system [10]. Numerical experiments and modelling allows you to quickly assess the impact of varying parameters on transients and theoretical foundations of automatic control with the practice of design and adjustment of systems.

Formulation of the problem.

Modern systems of automatic control of technological objects require adequate mathematical models that allow not only to describe the dynamic behaviour in a wide range of modes, but also to assess stability, quality of transients and sensitivity to parameter changes. In the context of furnace temperature control, it is necessary to have a model that takes into account the inertia of all key stages of energy conversion: from the actuator supplying fuel to the thermal capacity and dynamic properties of the furnace, as well as the inertia and lag of the thermocouple providing measurement of the controlled variable.

The main task of this work is to form a mathematical model of the automatic furnace temperature control system based on the cascade representation of the object in the form of several aperiodic links [11]. The model should take into account the influence of the proportional regulator, correcting the controlled variable based on the deviation of the current temperature from the set point. The goal is to obtain a final differential equation describing the dynamics of the entire system based on the given parameters of time constants and gains of the links, as well as the coefficient of

the proportional controller. It is proposed to divide the general control object into several aperiodic links, each of which characterises a separate stage of signal conversion. The first link describes the action of the actuator supplying fuel, the second - the actual thermal response of the furnace, the third - the inertia of the thermocouple measuring subsystem. The proportional controller will close the feedback loop. Express each of the aperiodic links in the form of first order differential equations with certain time constants and coefficients. Based on these equations, form a generalised mathematical model of the control object. By means of transformations, including sequential connection of links, obtain a higher-order equation reflecting the total dynamics of the system. This equation should include parameters defined by time constants T_1, T_2, T_3 and gain coefficients k_1, k_2, k_3, k_4. Set the initial conditions corresponding to the initial control error, the initial temperature deviation from the set temperature, and also establish that the initial time derivatives are equal to zero. Investigate the influence of the system parameters on the quality of the transient process. Determine under what conditions the fastest and most accurate steady-state output is achieved, overshoot and oscillations are minimized [12]. On this basis, to offer recommendations on the selection of proportional controller parameters.

The formulated problem is reduced to the mathematical description, analysis and evaluation of the dynamic characteristics of the automatic temperature control system on the basis of a cascade model with aperiodic links, with subsequent determination of the nature of the transient process for specific given parameters and initial conditions.

At the same time, the formulation of the problem is not reduced solely to the mathematical description. It is necessary to take into account the engineering aspect as well: the production of the obtained models on electronic models (for example, on a specialised hardware-software complex or in environmental conditions) should be convenient enough to allow the engineering practitioner to promptly conduct experiments ‘what will happen if...’. Which allows the consequences of changes in regulator or structural system parameters that were not originally set, to be tested, and safety and cost-effectiveness are enhanced in a virtual test bed environment [14].

An important practical criterion when considering the problem is the definition of target parameters of regulation quality. In industrial practice, one strives to minimise the transient time and reduce overshoot, the difference between the temperature reached during the run and the target temperature. In most cases, not only the accuracy of steady-state results, but also the speed of the system response to the perturbation may be important. Production is used in processes that require frequent reconfigurations or abrupt changes in production programmes, then the priority may shift towards the faster process, even if the overshoot is constantly expanding. Equations derived from aperiodic links work well when the system is close to linear conditions. The external climate object may be non-linear and the parameters may be a defence against temperature, fuel consumption and other factors. This task may also include assessing sensitivity to parameter variations, robustness in showing coefficients and analysing time delays, and validating results when moving into regions where the linear approximation becomes less accurate.

The formulation of the problem should also take into account the possibilities of computational technology. For numerical integration of high-order differential describing the system, it is possible to call sufficiently powerful computing resources or apply special methods of numerical solution, reducing computational costs and increasing the accuracy of calculations. Clear definition of the structural scheme of the control system including a series connected aperiodic links to describe the actuator, object and measuring sensor. Formation of a high-order differential equation linking the output quantity with the input control action and parameters of the proportional regulator. Selection of adequate initial conditions reflecting the real production situation, for example, the moment of switching on the system with some initial deviations from the set temperature and zero initial derivatives. Determination of transient quality, including regulation time, overshoot, possibly - integral quality indices. Consideration of physical regulation, parameter variations, non-linear effects and determination of sensitivity to these factors. Preparing the model

for numerical experiment and checking its correctness, verifying the results using analytical estimates and capabilities, comparing with experimental data or more detailed simulation models.

In the context of the problem statement, other aspects that influence the accuracy and practical applicability of the developed model must also be considered. One of the key difficulties is that a real industrial furnace may be operated under conditions that differ significantly from the idealised assumptions of the model. Uncontrolled external perturbations such as ambient temperature fluctuations, changes in fuel quality or instability in the power grid can affect the dynamics of the system. The problem formulation should provide for the possibility of supplementing the model with perturbing factors and assessing the stability of the solution to such external influences.

The coefficients and time constants of the links used in the model are not absolutely constant in reality. They may change over time due to aging of equipment, gradual contamination of working surfaces, wear of structural elements and other factors. In this regard, the problem may raise the question of the need for robust analysis or consideration of parametric uncertainty. This makes it possible to estimate how much the results obtained at nominal values of parameters will be stable to their variations, and will allow to identify the most critical parameters affecting the quality of regulation. In addition to the standard transient quality indicators, there are set-up times, overshoot, integral deviation indicators, and the fuel or power consumption required to maintain the desired temperature. The problem is extended to multi-objective optimisation, where trade-offs have to be made between speed and accuracy of control and the inclusion of non-linear effects in the model. At very high or very low temperatures, the material properties of the furnace or fuel can change non-linearly. In such cases, aperiodic linear links provide only an approximation of the real system. If the objective of the study is to obtain more accurate results, it is possible to involve nonlinear equations of state, which will considerably complicate the analysis, but will increase the adequacy of the model. In this case, the problem statement can be supplemented by mentioning linearisation methods applied to certain operating modes or by using numerical methods capable of detecting nonlinear effects and nonlinear steady or unsteady modes [16-18]. After theoretical derivation of the equations and numerical experiments, it will be necessary to compare the modelling results with data obtained from test tests of a real furnace or with already available industrial measurements. This approach will make it possible to determine to what extent the model reflects reality and, if necessary, to adjust its parameters or structure. The problem formulation is not limited to purely mathematical aspects, including experiments, verification and validation, as well as further refinement and improvement of models.

To represent an industrial furnace and its automatic temperature control system as a cascade chain of aperiodic links with a proportional regulator. On the basis of physical laws of heat transfer, properties of the actuator, furnace, thermocouple measuring sensor and regulator, make a differential equation describing the dynamics of the system. Determine initial conditions and select quality criteria for the transient process.

Analyse the influence of link parameters and controller coefficient on the nature of the transient process, including stability, monotonicity or oscillation of the solution, the magnitude of overshoot and the time of transition to steady state. Consider the possibility of external disturbances, parametric uncertainty and nonlinear effects, and evaluate the robustness of the results to variations in conditions and parameters. Provide for comparison of modelling results with experimental data to confirm the adequacy of the model, and, if necessary, correct the parameters or structure of the model. Such a detailed approach to the problem statement provides a comprehensive understanding of the problem, sets the direction for subsequent stages of research and creation of optimisation tools, as well as serves as a basis for practical application of the developed model in industrial conditions.

Solution of the problem.

Let us consider an example of modelling the system of automatic temperature control in the furnace working space, the structural diagram of which is shown in Fig. 1. The differential equation

for the error variation $x = X - X_0$, where X is the true temperature in the furnace in deg, and X_0 is the set temperature also in deg, is as follows

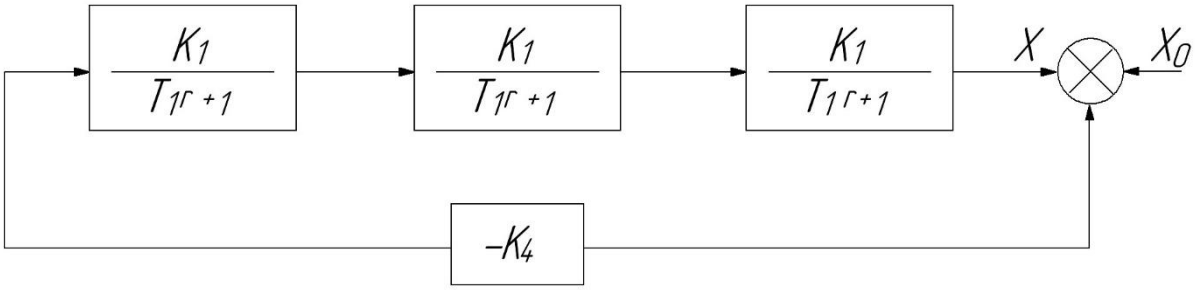

Figure 1. Multi-stage adaptive control system with negative feedback to stabilize the output signal in conditions of dynamically changing parameters

$$T_1T_2T_3\frac{d^3x}{dt^3}+(T_1T_2+T_1T_3+T_2T_3)\frac{d^2x}{dt^2}$$

The aperiodic unit with coefficient k_1 corresponds to the actuator feeding fuel to the furnace, the aperiodic unit with coefficient k_2 corresponds to the temperature of the furnace itself and finally the aperiodic unit with coefficient k_3 corresponds to the inertia of the thermocouple measuring the furnace temperature. The unit with coefficient k_4 corresponds to the proportional furnace temperature controller.

Let the parameters of the systems take the following values:

$$T_1 = 3\,\text{min} = 180\,\text{sec}, T_2 = 10\,\text{min} = 600\,\text{sec}, T_3 = 1\,\text{min} = 60\,\text{sec},$$
$$k_1 = 10(\frac{kg}{\text{min}\cdot V}), k_2 = 2(\frac{\text{deg}\cdot\text{min}}{\kappa 2}), k_3 = 0{,}1, k_4 = 2(\frac{V}{\text{deg}})$$

It is necessary to determine the character of the transient process at the initial value of the error

$$x(0) = 50\,\text{deg} \tag{2}$$

and zero initial values

$$x'(0) = x''(0) = 0 \tag{3}$$

Let us calculate the values of the coefficients in equation (1):

$$a_0 = T_1T_2T_3 = 3\cdot 10\cdot 1 = 30\,\text{min}^3 = 648\cdot 10^3\,\text{sec}^3$$
$$a_1 = T_1T_2 + T_1T_3 + T_2T_3 = 3+10+1 = 14\,\text{min} = 840\,\text{sec}$$
$$a_2 = T_1 + T_2 + T_3 = 3+10+1 = 14\,\text{min} = 840\,\text{sec}$$
$$a_3 = k_1k_2k_3k_4 = 10\cdot 2\cdot 0.1\cdot 2 = 4$$

Equation (1) takes the form

$$648\cdot 10^3\frac{d^3x}{dt^3}+1548\cdot 10^2\frac{d^2x}{dt^2}+840\frac{dx}{dt}+4x = 0 \tag{4}$$

$$x(0) = 50\,\text{deg} \tag{5}$$

To ensure high-precision signal processing in automated control systems, a combined structure of resistance and capacitance circuits is often employed. This type of design enables flexible management of filtering characteristics and suppression of unwanted signals. The diagram below illustrates a functional scheme of this kind, comprising resistors $R1, R2, ...R9$ and capacitors $C1, C2, C3$. Additionally, the scheme incorporates registers and operational elements, facilitating interaction with external recorders Fig. 2.

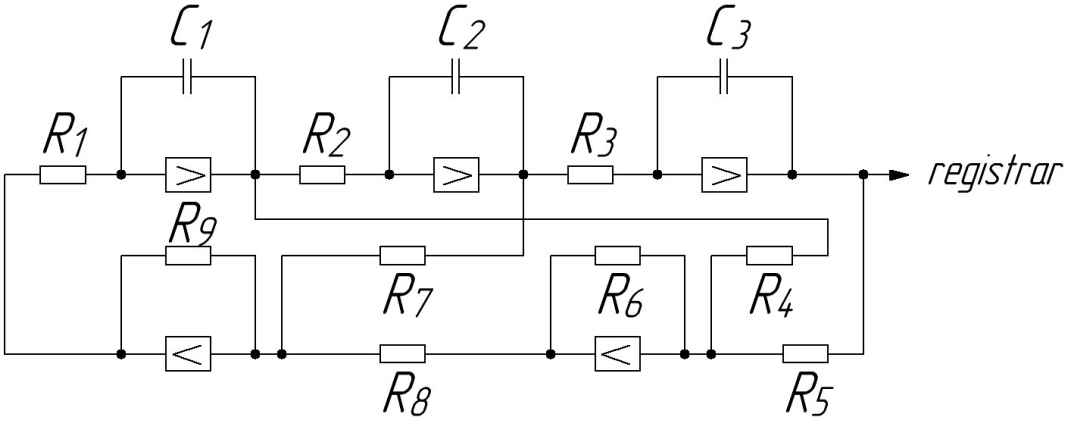

Figure 2. Multilevel parametric signal filtering scheme with nonlinear comparison nodes for dynamic adaptation to input impedance changes

At the initial moment of time, in order to increase the accuracy of the solution, it is necessary to use the whole range of output voltages of the solver amplifiers, equal to ±100 V.

Therefore, we take ξ as the machine variable ξ

$$\xi = kx \text{ or } x = \frac{1}{k}\xi \tag{6}$$

where $k = 2$ in grads and, hence, the initial value for ξ will be equal to

$$\xi(0) = 2.50 = 100\xi$$

One of the advantages of modelling on electronic models is that we can simulate slow processes on an accelerated time scale, which gives a huge gain in the time needed to investigate the processes.

As can be seen from the problem condition, the real transient process lasts tens of minutes. Taking the time scale of 1:100, we can define the transient process on the model 100 times faster than the real process. So, let's introduce the machine time τ by the formula

$$\tau = \frac{1}{100}t \text{ or } t = 100\tau \tag{7}$$

Thus, in the new variables ξ and τ the original equation (4) will take the form

$$\frac{648 \cdot 10^3}{100^3 \cdot 2}\xi''' + \frac{1548 \cdot 10^2}{100^2 \cdot 2}\xi'' + \frac{840}{100 \cdot 2}\xi' + \frac{4}{2}\xi = 0$$

or

$$0.648\xi''' + 15.48\xi'' + 84\xi' + 4\xi = 0 \tag{8}$$

Equation (8) after elementary calculations can be written in the form

$$-\xi''' = 24\xi'' + 130\xi' + 6.2\xi \tag{9}$$

This equation corresponds to the scheme of the electronic model shown in Fig. 3

In this scheme it is assumed

$$R_1C_1 = 1cet, R_2C_2 = 1cet, R_3C_3 = 1cer$$
$$\frac{R_6}{R_5} = 6.2, \frac{R_6}{R_4} = 14.3, \frac{R_9}{R_8} = 1, \frac{R_9}{R_7} = 130$$

The initial voltage on the capacitance C_3 is $\xi(0) = 100V$, the initial voltages on the capacitances C_1 and C_2 are zero, which corresponds to zero initial conditions on the first and second derivatives $\xi'(0) = \xi''(0) = 0$. Changes in voltage $\xi(t)$ are usually recorded on some recorder, such as a loop oscilloscope. The resulting oscillogram gives us full information about the nature of the variation in the deviations of the true oven temperature from the set point. In order to pass from the machine variables ξ and τ to the original variables x [deg] and t [sec], it is necessary to remember that

$$x = \frac{1}{2}\xi[\text{deg}]; t = 100\tau[\text{sec}]$$

In automated signal control systems, the proper configuration of filtering elements plays a crucial role in ensuring data processing with minimal losses. The presented diagram illustrates an advanced structure comprising resistors $R1, R2, \ldots, R10$, capacitors $C1, C2, C3$, and signal output points. This design enables efficient signal separation, optimization of processing, and seamless integration with external recorders. The structural diagram of such a model is shown in Fig. 3.

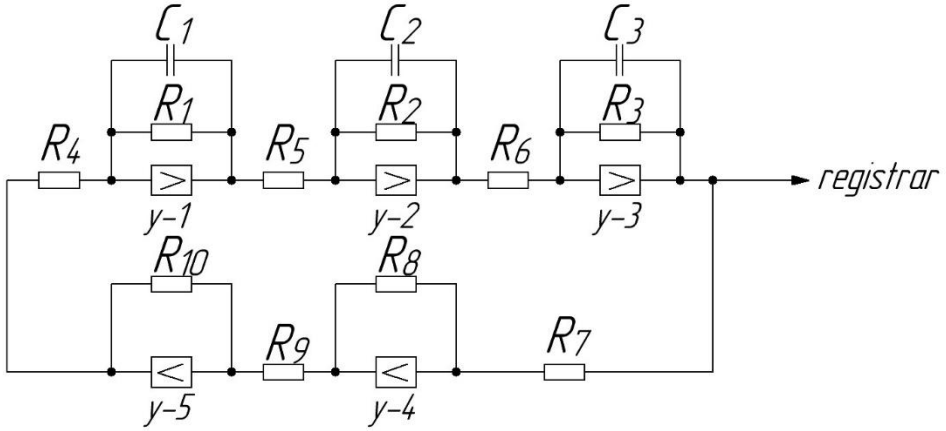

Figure 3. Three-channel logic control circuit based on elements using registers

It is also possible to draw up a scheme of the electronic model without going to the differential equation (1), but starting directly from the structural diagram of the automatic control system shown in Fig. 1, using the solver amplifiers of the model in the aperiodic link mode.

Amplifiers y-1, y-2, y-3 correspond to aperiodic links with time constants T_1, T_2, T_3. In order to obtain an accelerated modelling process, the time constants of amplifiers y-1,y-2, y-3 can be chosen 100 times smaller than the time constants T_1, T_2, T_3 respectively.

$$C_1R_1 = \frac{1}{100}T_1 = \frac{180}{100} = 1.8\,\text{sec}$$

$$C_2R_2 = \frac{1}{100}T_2 = \frac{600}{100} = 6\,\text{sec}$$

$$C_3R_3 = \frac{1}{100}T_3 = \frac{60}{100} = 0.6\,\text{sec}$$

Amplifiers y - 4 and y -5 correspond to negative feedback with coefficient - k_4.

Using the initial data for the coefficients k_1, k_2, k_3, k_4 in the control system, the resistances in the electronic model are defined as follows:

$$\frac{R_1}{R_3} = k_1 = 10, \frac{R_2}{R_4} = k_2 = 2, \frac{R_3}{R_5} = k_3 = 0.1, \frac{R_8}{R_7} = k_4 = 2$$

The U-5 amplifier plays the role of an inverter. Therefore, it is necessary to put

$$\frac{R_{10}}{R_9} = 1$$

In order to use the whole scale range of the model ±100 V, we take the initial voltage on the capacitance C_3 as follows

$$\xi(0) = 100\varepsilon$$

The voltages on the capacitances C_1 and C_2 must first be zero, which corresponds to the zero initial conditions $x'(0) = x''(0) = 0$.

Thereby we have introduced a temperature scale equal to $k = 2\left[\frac{V}{\text{deg}}\right]$, i.e.

$$x = \frac{1}{2}\xi$$

As in the previous model scheme, in order to pass from the machine variables ξ and time τ to the original variables x deg and t [sec], we need to recall that

$$x = \frac{1}{2}\xi\left[\text{deg}\right], t = 100\tau\left[\text{sec}\right]$$

For the analysis of dynamic systems in automation and simulation, understanding the behaviour of machine variables plays a key role. One such variable $\xi = e^{-\tau}\sin(2\pi\tau)$ describes the process of damped oscillations. This function combines two physical processes: exponential damping $e^{-\tau}$ and harmonic oscillations $\sin(2\pi\tau)$. To clearly interpret the behaviour of the variable ξ, , we plot its dependence on machine time τ. At the initial moments of time $\tau \to 0$ the value of ξ is maximally close to the amplitude of $\sin(2\pi\tau)$, because of the exponential multiplier $e^{-\tau} \to 0$. As τ increases, the amplitude of oscillations gradually decreases due to exponential damping This allows to model real physical processes, such as oscillations of a system with friction or resistance

The graph illustrates how the value of ξ changes as τ increases Fig. 4

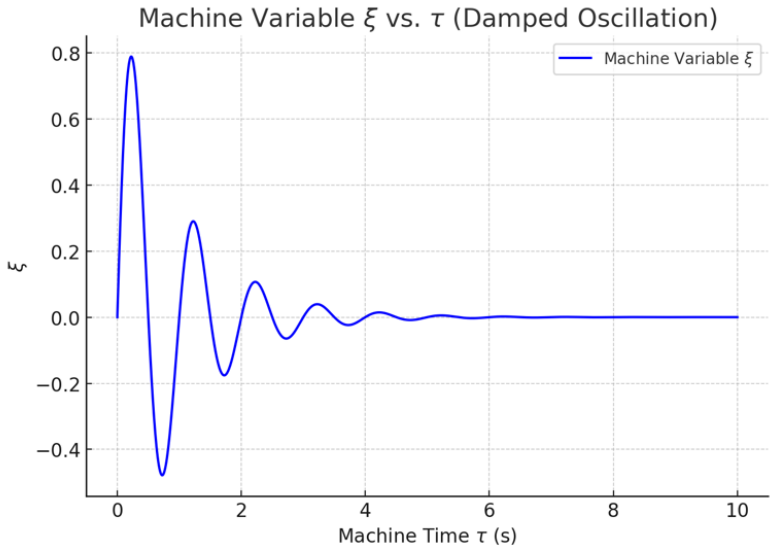

Figure 4. Graph ξ plot of amplitude attenuation

At the average time duration $0<\tau<5$, the influence of damping becomes noticeable. The exponential multiplier begins to dominate, significantly reducing the amplitude. In this phase, the system rapidly loses energy but retains the oscillation frequency. The obtained characteristic is especially important in the design of automatic control systems. At large time intervals $\tau<5$ the oscillations practically stop. The variable ξ tends to zero, which corresponds to the resting state of the system. This is a key indicator of damping efficiency, important for stabilising the system in the final state. The graph of the variable $\xi = e^{-\tau}\sin(2\pi\tau)$ demonstrates all stages of damped oscillations: from the initial phase of active oscillations to the complete cessation of oscillations Fig. 5.

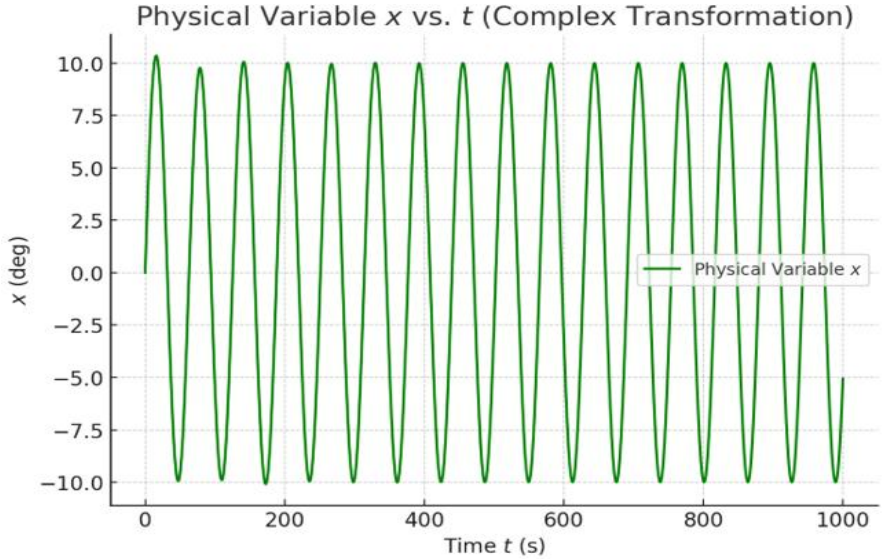

Figure 5. Graph x complex transformation

The plot of the variable $x = 0,5\xi + 10sin(0,1t)$ is a complex transformation that combines the damped oscillations of the machine variable $\xi = e - \tau sin(2\pi\tau)$ with an additional low-frequency sinusoid $10sin(0,1t)$. This combination models the behaviour of a system in which the effects of damping and low-frequency modulation are simultaneously present. At the initial stage $t \to 0$, the influence of damped oscillations dominates. The $0,5\xi$ component dominates due to the high

amplitude of damped oscillations. As time $t > 0$ progresses, the amplitude of ξ decreases due to exponential damping, and the low-frequency component $10sin(0{,}1t)$ comes to the forefront.

At the intermediate stage $t \approx 20$, the variable x acquires a complex character. Here we can see how both components - damped oscillation ξ and sinusoid - interact to form a superposition. Behaviour of systems with modulated signal, where the amplitude of one process changes under the influence of the other. At large time intervals $t > 50$ the damped oscillations ξ practically disappear and the graph x tends to a pure low-frequency sinusoid $10sin(0.1t)$. Which demonstrates the transition of the system to the dominance of one of the effects.

The plot of variable $\zeta = ln(1+t)cos(t)$ shows a complex behaviour combining logarithmic amplitude growth and cosine oscillations, to model a system in which there is an accumulation of effect logarithmic component and periodic changes cosine component.

At the initial stage $t \to 0$, the logarithmic component of $ln(1+t)$ is almost constant and close to zero. Here the amplitude of the variable ζ is determined only by the oscillatory component $cos(t)$ Fig. 6.

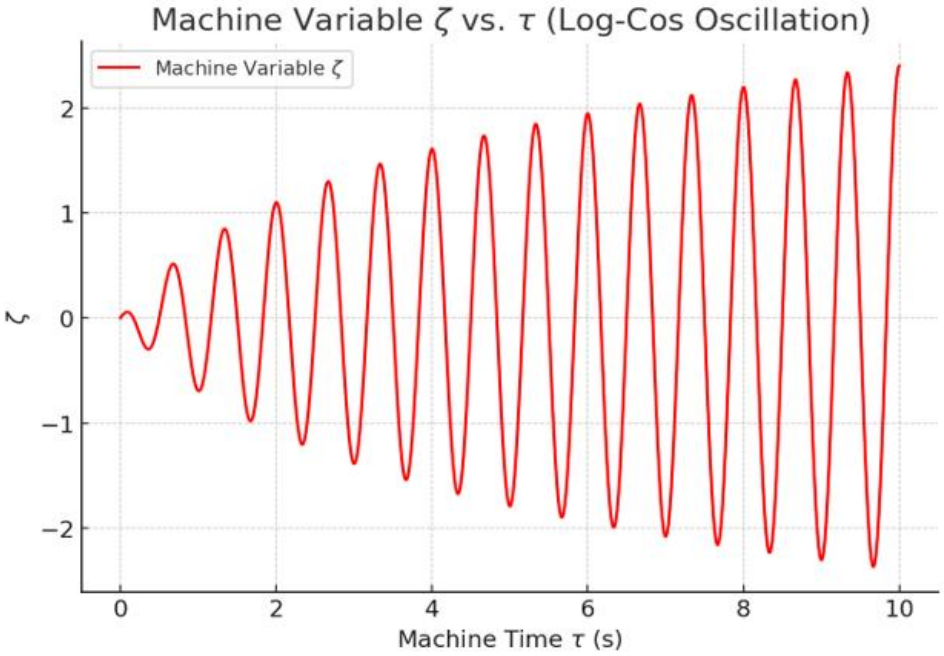

Figure 6. Graph ζ logarithmic-cosine behaviour

As the time $t > 0$ increases, the logarithmic component begins to increase, which leads to an increase in the amplitude of oscillations. At this stage, the system demonstrates complex dynamics due to the interaction between the increasing logarithmic effect and the persisting oscillations.

At large time intervals $t > 10$, the logarithmic component of the $ln(1+t)$ becomes dominant. Despite this, the cosine oscillations persist, but their relative amplitude decreases and they are perceived as modulation of the logarithmic rise

Results and conclusions.

Modelling of the automatic temperature control system on the electronic model confirmed its high efficiency and reliability. The developed system demonstrates fast and stable achievement of the set temperature regime with minimal fluctuations, which is achieved due to a properly adjusted proportional controller and taking into account the inertial characteristics of the actuator and thermocouple. Transient analyses revealed optimal system parameters that provide a balance

between response speed and stability, which is especially important for industrial applications requiring precise and fast temperature control.

The obtained results indicate the feasibility of using the cascade representation of control objects and the electronic model to analyse and develop automatic control systems. Further research can be aimed at optimising the regulator coefficients in order to improve the accuracy of regulation, reduce power consumption and improve the stability of the system to external disturbances. A possible direction is the introduction of more complex regulator schemes, such as integral or differential regulators, to achieve even higher dynamics and stability of the system.

REFERENCES

[1]. V.A. Besekersky. E.P. Popov. *Theory of automatic control systems*. – St. Petersburg: Profession, 2003. – 752 p.

[2]. Avvakumov, S.N., Kiselev, Y.N. *Some algorithms of optimal control.* Proc. Steklov Inst. Math. 255 (Suppl 2), S1–S15 (2006). https://doi.org/10.1134/S0081543806060010.

[3]. Boris S. Mordukhovich, M. Ebrahim Sarabi. *Variational analysis and full stability of optimal solutions to constrained and minimax problems, Nonlinear Analysis: Theory, Methods & Applications.* Volume 121, 2015, Pages 36-53, ISSN 0362-546X, doi.org/10.1016/j.na.2014.10.013

[4]. Kosheleva I.V., Danilov A.I., Mokrova N.V. *Decomposition control of a cascade of catalytic reforming reactors. / Advances in chemistry and chemical technology.* Volume XVI. 2002. No. 1 (18). p.32-33.

[5]. Artemyev, V. S. *Method of the first approximation of stability analysis of control systems of electrical equipment* / V. S. Artemyev, N. V. Mokrova // Computational Nanotechnology. – 2024. – Vol. 11, No. 3. – pp. 52-56. – DOI 10.33693/2313-223X-2024-11-3-52-56.

[6]. Artemyev, V. S. *Automated methods of analysis and forecasting of self-oscillations in agricultural systems* / V. S. Artemyev, N. V. Mokrova // Waste and resources. – 2024. – Vol. 11, No. 1. – DOI 10.15862/19INOR124.

[7]. Artemyev, V. *Theoretical and practical aspects of the application of the dynamic programming method in optimal control problems* / V. Artemyev, N. Mokrova, A. Hajiyev // Machine Science. – 2024. – Vol. 13, No. 1. – P. 46-57. – DOI 10.61413/GIPV6858.

[8]. Bellman R. *Dynamic programming*. Transl. from English – M.: Izdatinlit, 1960. – 400 p.

[9]. Hu Wen-Tsen., Umbetov U. *Decentralized control of multidimensional objects with decomposition by situations.* News of the National Academy of Sciences of the Republic of Kazakhstan, Physics and Mathematics Series, 2007, No. 1, pp. 82 – 85.

[10]. Mokrova, N. V. *Synthesis of finite management in the agro-industrial complex under pulsed loads* / N. V. Mokrova, A. O. Grigoriev, V. S. Artemyev // Bulletin of the Chuvash State Agrarian University. – 2024. – № 3(30). – Pp. 189-197. – DOI 10.48612/vch/3t59-rm1b-2mte.

[11]. Wilco van Harselaar, Niels Schreuders, Theo Hofman, Stephan Rinderknecht. *Improved Implementation of Dynamic Programming on the Example of Hybrid Electric Vehicle Control*, IFAC-PapersOnLine, Volume 52, Issue 5, 2019, Pages 147-152, ISSN 2405-8963, doi.org/10.1016/j.ifacol.2019.09.024.

[12]. Artemyev V. S. *Development of automation and control systems for production processes* / V. S. Artemyev // Scientific and information support for the innovative development of the agro-industrial complex : Proceedings of the XVI International Scientific and Practical

Internet Conference, Pravdinsky settlement, Moscow region, June 06, 2024. Moscow: Russian Scientific Research Institute of Information and Techno-economic Research on engineering and technical support of the agro-industrial complex, 2024, pp. 478-483.

[13]. V. Artemyev, A. Medvedev, V. Yaroshevich. *Investigation of optimal control of variable systems in the dynamic spectrum.* Machine Science. – 2023. – Vol. 12, No. 1. – P. 68-75.

[14]. V. Artemyev, S. Mokrushin, S. Savostin [et al.].*Processing of time signals in a discrete time domain.* Machine Science. – 2023. – Vol. 12, No. 1. – P. 46-54.

[15]. V. S. Artemyev, M. N. Makhiboroda, S. L. Yablochnikov [et al.]. *Implementation of Adaptive Control with Parametric Uncertainty*. Intelligent Technologies and Electronic Devices in Vehicle and Road Transport Complex (TIRVED), Moscow, 10–11 november 2022. – Moscow: IEEE, 2022. – P. 9965505. – DOI 10.1109/TIRVED56496.2022.9965505.

[16]. A. Haag, M. Bargende, P. Antony, F. Panik. *Iterative refinement of the discretization of the dynamic programming state grid*. In 16. Int. Stuttgarter Symposium, Springer (2016), pp. 145-154.

[17]. Wei Zhou, Lin Yang, Yishan Cai, Tianxing Ying. *Dynamic programming for New Energy Vehicles based on their work modes part I: Electric Vehicles and Hybrid Electric Vehicles.* Journal of Power Sources, Volume 406, 2018, Pages 151-166, ISSN 0378-7753, doi.org/10.1016/j.jpowsour.2018.10.047

[18]. Mokrova N.V. *Problem of optimum control of manufacture of the activated coals.* Ugol. 2007. №7. с.72-74. ISSN: 0041-5790.

Received: 14.05.2024
Accepted: 22.08.2024

MACHINE SCIENCE

ISSN: 2227-6912
E-ISSN: 2790-0479

2024, № 2 Pages 77-83

PHASE ANALYSIS AND ELECTRICAL PROPERTIES OF COMPOSITES BASED ON HIGH PRESSURE POLYETHYLENE WITH Na^+-MONTMORILLONITE FILLER

Matanat MEHRABOVA[1,a], Kamal GULMAMMEDOV[1,b], Sevinj SAFAROVA[1,c]

[1]Azerbaijan Technical University, department of "Engineering Physics and Electronics"

E-mail: *[a]*metanet.mehrabova@aztu.edu.az* , [b]*kamal.gul@aztu.edu.az*, [c]*seferova_sevinc@aztu.edu.az*

https://doi.org/10.61413/GMGO5334

Abstract. One of the promising areas in polymer science is the development of methods for obtaining and studying polymer composites and nanocomposites. An important advantage of composites is their higher functionality and electrical stability compared to polymer analogues. The functioning of composite structures as an active element is associated, in particular, with charge formation phenomena. Therefore, in the development of new dielectric composites, researcher's attention mainly focuses on their production and study of dielectric properties under effect of various factors (temperature, frequency). These studies can serve as a basis for selecting components of compositions for obtaining elements with predetermined parameters and assessing the possibility of their use as a dielectric. Analysis of literature data shows that fillers impart increased thermal and electrical conductivity, new magnetic properties to polymer materials, improve mechanical and electrical strength, etc. In the work presented the results of a study of surface microrelief and X-ray phase analysis of high pressure polyethylene with Na^+-montmorillonite filler **(**HPPE+x wt% Na^+-MMT) composites, the results of the study on the temperature dependences of dielectric permittivity and the tangent of the dielectric loss angle. It was found that with an increase in the filler content, the degree of crystallinity of the composites decreases, dielectric permittivity increases, and dielectric losses decrease. The results of the X-ray phase analysis of the composites show that with an increase in the filler content of Na^+MMT, the degree of crystallinity of the composites decreases from 50.5% (for 10 wt.%) to 62.1% (for 5 wt.%).

Keywords: *High pressure polyethylene, bentonite montmorillonite, surface microrelief, X-ray phase analysis, dielectric properties*

Introduction.

The development of technology is closely linked to advances in the creation of new materials such as semiconductors and polymers [1-5]. Polymer materials with a special properties are widely used in the fields of modern mechanical engineering, space technology, electrical engineering, radio engineering, etc. [6-9]. Controlling and varying the diverse properties of a new polymer material through modification allows for the creation of valuable industrial products. With a complex of physical properties, medium and highly crystalline polymer materials have specific features. Moreover, there is a vast raw material base for their production, their cost is relatively low, and their high chemical resistance is combined with excellent mechanical and dielectric properties. Based on this, high pressure polyethylene (HPPE) has secured a prominent position among other polymer materials of industrial significance. The production and application of HPPE in various fields of modern technology are steadily growing [10-14]. Therefore, it is not surprising that there is significant research interest in these materials, their structure, and the relationship between their structure and properties. Recent research dedicated to methods of evaluating the technological, physical-mechanical, and electrophysical characteristics of HPPE and the development of fundamentally new methods of regulating the properties of its melts and solid states, based on modern concepts of

polymer structure and the ability to control their supramolecular structure and properties, is of certain importance. It should be noted that one of the most accessible methods for developing technology to obtain new dielectric materials with specified properties is the method of modifying ready-made polymers by introducing functional groups and various additives into their macromolecules. Based on this, the determination of the physicochemical basis for obtaining new polymer modifications based on HPPE with additives that improve their electrophysical properties is of great scientific and practical interest.

To obtain new composite materials, HPPE (grade M-150) was used as the matrix, and bentonite montmorillonite (Na^+-MMT) were used as fillers. The main feature of montmorillonite, determined by its structure and crystalline composition, is its ability to adsorb various ions and perform ion exchange. The presence of amorphous substitutions, a large specific surface area, and the ease of ion penetration into the interatomic space provide a significant capacity for cation exchange [15-17].

Experimental Methodology

The HPPE+x wt.% Na^+-MMT composites were obtained using the method described in [18-21]. The polyethylene and bentonite powders were pre-ground in a ball mill with porcelain balls to a particle size of no more than 60 μm. The surface microrelief of the HPPE+x wt.% Na^+-MMT composites was studied using a Solver Next AFM atomic force microscope in MD mode. The diagrams were obtained on a 'D2 Phaser' diffractometer (“Buker”).

The tangent of the dielectric loss angle (tgδ) and the capacitance of the studied samples were measured using an AC bridge R-589 at a frequency of 1 kHz in the temperature range of 300-450 K, according to the method described in [22,23]. The measurement ranges for capacitance were 0.001 pF to 100 μF, and for the tangent of the loss angle, 10^{-5}-0,5. The bridge was powered by an AC network with a voltage of 220 V and a frequency of 50 Hz. The measuring electrodes were polished brass discs. The sample temperature was measured using copper-constantan thermocouples with an accuracy of ±1°C. The study was conducted on composites with filler contents of 3, 5, 7, and 10 wt. % Na^+-MMT.

Experimental Results and Their Discussion

The results of the study of the surface microrelief of the composites in 2D and 3D models and their histograms are shown in Fig. 1. From Fig. 1, it follows that with changes in the filler content of Na^+-MMT, the surface condition changes significantly. This is apparently due to changes in the interaction between the matrix and the filler in the boundary layer.

However, the intensities of the peaks on the X-ray diffraction patterns increase with an increase in the content of Na^+-MMT filler.

The results of the X-ray phase analysis of the composites, shown in Fig. 2, demonstrated that with an increase in the filler content, the degree of crystallinity of the composites decreases. Specifically, the degree of crystallinity with fillers of 5, 7, and 10 wt.% is 62.1%, 52.2%, and 50.5%, respectively. No significant changes occur in the X-ray diffraction patterns of the composites as the filler content increases.

The dielectric properties of the composites based on high pressure polyethylene (HPPE) with Na^+-MMT fillers were studied in the temperature range of 300-380 K. The studies were conducted on composites with fillers of 3, 5, 7, and 10 wt. % Na^+-MMT. Fig. 3 presents the temperature dependencies of the dielectric permittivity (ε), and Fig. 4 shows the tangent of the dielectric loss angle (tgδ) of these composites.

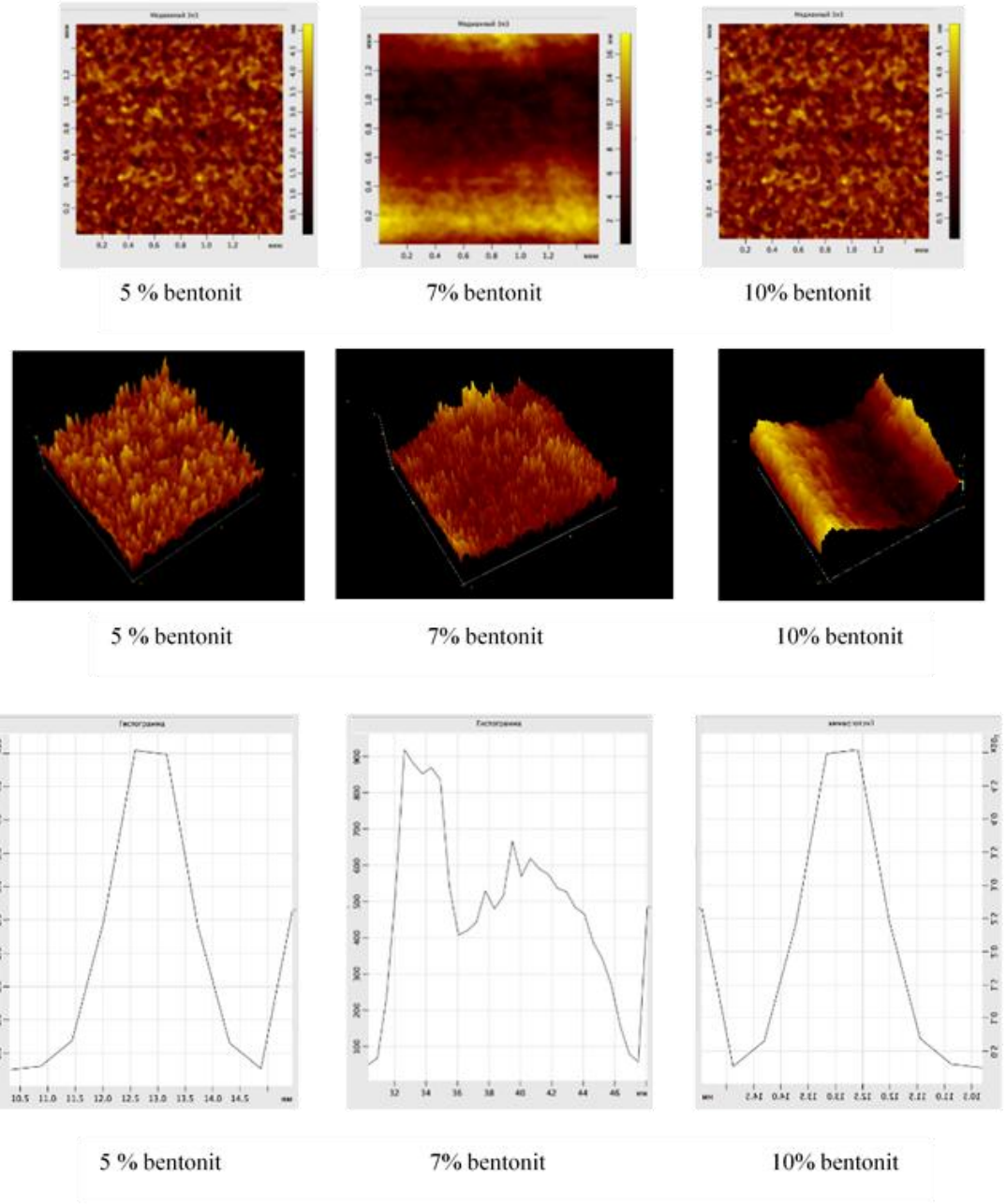

Figure 1 Results of the study of the surface microrelief of HPPE + x wt.% Na^+-MMT composites in 2D and 3D modes, 1 - x = 5; 2 - x = 7; 3 - x = 10, and their histograms.

As seen in Fig. 3, the dielectric permittivity increases linearly with rising temperature, and no specific responses were detected in the ε(T) dependency. The changes in the tangent of the dielectric loss angle with temperature variation are relatively complex. In the temperature range of 340-350 K, distinct maxima are observed on the tgδ(T) curves. Apparently, the appearance of maxima in tgδ(T) at high temperatures is the result of changes in the parameters of the interphase boundary layer. It should be noted that as the filler content of Na^+-MMT increases, the dielectric permittivity of the composites increases, while the tangent of the dielectric loss angle decreases.

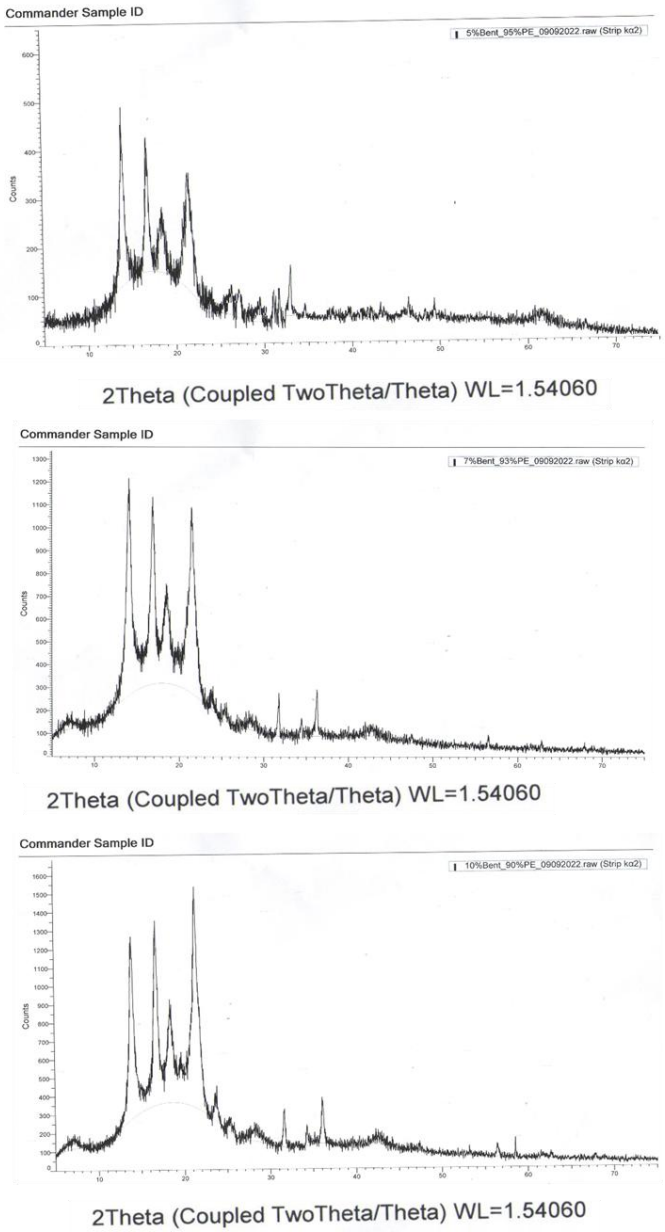

Figure 2. X-ray phase analysis of HPPE + x wt.% Na+-MMT composites with 5, 7, and 10 wt.%.

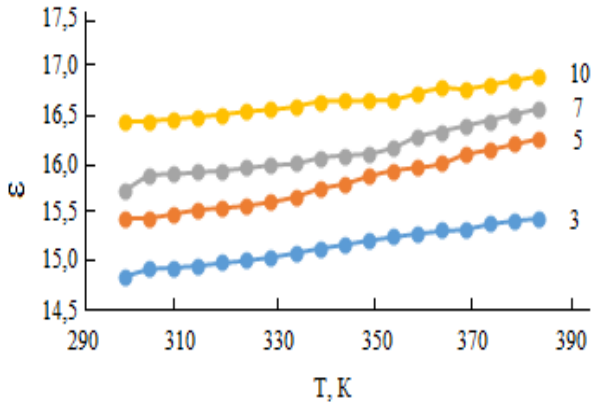

Figure 3 Temperature dependence of the dielectric permittivity of HPPE + x wt.% Na^+-MMT composites, where 1 - x = 3; 2 - x = 5; 3 - x = 7; 4 - x = 10

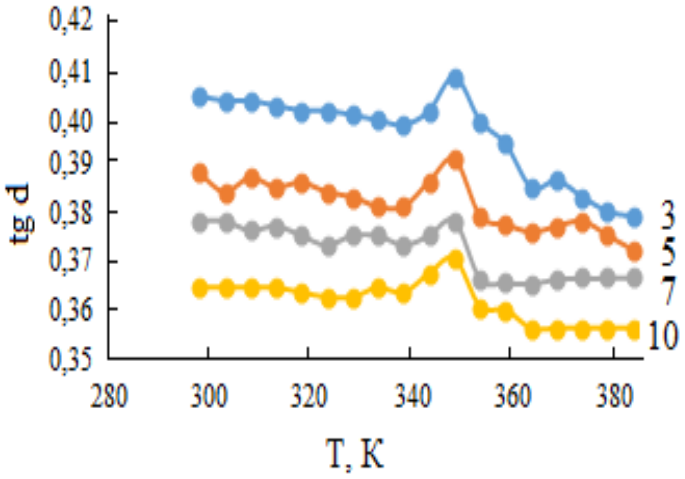

Figure 6. Temperature dependence of the tangent of the dielectric loss angle of HPPE + x wt.% Na^+-MMT composites.

Results and conclusions.

The surface microrelief and X-ray phase analysis of high pressure polyethylene composites with Na+-montmorillonite filler (HPPE+x vol.% Na+-MMT) were studied. The results of the study of temperature dependences of permittivity and dielectric loss tangent showed that with an increase in the volumetric filler content, the degree of crystallinity of the composites decreases, the permittivity increases, and dielectric losses decrease. According to the results of X-ray phase analysis of the composites, it was revealed that with an increase in the volumetric filler content Na+MMT, the degree of crystallinity of the composites decreases from 50.5% (for 10 vol.%) to 62.1% (for 5 vol.%).

REFERENCES

[1]. I.R. Nuriyev, M.A. Mehrabova, A.M. Nazarov, R.M. Sadigov, N.G. Hasanov. *On the growth, structure, and surface morphology of epitaxial CdTe films. Semiconductors*. 2017, 51, p. 34-37

[2]. I.R.Nuriyev, M.A.Mehrabova, A.M.Nazarov, N.H.Hasanov, R.M.Sadigov, S.S. Farzaliyev, N.V.Farajov. *Structure and surface morphology of Cd1− x(Mn,Fe)xSe epitaxial films.Journal of surface investigation: X-ray, synchrotron and neutron techniques*, 2019, 13, 6, 1083-1085.

[3]. M.A.Mehrabova, N.T.Panahov, N H.Hasanov *Ab initio calculations of electronic band structure of ideal and defective CdMnS.“Materials Physics and Mechanics*” Журнал "Физика и механика материалов", Россия, Санкт-Петербург, 2022;48, 3, 419-427.

[4]. I.R.Nuriyev, M.A.Mekhrabova, A.M.Nazarov, R.M.Sadygov *Growth of epitaxial Cd1–x Mn x Te films.* Inorganic Materials, 2016, 52, 886–889. DOI 10.1134/S0020168516090132

[5]. M.A.Mehrabov, S.I.Mammadova, F.Sh.Kerimov, S.I.Safarova, K.J.Gulmamedov, I.H.Hamdillayeva. *Influence of discharges and UV Irradiation on the electrical properties of high pressure polyethylene and compositions on its base.* Polymer-Plastics Technology and Materials. 2024, Volume 63, 2024 - Issue 16, p.2237-2245. DOI 10.1080/25740881.2024.2369677

[6]. P.Olesik, M.Godzierz, M.Kozioł, J.Jała, U.Szeluga, J.Myalski. *Structure and mechanical properties of high-density polyethylene composites reinforced with glassy carbon*. Materials, 2021, 14(14), 4024. DOI 10.3390/ma14144024

[7]. N. Abduljabbar, Sh. Al-Busaltan, A. Dulaimi, R.Al-Yasari, M. Sadique, H. Al Nageim.*The effect of waste low-density polyethylene on the mechanical properties of thin asphalt overlay.* JURNAL

2021. 125722.
[8]. A.A.A. Alim, A. Baharum, S.S.M. Shirajuddin, F.H. Anuar. *Blending of Low-Density Polyethylene and Poly(Butylene Succinate) (LDPE/PBS) with Polyethylene–Graft–Maleic Anhydride (PE–g–MA) as a Compatibilizer on the Phase Morphology*, Mechanical and Thermal Properties. Polymers (Basel). 2023 Jan; 15(2): 261. DOI 10.3390%2Fpolym15020261.
[9]. Fang Zhi-Jie, Zhang Ping, He Man-Chao. *Atomic and electronic structures of montmorillonite in soft rock*. Chinese Physics B, 2009. V.18, № 7, p. 2933. DOI 10.1088/1674-1056/18/7/053
[10]. Kumykov E.S., Karmov M.A., Nafonova M.N., Tkhakakhov R.B. et al. *Dielectric properties of polymer composites based on SKN-26 and PVC containing nanosized particles*. Magazine "Plastic Masses". 2012, No. 3, p. 4.
[11]. Stadnik A.D., Moroz I.A., Medvedovskaya O.G., Bilyk V.N. *Structure and properties of polymer composites and nanocomposites subjected to thermomagnetic treatment*. Journal of Nano- and Electronic Physics. 2015, v. 7, no. 3, 03046-
[12]. Godjaev E.M., Safarova S.I,.Ahmedova H.R, Osmanova S.S..*Composite dielectric properties with nanoadditions of aluminum particles.* Azerbaijan journal of Fhysiscs, Volume XIX, N4, Section:En, October2013 s.14-17.
[13]. Gojayev E.M., Safarova S.I.,.Ahmadova Kh.R,.Djafarova G.S,.Mextiyeva Sh.M. *Effect of Aluminum Nano-Particles on Microrelief and Dieectric Properties of PE+ $TlInSe_2$ Composite Materials.* Journal of Non-Metallic Materials, January 2015, №5, p.11-19.DOI: 10.4236/ojinm.2015.51002
[14]. Turik A.B., Rodinin M.Yu. *Dielectric losses in materials with a limited relaxation time distribution region*. JTP Letters. 2010, 36(1), 37–43.
[15]. Gojayev E.M., S.S. Osmanova, Safarova S. I., Gafarova D. M.*Synthesis, XRD analysis and electronic structure of InGaTe2 chain semiconductor*. International Journal of Modern Physics B,Vol.35,No.2(2021)2150029(9pages) DOI 10.1142/S0217979221500296
[16]. Debasis Borah , Harshajit Nath and Hemaprobha *Saikia.Modification of bentonite clay and its applications* Reviews in Inorganic Chemistry 42(3), November 2021. DOI: 10.1515/revic-2021-003
[17]. Jianwei Lin, Siqi He, Yanhui Zhan, Zhe Zhang, Xiaolong Wu, Yang Yu, Yuying Zhao ,Yan Wang .*Assessment of sediment capping with zirconium-modified bentonite to intercept phosphorus release from sediments.*Environmental Science and Pollution Research 26(4), 2019, pages 3501–3516. DOI: 10.1007/s11356-018-3869-y
[18]. Gojayev E.M., Gulmamedov K.J., Safarova S.İ., Aliyeva Sh.V. *Mechanical Strength of Low Density Polyethylene Composites Modified Montmorillonite Na+MMT* International Conference on Engineering Sciences held on November 11-12 2022 Baku,Azerbaijan Technical University
[19]. J.Golebiewski, A. Rozanski, J.Dzwonkowski, A.Galeski. *Low density polyethylene–montmorillonite nanocomposites for film blowing.* European Polymer Journal. Volume 44, Issue 2, February 2008, Pages 270-286, DOI 10.1016/j.eurpolymj.2007.11.002
[20]. Chi-Nhan Ha Thuc , AnneCécile Grillet, Laurence Reinert , Fumihiko Ohashi Huy Ha Thuc , Laurent Duclaux .*Separation and purification of montmorillonite and polyethylene oxide modified montmorillonite from Vietnamese bentonites*. Applied Clay Science.Volume 49, Issue 3, July 2010, Pages 229-238. DOI 10.1016/j.clay.2010.05.011
[21]. Muñoz-Shugulí, Francisco J. Rodríguez , Julio E. Bruna, María J. Galotto, Claire Sarantópoulos, Mary A. Favaro Perez, Marisa Padula .*Cetylpyridinium bromide-modified montmorillonite as filler in low density polyethylene nanocomposite films*. Applied Clay Science.Volume 168, February 2019,

Pages 203-210, https://doi.org/10.1016/j.clay.2018.10.020
[22]. Khaliq Majeed, Azman Hassan, Aznizam Abu Bakar, Mohammad Jawaid.*Effect of montmorillonite (MMT) content on the mechanical, oxygen barrier, and thermal properties of rice husk/MMT hybrid filler-filled low-density polyethylene nanocomposite blown films*. Journal of Thermoplastic BComposite Materials. 2016.Volume 29, Issue 7, DOI 10.1177/0892705714554492
[23]. Pamela Rodrigues Passos Severino,Thais Larissa do Amaral Montanheiro, Oreste Ferro,Fabio Roberto Passador, Larissa Stephen Montanha.*Protective Low-Density Polyethylene Residues from Prepreg for the Development of New Nanocomposites with Montmorillonite*: Recycling and Characterization.Recycling 2019, 4(4), 45; DOI 10.3390/recycling4040045

Received: 15.01.2024
Accepted: 22.09.2024

MACHINE SCIENCE

ISSN: 2227-6912
E-ISSN: 2790-0479

web site: msj.aztu.edu.az; e-mail: msj@aztu.edu.az **Tel: (+994 12) 538 94 12**

SUBMISSION GUIDELINES

General requirements.
Article should not be earlier published in any edition, stated in the short form and edited. The scientific article maintenance should correspond to one of the following scientific directions: Designing of machines; Materials technology; Mechanics; Manufacturing engineering; Economy and management; Automatics and ICT; Technical information.

The documents applied to article.
The conclusion of the corresponding organization (chair, etc.); The expert opinion on expediency of the publication of the article; The covering letter; The Information on the authors (name, patronymic, surname, the exact address, place of work and position, scientific degree, area of scientific activity, contact phones, e-mail address ,etc.).

Preparation rules.
Format - A4; *Margins from each party* - 20 mm; *Program* - Microsoft Office Word; *Font* - Times New Roman, a font size - 12, an interval – 1,15.
The scientific article can be written only in English language, and it is represented in duplicate.
Article volume - 5 … 8 pages.

Sequence of compilation:
1. Article name - on the center;
2. Names and surnames of the authors - on the center;
3. Full addresses of a place of work of authors - on the center;
4. Co-ordinates of authors: e-mail address, phone numbers.
5. The abstract: not less than two-three offers, and no more than 100 words. In the summary: article summary, problem statement, and the information on the received results should be reflected.
6. Keywords: often used 3 ÷ 5 terms under the article.
7. The basic text.
8. The references.

The main text of article should be divided as follows:
For example: "*Introduction*", "*Problem statement*", "*Decision or test methods*", "*Results of the decision or tests and their estimation*".
In introduction: the description of the problem statement, the work purpose and etc.;
In the main part: formation of problem statements; research and methods of the decision, their advantage and difference from existing methods; examples confirming efficiency of the offered method of the decision and the results received.
In the conclusion: evaluation of the results.

Drawings. *Formats* - DOC, JPEG, TIFF and PDF (600 dpi). *The size* – min. 5 × 5, max. 10 × 15. *Arrangement* - ("In the text", in the center). Images of drawings should be accurately visible, and all symbols well are read.
Drawings, paintings, schedules and algorithms should correspond to standard requirements.

Tables are located in the text and are numbered, and the name of each table should be specified in the right top corner.

Formulas should be written down in format *Equation* in the separate line. It is not recommended to use special symbols in the text written on the same line in format *Equation*. Formulas should be written down in certain sequence and are numbered on the right.

The references should correspond to the text and sequence of article. It is recommended to refer to sources published in last 10 years.

The additional information. Edition has the right to spend necessary updating and reductions. Authors bear a scientific article maintenance responsibility. To the publication those articles which have received a positive response are represented only. If article is not published, the edition decision is possible to data of authors, the manuscript and disks do not come back.